Geochemical News 143 - April 2010

In This Issue

Geochemistry in China: Current Topics

GNews 143 Staff

Stephen Komor, Ph.D. (Editor)
U.S. Geological Survey (retired)
sck15@cornell.edu

Seth Davis (Webmaster)
Geochemical Society
seth.davis@geochemsoc.org

Introductory Remarks

Full Text (467 Kb PDF)

This issue of the *Geochemical News* is devoted to geochemical research in China. The papers included in the issue are all peer reviewed, and exemplify the research achievements of our geochemistry colleagues in China. These colleagues and the Geochemical Society have the same motives for publishing these papers: 1. To illustrate the extremely high quality of Chinese geochemical research; 2. To alert Western geochemists that to stay abreast of the forefronts of their fields, they need to regularly read the Chinese literature written in English, and; 3. Perhaps most importantly, to promote collaboration among Western and Chinese geochemists.

I have made five close-to-evenly-spaced trips to China over the past 22 years, three because of research collaborations and two because of international conferences. It has been said by others before me that the economic transformation of the country over that 22-year period since my first visit has been nothing short of breathtaking and miraculous. Less well documented is the equally impressive transformation of China's basic research enterprise across the board, and particularly in geochemistry. Whereas 22 years ago many researchers in geochemistry had outdated analytical equipment, many labs in China today have state-of-the-art mass spectrometers, electron microprobes, ion microprobes, and the like, most as part of state key laboratories, including two (Environmental Geochemistry and Ore Deposit Geochemistry) in Guiyang. Government spending on research in science and technology has grown at a staggering 20% per year for over a decade. The country continues to exhibit tremendous energy and motivation to overhaul its research infrastructure, and has so far shown careful planning to develop a diversified yet balanced research portfolio in which all sciences receive close-to-equal billing. Some 1,500 individuals belong to the Chinese Society for Mineralogy, Petrology, and Geochemistry, and overall, practicing geochemists in academia and industry are approximately three to four times this number.

Each of the papers in this issue has the contact email address of the authors, provided to encourage establishment of communication between these colleagues and members of the Geochemical Society. Dr. Yong-Fei Zheng recruited the authors for this issue. Letters may be directed to him to identify a geochemist who specializes in your particular field. The impetus for this project came from Dr. Martin Goldhaber, Past President of the Geochemical Society. You will profit by reading these papers, and I encourage you to take advantage of the opportunities to collaborate with our colleagues in the Chinese geochemistry community.

Samuel Mukasa

About the Author

Samuel Mukasa is President of the Geochemical Society and the Eric J. Essene Collegiate Professor of Geological Sciences at University of Michigan in Ann Arbor, MI, USA.

Metamorphic chemical geodynamics of continental subduction zones in China

Yong-Fei ZHENG [a,*]

[a] CAS Key Laboratory of Crust-Mantle Materials and Environments, School of Earth and Space Sciences, University of Science and Technology of China, Hefei 230026, China

[*] corresponding author's email: yfzheng@ustc.edu.cn

Full Text (7.5 Mb PDF)

Abstract

Ultrahigh-pressure (UHP) terranes as well as UHP metamorphic minerals and rocks represent a special natural laboratory to investigate the geodynamics and fluid regime during subduction and exhumation of continental crust. Studies of UHP rocks have represented a new frontier in the earth sciences during the past two decades, significantly advancing our understanding of geological processes in continental subduction zones. This is particularly so from intensive studies of geochemical records in deeply subducted continental crustal rocks from the Dabie-Sulu orogenic belt in China. Such studies have addressed the following issues: the time and duration of UHP metamorphism, the origin and activity of metamorphic fluid during continental collision, and element mobility in continental subduction zones. This extends metamorphic chemical geodynamics of subduction zones from the oceanic crust to the continental crust, enabling important contributions to development of the plate tectonic theory.

Keywords: Continental subduction, UHP metamorphism, plate tectonics, metamorphic geochemistry, chemical geodynamics

About the Author

Yong-Fei Zheng is a professor of geochemistry and director of the Key Laboratory of Crust-mantle Materials and Environments in Chinese Academy of Sciences. He obtained a Dr. rer. nat. in 1991 from Geochemical Institute at University of Goettingen in Germany. His primary research interest concerns the fundamentals of isotope geochemistry and their applications to high-temperature geological systems. His current research largely focuses on chemical geodynamics and fluid regime of continental subduction zones. He was elected as a Fellow of the Mineralogical Society of America in 2005 and a Member of the Chinese Academy of Sciences in 2009. He also serves as associate editors for *Terra Nova* and *Geochemical Journal*, and a member of editorial boards for *Chemical Geology*, *Lithos*, *Ore Geology Review* and *Journal of Asian Earth Sciences*.

1. Introduction

The study of ultrahigh-pressure (UHP) metamorphism and continental deep-subduction was initiated by findings of coesite (Chopin, 1984; Smith, 1984) and diamond (Sobolev and Shatsky, 1990; Xu et al., 1992) in metamorphic rocks of supracrustal origin. These findings have provided compelling evidence that segments of the continental crust were subducted to mantle depths in excess of 100 km and returned to the surface during continental collision orogeny. This challenges the precept in the plate tectonics theory that the continental crust cannot be subducted to mantle depths because of its lower density than the oceanic crust. Thus far, 22 coesite- and diamond-bearing UHP terranes have been recognized in the world; most of them are of Phanerozoic ages (Chopin, 2003; Liou and Ernst, 2008). These UHP terranes lie within major continental collision belts and extend for several hundred km or more; most are in Eurasia (e.g., Alps, Norway, Erzgebirge, Kokchetav, Tianshan, Himalaya, Dabie-Sulu), with rare examples in Africa, South, Central and North America and Antarctica. These deep processes would not only result in phase changes and mineralogical reactions within UHP slabs, but also bring about crust-mantle interactions in continental subduction zones.

A group of Chinese earth scientists were involved in the study of UHP terranes as soon as coesite (Okay et al., 1989, Wang et al., 1989) and diamond (Xu et al., 1992) were identified in eclogites from the Dabie orogen, east-central China. Besides Dabie, five additional coesite- and diamond-bearing UHP terranes have been discovered in China, including Sulu (Enami and Zang, 1990), North Qaidam (Yang et al., 2001), Altun Tagh (Liu et al., 2002), Western Tianshan (Zhang et al., 2002), and North Qinling (Yang et al., 2003). Some special textures of mineral exsolution were also discovered in UHP metamorphic rocks (Ye et al., 2000; Song et al., 2005; Liu et al., 2007a, b), suggesting a possible origin of these rocks from depths in excess of 200 to 300 km. These six UHP terranes occur from east to west along the central orogenic belt of China, forming in the Early Paleozoic and Early Mesozoic, respectively. All UHP rocks consist mainly of felsic and intermediate gneissic rocks with minor eclogites and garnet peridotites. Nevertheless, the mafic-ultramafic rocks appear to have originated from different tectonic settings and were subjected to coeval UHP metamorphism, deformation, and retrogression with their enclosing granitic gneisses and supracrustal rocks. Since UHP eclogites and garnet peridotites more easily preserve petrological and geochemical relics of the UHP stages, they have been studied more intensively to constrain the major processes attending continental subduction, collision and subsequent exhumation. This is particularly so for these rock types in the Dabie and Sulu terranes (e.g., Wang et al., 1995; Cong, 1996; Li et al., 1999; Jahn et al., 2003; Zheng et al., 2003a, 2009a; Xu et al., 2006; Zhang et al., 2009a).

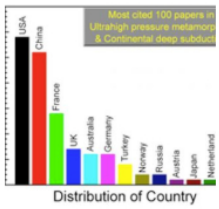

Figure 1

The study of UHP metamorphism and continental deep-subduction has greatly promoted the development of solid earth sciences in China. As illustrated by Fig. 1, there are 26 papers in principal affiliation with Chinese institutions that are among the most cited 100 papers for this increasingly recognized topic. While in the past Chinese scientists failed to make their own contributions to the establishment of the plate tectonics theory, at present they highly contribute to its development with respect to continental dynamics. This paper mainly focuses on the progress in metamorphic chemical geodynamics based on studies of UHP rocks from the Dabie-Sulu orogenic belt since no equivalent studies of deeply subducted continental crustal rocks are available from the other UHP terranes in the world.

2. Timing of UHP metamorphism

Determining the age of UHP metamorphism holds the key to unraveling the geodynamics of continental subduction and exhumation. This is particularly so for UHP eclogites in the Dabie-Sulu orogenic belt that resulted from subduction of the South China Block beneath the North China Block. This belt contains one of the largest (>30,000 km^2) and best-exposed two UHP metamorphic terranes (Carswell and Compagnoni, 2003). There are three very important geochemical anomalies in the Dabie-Sulu UHP rocks: excess argon in phengite (Li et al., 1994), a negative oxygen isotope anomaly (Yui et al., 1995; Zheng et al., 1996), and a positive Nd isotope anomaly (Jahn et al., 1996). These provide us an excellent opportunity to study the physico-chemical changes that occurred during subduction and exhumation of the continental crust.

Geochronology of UHP metamorphic event is a key to understanding subduction and exhumation of the continental crust. Because eclogite has mineral paragenesis of garnet + omphacite + phengite ± rutile, mineral Sm-Nd isochrons have been successfully used to date eclogitization. By means of this classic method, Li et al. (1993) first determined that the Dabie-Sulu UHP metamorphism occurred in the

Triassic. Later TIMS and SIMS zircon U-Pb dating gave Early Paleozoic and Neoproterozoic ages for some eclogites in this region, casting doubt on reliability of the Triassic age for UHP metamorphism. Finally, it has been realized that the optical purity of eclogitic minerals is critical to success the Sm-Nd isochron dating (Li et al., 2000). Furthermore, inspection of mineral O isotope equilibrium in the isochron minerals provides a test to the validity of mineral Sm-Nd isochrons in UHP eclogites and gneisses (Zheng et al., 2002, 2003b; Xie et al., 2004). Consequently, the Triassic eclogite-facies UHP metamorphic event is verified by SHRIMP U-Pb dating of metamorphically grown zircons in combination with identification of either mineral inclusions (Liu and Xu, 2004; Liu et al., 2004a, b) or REE distribution patterns (Li et al., 2005), or both (Liu et al., 2006a, 2006b, 2008).

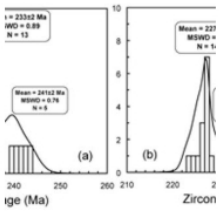

Figure 2

While the Dabie-Sulu UHP metamorphic event is resolved as having occurred in the Triassic, there are two contrasting views on its exact age. Hacker et al. (1998, 2000) suggested an age of ~245 Ma based on zircon U-Pb dates, whereas Li et al. (2000) preferred an age of 226±2 Ma based on mineral Sm-Nd isochrons. This controversy has more recently been resolved by SHRIMP U-Pb dating of coesite-bearing domains of metamorphic zircon (Wan et al., 2005; Liu et al., 2006a, 2008), bracketing the UHP metamorphic event between 241±2 Ma and 226±2 Ma (Fig. 2a). In doing so, the identification of mineral inclusions in metamorphically grown zircon has played an important role in distinguishing the peak UHP phase from HP eclogite- and amphibolite-facies metamorphic events.

3. Duration of the UHP metamorphism

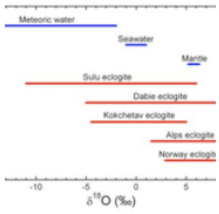

Figure 3

Highly negative $\delta^{18}O$ values are a very remarkable feature observed in UHP metamorphic rocks from the Dabie-Sulu orogenic belt (Fig. 3). They occur not only in rock-forming minerals of UHP eclogite, granitic gneiss and quartz schist (Rumble and Yui, 1998; Zheng et al., 1998, 1999; Fu et al., 1999; Tang et al., 2008a), but also in granitic minerals such as garnet (Zheng et al., 2007a) and zircon (Tang et al., 2008b). The negative oxygen isotope anomalies represent four global extremes, including the most negative $\delta^{18}O$ values for (1) metamorphic minerals (Rumble et al., 2003; Zheng et al., 2003a), (2) intrusive minerals (Zheng et al., 2007a), (3) zircon of magmatic origin (Zheng et al., 2004; Valley et al., 2005; Tang et al., 2008b), and (4) zircon of metamorphic origin (Zheng et al., 2004). These low $\delta^{18}O$ values have been interpreted to record the meteoric isotope signature of the cold paleoclimate that predates the snowball Earth event in the middle Neoproterozoic (Zheng et al., 2007a).

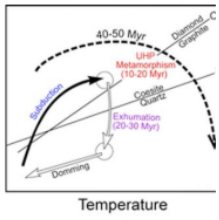

Figure 4

Preservation of the extreme ^{18}O depletion in the Dabie-Sulu UHP rocks provides a key example of chemical competition between thermodynamics and kinetics during UHP metamorphism at mantle depths. While the thermodynamics always tends to decline the $\delta^{18}O$ difference between the supracrustal protolith and the mantle in order to drive them toward O isotope homogenization, the kinetics requires enough time for the homogenization to be completed at given P-T conditions (depending on the amount of fluid passing through the UHP rocks and driving fluid-mineral O exchange). The competition between the two physico-chemical parameters determines the final status of the $\delta^{18}O$ values recorded in the UHP mineral assemblages. Accordingly, Zheng et al. (1998) estimated a timescale of 10 to 20 Myr for the UHP metamorphism at mantle depths (Fig. 4) based on the preservation of negative O isotope anomaly in the UHP minerals and the kinetics of mineral O transport by diffusion and dissolution-recrystallization under UHP conditions. This estimate is quantitatively confirmed by SHRIMP U-Pb dating on different types of metamorphic zircon (Fig. 2), which indicates that entire UHP metamorphic event in the coesite stability field lasted 15±2 Myr (Hacker et al., 2006; Liu et al., 2006b; Wu et al., 2006). Thus, both subduction and exhumation processes of the continental crust take place at faster rates than those of the oceanic crust, with short residence time of supracrustal rocks at mantle depths. These processes were imaged as if frying an icecream by boiling oil without melting (Zheng et al., 2003a). This interpretation also removes the doubt that the occurrence of negative $\delta^{18}O$ UHP rocks could indicate their formation by dynamic collision of two continental blocks at lower crustal levels without one of them being deeply subducted to mantle depths.

4. Fluid regime in continental subduction zones

Numerous studies have revealed the widespread existence of diverse water species in minerals at UHP conditions (Zheng, 2009b), including structural hydroxyl and molecular water (occurring as aqueous inclusions of different size) in the minerals usually considered stoichiometrically anhydrous (namely the nominally anhydrous minerals). The presence of molecular water in metamorphic minerals was detected by the micro-FTIR and TEM techniques (Su et al., 2002; Wu et al., 2004; Meng et al., 2009). Total water and molecule water were quantified by total and stepwise extraction analyses, respectively, using the TC/EA-MS online technique (Chen et al., 2007a; Gong et al., 2007a). Further distinction in the fluid origin between the structural hydroxyl and molecular water can be made by the hydrogen isotope analysis, because the molecular water is depleted in deuterium relative to the structural hydroxyl at thermodynamic equilibrium (Chen et al., 2007a; Gong et al., 2007b). Thus, the UHP minerals would act as water sinks (with the maximum water solubility at the peak UHP conditions) during the subduction on one hand, and as water sources during exhumation on the other hand (Zheng, 2009b). Occurrence of coesite pseudomorph as inclusion in allanite from allanite-quartz veins within UHP eclogite indicates fluid flow in the UHP regime (Zhang et al., 2008).

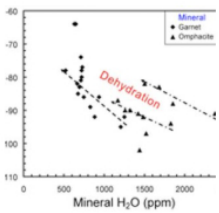

Figure 5

Many studies have been devoted to petrology, stable isotopes, fluid inclusions and mineral water contents in the Dabie-Sulu UHP metamorphic rocks. The results indicate that the scale of fluid flow is very small during the UHP metamorphism of continental crustal rocks (Zheng et al., 1999; Rumble et al., 2000; Fu et al., 2001). Inspection of the relationship between the distance, petrography and $\delta^{18}O$ values of adjacent samples from the main hole of Chinese Continental Scientific Drilling (CCSD) reveals O isotope heterogeneities between the different and same lithologies on scales of 20 to 50 cm (Chen et al., 2007b), corresponding to the maximum scales of fluid mobility during the continental collision. However, the fluid activity became significantly large during the initial exhumation because waters derived from the decomposition of hydrous UHP minerals and the exsolution of structural hydroxyl and molecular water in nominally anhydrous UHP minerals can be accumulated to form the retrograde fluid (Chen et al., 2007a; Sheng et al., 2007; Zheng, 2009b). This is indicated by negative correlations between water concentration and hydrogen isotope composition of omphacite and garnet from UHP eclogites (Fig. 5). The decreasing water contents of omphacite and garnet with increasing δD values are caused by a solubility decrease of the D-depleted molecular water in the two UHP minerals with decreasing pressure.

It has been well established that subduction of the altered basaltic oceanic crust and overlying sediments is characterized by significant release of aqueous fluid from metamorphosing slabs (Peacock, 1990; Tarrard, 2003; Bebout, 2007). However, this appears not to be the case for the deep subduction of

continental crust. In particular, the exhumation of deeply subducted continental crust is characterized by profound flux of aqueous fluid out from UHP metamorphic minerals due to the decomposition of hydrous minerals and the exsolution of structural hydroxyl and molecular water from nominally anhydrous minerals (Zheng, 2009b). This recognition provides a resolution to the controversy on the origin of retrograde fluid in subduction zones. The traditional viewpoint holds that fluids enhancing retrograde alteration of HP and UHP metamorphic rocks originate from external infiltration at shallow depths (e.g., Yardley et al., 2000; Guiraud et al., 2001; Proyer, 2003). In contrast, retrograde fluids is suggested to derive from the decomposition of hydrous minerals and the exsolution of structural-bound hydroxyl within UHP minerals during decompression exhumation (e.g., Vallis and Scambelluri, 1996; Zheng et al., 1999; Li et al., 2004). A study of fluid inclusions in rutile from UHP eclogites gave a narrow range of homogenization temperatures but a wide range of salinities for aqueous inclusions that were trapped during the exhumation (Ni et al., 2008). This suggests mixing of two fluids, with the high salinity one from the decomposition of hydrous minerals but low salinity one from the exsolution of structural hydroxyl and molecular water.

5. Element mobility in deeply subducted continental crustal rocks

By comparing the composition of HP metamorphic rocks to their protoliths, a number of studies indicate considerable removal of LILE and/or LREE from metabasites during subduction of the oceanic crust to eclogite-facies conditions (e.g., Becker et al., 2000; Scambelluri et al., 2001; John et al., 2004). On the other hand, mafic rocks do not lose significant amounts of trace elements during HP metamorphism up to eclogite-facies (e.g., Chalot-Prat et al., 2003; Spandler et al., 2004; Volkova et al., 2004). This implies the decoupling between dehydration and trace element loss during prograde HP metamorphism. Therefore, it has been intriguing how elements are liberated from subducting crusts. This principally concerns the degree and mechanism of element transport with respect to open or closed systems during prograde HP-UHP metamorphism in oceanic subduction zones. It is possible that the subducting slab does not release abundant fluid until a major dehydration reaction like antigorite breakdown (Ulmer and Trommsdorff, 1995; Schmidt and Poli, 1998; Scambelluri and Philippot, 2001), and thus rocks behave as relatively closed systems up to HP-UHP conditions (Spandler et al., 2004). After that, the fluid moves and enhances element mobility and melting or supercritical fluid production in other rock reservoirs like mafic or pelitic rocks. Because the high solubility of trace elements occurs in hydrous melts and supercritical fluids (Kessel et al., 2005; Hermann et al., 2006), their formation or not during subduction-zone metamorphism may play a critical role in dictating the coupling or decoupling of dehydration and trace element loss (Zhao et al., 2007; Xia et al., 2008).

SHRIMP U-Pb dating on different types of zircons from UHP metamorphic rocks indicates that zircon growth is dictated by episodic activity of metamorphic fluid during subduction and exhumation of the continental crust (Li et al., 2004; Wu et al., 2006; Zhao et al., 2006; Zheng et al., 2007b), suggesting Zr and Si mobility at mantle depths in subduction zones. Furthermore, omphacite, garnet, paragonite, kyanite, rutile and zircon is present in UHP kyanite-quartz vein within eclogite (Li et al., 2004; Zheng et al., 2007b; Wu et al., 2009), indicating relative enrichment of Na, Si, Al, HFSE and HREE in metamorphic fluid. The high solubilities of Al, HFSE and HREE are required to precipitate sufficient amounts of garnet, kyanite, rutile and zircon from the fluid as a response to changes in temperature, pressure or chemical potential. It can only be achieved by a substantial extent of Al-Si complexing with relative enrichment of HFSE and HREE in the supercritical aqueous fluid (Wu et al., 2009; Zheng, 2009b).

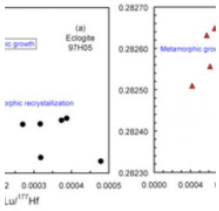

Figure 6

Zheng et al. (2005) made a combined in-situ study of U-Pb and Lu-Hf isotopes in zircon from UHP eclogite and granitic gneiss, leading to the first finding of decreased $^{176}Lu/^{177}Hf$ ratios but increased $^{176}Hf/^{177}Hf$ isotope ratios for metamorphic growth (Fig. 6). This finding has been confirmed by later studies (Wu et al., 2006; Liu et al., 2008), suggesting chemical exchange between zircon-grown medium and HREE-rich garnet. With the advance of combined LA-MC-ICPMS and LA-ICPMS techniques, simultaneous in-situ analyses of trace elements, U-Th-Pb and Lu-Hf isotopes can be made in the same volume of a single zircon (Yuan et al., 2008; Xie et al., 2008). This provides insights into metamorphic zirconology with implications for fluid action on the recrystallization and growth of zircon during subduction-zone metamorphism. As a consequence, metamorphic recrystallization is subdivided into three mechanisms of solid-state transformation, replacement alteration and dissolution reprecipitation, and the metamorphic growth into new precipitation from aqueous fluid or hydrous melt (Xia et al., 2009, 2010; Chen et al., 2010).

From geochemical analyses of mid-T/UHP eclogite and granitic gneiss from core samples of the CCSD main hole, Zhao et al. (2007) found large variations in the abundance of elements like SiO_2, LREE and LILE at the contact between eclogite and granitic gneiss, indicating their mobility between different slice components. On the other hand, Tang et al. (2007) observed high LILE mobility but REE and HFSE immobility within UHP eclogites in which trace element distribution equilibrium is approached between garnet and clinopyroxene. It is known that the supercritical fluid attending the UHP conditions mainly comprises SiO_2 + Al_2O_3 + CaO +MgO +FeO +Na_2O + H_2O, and is enriched in LREE, HFSE, P, V, Sr, Ba and Pb (Zhang et al., 2008). From a comprehensive study of metamorphic zirconology, Xia et al. (2010) suggested that a supercritical fluid transported LREE, HREE, Th, U and HFSE in accessory minerals to recrystallized zircons during subduction-zone metamorphism.

Variable extents of fluid/melt metasomatism are evident at contacts between contrasting lithological units (e.g., Malaspina et al., 2006a, b; Zhao et al., 2007). This is particularly so for some UHP peridotites, in which melt-peridotite reactions at UHP conditions represent an analogue to crust-mantle interaction in continental subduction zones. However, there is no documentation that these orogenic peridotites belong to the mantle wedge above the subducted continental slab. In other words, it is only assumed to be the mantle wedge without any demonstration of its origin (e.g., Zheng et al., 2008; Zhang et al., 2009b). Available Re-Os isotope data argue against the assumption of mantle wedge for the peridotites (Yuan et al., 2007; Zheng et al., 2009b). In this regard, the observed metasomatism in the UHP peridotites has nothing to do with not only the crust-mantle interaction but also fluid mobility and output from the continental slab.

6. Concluding remarks

The plate tectonics theory, which has influenced nearly all branches of the earth sciences, has its roots in the great upsurge of research on the oceanic crust and its deep subduction. By introducing the basic idea that the oceanic crust is recycled from the Earth's surface into the mantle, Armstrong (1968) first recognized the very important implications of geochemical recycling for crust and mantle evolution. Chemical geodynamics, firstly proposed by Allegre (1982) and further propogated by Zindler and Hart (1986), is primarily a field focusing on mantle geochemistry. Now it has been developed as an integrated study of the chemical structure and tectonic evolution of geospheres, extending from geochemical recycling in oceanic subduction zones to HP and UHP metamorphic reworking in both oceanic and continental subduction zones (Bebout, 2007; Zheng et al., 2009a). This enables to trace the possible contribution of deeply subducted continental crust to mantle geochemical heterogeneity.

Through independent and cooperative research efforts, Chinese geochemists have contributed to elucidate of many important problems by seeking answers to questions such as: (1) which geochemical processes occur during subduction and exhumation of the continental crust? (2) how can geochemical records be used to distinguish in-situ from exotic UHP rocks with respect to the enclosing country rocks? (3) what kind of crust-mantle interaction takes place when continental slices are subducted to mantle depths? (4) how does the dehydration of UHP metamorphic minerals during exhumation provide internally-derived fluid for metamorphic veining and amphibolite-facies retrogression? (5) how does the

dehydration melting of UHP metamorphic rocks during exhumation produce varying degrees of migmatization and even K-rich magmatism? (6) which mechanism and rate of ascent prevent UHP mineral assemblages from being completely obliterated by metamorphic overprinting and partial melting during exhumation? (7) how can we recognize and distinguish post-collisional melting products with contrasting sources between the subducted and obducted continental lithospheres? (8) how can we quantify element mobility via aqueous fluid, hydrous melt and supercritical fluid during the continental subduction-zone metamorphism? As a consequence, contributions from the Chinese geochemical community have greatly facilitated the understanding of geodynamic processes attending the overall evolution of convergent plate margins: from oceanic crust subduction to continental collision (Zheng et al., 2009c).

Acknowledgments

This study was supported by funds from the Chinese Ministry of Science and Technology (2009CB825004) and the Natural Science Foundation of China (40921002). Thanks are due to Gray E. Bebout and Marco Scambelluri for their comments that helped improvement of the presentation.

References

Allegre C.J. (1982) Chemical geodynamics. *Tectonophysics* **81**, 109-132.

Amstrong R.L. (1968) A model for Sr and Pb isotope evolution in a dynamic Earth. *Rev. Geophys.* **6**, 175-199.

Bebout G.E. (2007) Metamorphic chemical geodynamics of subduction zones. *Earth Planet. Sci. Lett.* **260**, 373-393.

Becker H., Jochum K.P. and Carlson R.W. (2000) Trace element fractionation during dehydration of eclogites from high-pressure terranes and the implications for element fluxes in subduction zones. *Chem. Geol.* **163**, 65-99.

Chalot-Prat F., Ganne J. and Lombard A. (2003) No significant element transfer from the oceanic plate to the mantle wedge during subduction and exhumation of the Tethys lithosphere (Western Alps). *Lithos* **69**, 69-103.

Carswell D.A. and Compagnoni R. (2003) *Ultrahigh Pressure Metamorphism*. European Mineralogical Union Notes in Mineralogy, vol. 5, 508 pp.

Chen R.-X., Zheng Y.-F., Gong B., Zhao Z.-F., Gao T.-S., Chen B. and Wu Y.-B. (2007a) Origin of retrograde fluid in ultrahigh-pressure metamorphic rocks: constraints from mineral hydrogen isotope and water content changes in eclogite-gneiss transitions in the Sulu orogen. *Geochim. Cosmochim. Acta* **71**, 2299-2325

Chen R.-X., Zheng Y.-F., Gong B., Zhao Z.-F., Gao T.-S., Chen B. and Wu Y.-B. (2007b) Oxygen isotope geochemistry of ultrahigh-pressure metamorphic rocks from 200-4000 m core samples of the Chinese Continental Scientific Drilling. *Chem. Geol.* **242**, 51-75.

Chen R.-X., Zheng Y.-F. and Xie L.W. (2010) Metamorphic growth and recrystallization of zircon: distinction by simultaneous in-situ analyses of trace elements, U-Th-Pb and Lu-Hf isotopes in zircons from eclogite-facies rocks in the Sulu orogen. *Lithos* **114**, 132-154.

Chopin C. (1984) Coesite and pure pyrope in high-grade blueschists of the western Alps: a first record and some consequence. *Contrib. Mineral. Petrol.* **86**, 107-118.

Chopin C. (2003) Ultrahigh-pressure metamorphism; tracing continental crust into the mantle. *Earth Planet. Sci. Lett.* **212**, 1-14.

Cong B.L. (1996) *Ultrahigh-Pressure Metamorphic Rocks in the Dabieshan-Sulu Region of China*. Science Press, Beijing, 224 pp.

Enami M. and Zang Q. (1990) Quartz pseudomorph after coesite in eclogites from Shandong Province, east China. Am. Mineral. **75**, 381-386.

Ernst W.G. and Liou J.G. (2008) High- and ultrahigh-pressure metamorphism: Past results and future prospects. *Am. Mineral.* **93**, 1771-1786.

Fu B., Zheng Y.-F., Wang Z.-R., Xiao Y.-L., Gong B. and Li S.G. (1999) Oxygen and hydrogen isotope geochemistry of gneisses associated with ultrahigh pressure eclogites at Shuanghe in the Dabie Mountains. *Contrib. Mineral. Petrol.* **134**, 52-66.

Fu B., Touret J.L.R. and Zheng Y.-F. (2001) Fluid inclusions in coesite-bearing eclogites and jadeite quartzites at Shuanghe, Dabie Shan, China. *J. Metamorph. Geol.* **19**, 529-545.

Gong B., Zheng Y.-F. and Chen R.-X. (2007a) A TCEA-MS online method for determination of hydrogen isotope composition and water concentration in geological samples. *Rapid Commun. Mass Spectrom.* **21**, 1386-1392.

Gong B., Zheng Y.-F. and Chen R.-X. (2007b) TC/EA-MS online determination of hydrogen isotope composition and water concentration in eclogitic garnet. *Phys. Chem. Minerals* **34**, 687-698.

Guiraud M., Powell R. and Rebay G. (2001) H_2O in metamorphism and unexpected behaviour in the preservation of metamorphic mineral assemblages. *J. Metamorph. Geol.* **19**, 445-454.

Hacker B.R., Ratschbacher L., Webb L., Ireland T., Walker D. and Dong S. (1998) U/Pb zircon ages constrain the architecture of the ultrahigh-pressure Qinling-Dabie orogen, China. *Earth Planet. Sci. Lett.* **161**, 215-230.

Hacker B.R., Ratschbacher L., Webb L., McWilliams M.O., Ireland T., Calvert A., Dong S., Wenk H.-R. and Chateigner D. (2000) Exhumation of ultrahigh-pressure continental crust in east central China: Late Triassic-Early Jurassic tectonic unroofing. *J. Geophys. Res.* **B105**, 13339-13364.

Hacker B.R., Wallis S.R., Ratschbacher L., Grove M. and Gehrels G. (2006) High-temperature geochronology constraints on the tectonic history and architecture of the ultrahigh-pressure Dabie-Sulu orogen. *Tectonics* **25**, TC5006, doi: 10.1029/ 2005TC001937.

Hermann J., Spandler C., Hack A. and Korsakov A.V. (2006) Aqueous fluids and hydrous melts in high-pressure and ultra-high pressure rocks: Implications for element transfer in subduction zones. *Lithos* **92**, 399-417.

Jahn B.-m., Cornichet J., Cong B.L. and Yui T.-F. (1996) Ultrahigh-ε_{Nd} eclogites from an ultrahigh-pressure metamorphic terrane of China. *Chem. Geol.* **127**, 61-79.

Jahn B.-m., Rumble D. and Liou J.G. (2003) Geochemistry and isotope tracer study of UHP metamorphic rocks. *European Mineralogical Union Notes in Mineralogy* **5**, 365-414.

Jarrard R.D. (2003) Subduction fluxes of water, carbon dioxide, chlorine, and potassium. Geochemistry Geophysics Geosystems 4, 8905, doi:10.1029/2002GC000392.

John T., Scherer E.E., Haase K. and Schenk V. (2004) Trace element fractionation during fluid-induced eclogitization in a subducting slab: trace element and Lu-Hf-Sm-Nd isotope systematics. *Earth Planet.*

Sci. Lett. **227**, 441-456.

Kessel R., Schmidt M.W., Ulmer P. and Pettke T. (2005) Trace element signature of subduction-zone fluids, melts and supercritical liquids at 120-180 km depth. *Nature* **437**, 724-727.

Li S.G., Xiao Y.L., Liu D.L., Chen Y.Z., Ge N.J., Zhang Z.Q., Sun S.-s., Cong B.L., Zhang R.Y., Hart S.R. and Wang S.S. (1993) Collision of the North China and Yangtse Blocks and formation of coesite-bearing eclogites: Timing and processes. *Chem. Geol.* **109**, 89-111.

Li S.G., Wang S.S., Chen Y.Z., Liu D.L., Qiu J., Zhou H.X. and Zhang Z.M. (1994) Excess argon in phengite from eclogite: Evidence from dating of eclogite minerals by Sm-Nd, Rb-Sr and $^{40}Ar/^{39}Ar$ methods. *Chem. Geol.* **112**, 343-350.

Li S.G., Jagoutz E., Lo C.-H., Chen Y.Z., Li Q.L. and Xiao Y.L. (1999) Sm/Nd, Rb/Sr, and $^{40}Ar/^{39}Ar$ isotopic systematics of the ultrahigh-pressure metamorphic rocks in the Dabie-Sulu belt, Central China: A retrospective view. *Intern. Geol. Rev.* **41**, 1114-1124.

Li S.G., Jagoutz E., Chen Y.Z. and Li Q.L. (2000) Sm-Nd and Rb-Sr isotopic chronology and cooling history of ultrahigh pressure metamorphic rocks and their country rocks at Shuanghe in the Dabie Mountains, Central China. *Geochim. Cosmochim. Acta* **64**, 1077-1093.

Li X.-P., Zheng Y.-F., Wu Y.-B., Chen F.K., Gong B. and Li Y.-L. (2004) Low-T eclogite in the Dabie terrane of China: Petrological and isotopic constraints on fluid activity and radiometric dating. *Contrib. Mineral. Petrol.* **148**, 443-470.

Li Q.L., Li S.G., Hou Z.H., Hong J.A. and Yang W. (2005) A combined study of SHRIMP U-Pb dating, trace element and mineral inclusions on high-pressure metamorphic overgrowth zircon in eclogite from Qinglongshan in the Sulu terrane. *Chinese Sci. Bull.* **50**, 5459-5465.

Liu L., Sun Y., Xiao P.X., Che Z.C., Luo J.H., Chen D.L., Wang Y., Zhang A.D., Chen L. and Wang Y.H. (2002) Discovery of ultrahigh-pressure magnesite-bearing garnet iherzolite (>3.8 GPa) in the Altyn Tagh, Northwest China. *Chinese Sci. Bull.* **47**, 881-886.

Liu F.L. and Xu Z.Q. (2004) Fluid inclusions hidden in coesite-bearing zircons in ultrahigh-pressure metamorphic rocks from southwestern Sulu terrane in eastern China. *Chinese Sci. Bull.* **49**, 396-404.

Liu F.L., Xu Z.Q. and Xue H.M. (2004a) Tracing the protolith, UHP metamorphism, and exhumation ages of orthogneiss from the SW Sulu terrane (eastern China): SHRIMP U-Pb dating of mineral inclusion-bearing zircons. *Lithos* **78**, 411-429.

Liu F.L., Xu Z.Q., Liou J.G. and Song B. (2004b) SHRIMP U-Pb ages of ultrahigh-pressure and retrograde metamorphism of gneisses, south-western Sulu terrane, eastern China. *J. Metamorph. Geol.* **22**, 315-326.

Liu F.L., Gerdes A., Liou J.G., Xue H.M. and Liang F.H. (2006a) SHRIMP U-Pb zircon dating from Sulu-Dabie dolomitic marble, eastern China: constraints on prograde, ultrahigh-pressure and retrograde metamorphic ages. *J. Metamorph. Geol.* **24**, 569-589.

Liu D.Y., Jian P., Kröner A. and Xu S.T. (2006b) Dating of prograde metamorphic events deciphered from episodic zircon growth in rocks of the Dabie-Sulu UHP complex, China. *Earth Planet. Sci. Lett.* **250**, 650-666.

Liu X.W., Jin Z.M. and Green II H.W. (2007a) Clinoenstatite exsolution in diopsidic augite of Dabieshan: Garnet peridotite from depth of 300 km. *Am. Mineral.* **92**, 546-552.

Liu L., Zhang J.F., Green II H.W. Jin Z.M. and Bozhilov K.N. (2007b) Evidence of former stishovite in metamorphosed sediments, implying subduction to > 350 km. *Earth Planet. Sci. Lett.* **263**, 180-191.

Liu F.L., Gerdes A., Zeng L.S. and Xue H.M. (2008) SHRIMP U-Pb dating, trace element and Lu-Hf isotope system of coesite-bearing zircon from amphibolite in SW Sulu UHP terrane, eastern China. *Geochim. Cosmochim. Acta* **72**, 2973-3000.

Malaspina N., Hermann J., Scambelluri M. and Compagnoni R. (2006a) Polyphase inclusions in garnet-orthopyroxenite (Dabie Shan, China) as monitors for metasomatism and fluid-related trace element transfer in subduction zone peridotite. *Earth Planet. Sci. Lett.* **249**, 173-187.

Malaspina N., Hermann J., Scambelluri M. and Compagnoni R. (2006b) Multistage metasomatism in ultrahigh-pressure mafic rocks from the North Dabie Complex (China). *Lithos* **90**, 19-42.

Meng D.W., Wu X.L., Fan X.Y., Meng X., Zheng J.P. and Mason R. (2009) Submicron-sized fluid inclusions and distribution of hydrous components in jadeite, quartz and symplectite-forming minerals from UHP jadeite-quartzite in the Dabie Mountains, China: TEM and FTIR investigation. *Applied Geochem.* **24**, 517-526

Ni P., Zhu X., Wang R.C., Shen K., Zhang Z.M., Qiu J.S. and Huang J.P. (2008) Constraining ultrahigh-pressure (UHP) metamorphism and titanium ore formation from an infrared microthermometric study of fluid inclusions in rutile from Donghai UHP eclogites, eastern China. *Geol. Soc. Am. Bull.* **120**, 1296-1304.

Okay A.I., Xu S.T. and Sengor A.M.C. (1989) Coesite from the Dabie Shan eclogites, central China. *Eur. J. Mineral.* **1**, 595-598.

Peacock S.M. (1990) Fluid processes in subduction zones. *Science* **248**, 329-337.

Proyer A. (2003) The preservation of high-pressure rocks during exhumation: metagranites and metapelites. *Lithos* **70**, 183-194.

Rumble D. and Yui T.-F. (1998) The Qinglongshan oxygen and hydrogen isotope anomaly near Donghai in Jiangsu province, China. *Geochim. Cosmochim. Acta* **62**, 3307-3321.

Rumble D., Wang Q.C. and Zhang R.Y. (2000) Stable isotope geochemistry of marbles from the coesite UHP terrains of Dabieshan and Sulu, China. *Lithos* **52**, 79-95.

Rumble D., Liou J.G and Jahn B.-m. (2003) Continental crust subduction and ultrahigh pressure metamorphism. *Treatise on Geochemistry* **3**, 293-319.

Scambelluri M. and Philippot P. (2001) Deep fluids in subduction zones. *Lithos* **55**, 213-227 .

Scambelluri M., Bottazzi P., Trommsdirff V., Vannucci R., Hermann J., Gomez-Pugnaire M.T. and Vizcaino V.L.-S. (2001) Incompatible element-rich fluids released by antigorite breakdown in deeply subducted mantle. *Earth Planet. Sci. Lett.* **192**, 457-470.

Schmidt M.W. and Poli S. (1998) Experimentally based water budgets for dehydrating slabs and consequences for arc magma generation. *Earth Planet. Sci. Lett.* **163**, 361-379.

Sheng Y.M., Xia Q.K., Yang X.Z., Hao Y.T. (2007) H_2O contents and D/H ratios of nominally anhydrous minerals from ultrahigh-pressure eclogites of the Dabie orogen, eastern China. *Geochim. Cosmochim. Acta* **71**, 2079-2103.

Smith D.C. (1984) Coesite in clinopyroxene in the Caledonides and its implications for geodynamics. *Nature* **310**, 641-644.

Nature **310**, 641-644.

Sobolev N.V. and Shatsky V.S. (1990) Diamond inclusions in garnets from metamorphic rocks; a new environment of diamond formation. *Nature* **343**, 742-746.

Song S.G., Zhang L.F., Chen J., Liou J.G. and Niu Y.L. (2005) Sodic amphibole exsolutions in garnet from garnet-peridotite, North Qaidam UHPM belt, NW China; implications for ultradeep-origin and hydroxyl defects in mantle garnets. *Am. Mineral.* **90**, 814-820.

Spandler C., Hermann J., Arculus R. and Mavrogenes J. (2004) Geochemical heterogeneity and element mobility in deeply subducted oceanic crust: insights from high-pressure mafic rocks from New Caledonia. *Chem. Geol.* **206**, 21-42.

Su W., You Z.D. and Cong B.L. (2002) Cluster of water molecules in garnet from ultrahigh-pressure eclogite. *Geology* **30**, 611-614.

Tang H.-F., Liu C.-Q., Nakai S.-i. and Orihashi Y. (2007) Geochemistry of eclogites from the Dabie-Sulu terrane, eastern China: New insights into protoliths and trace element behavior during UHP metamorphism. *Lithos* **95**, 441-457.

Tang J., Zheng Y.-F., Wu Y.-B., Gong B., Zha X.P. and Liu X.M. (2008a) Zircon U-Pb age and geochemical constraints on the tectonic affinity of the Jiaodong terrane in the Sulu orogen, China. *Precambr. Res.* **161**, 389-418.

Tang J., Zheng Y.-F., Gong B., Wu Y.-B., Gao T.-S., Yuan H.L. and Wu F.-Y. (2008b) Extreme oxygen isotope signature of meteoric water in magmatic zircon from metagranite in the Sulu orogen, China: implications for Neoproterozoic rift magmatism. *Geochim. Cosmochim. Acta* **72**, 3139-3169.

Ulmer P. and Trommsdorff V. (1995) Serpentine stability to mantle depths and subduction-related magmatism. *Science* **268**, 858-861.

Valley J.W., Lackey J.S., Cavosie A.J., Clechenko C.C., Spicuzza M.J., Basei M.A.S., Bindeman I.N., Ferreira V.P., Sial A.N., King E.M., Peck W.H., Sinha A.K. and Wei C.S. (2005) 4.4 billion years of crustal maturation: oxygen isotope ratios of magmatic zircon. *Contrib. Mineral. Petrol.* **150**, 561-580.

Vallis F. and Scambelluri M. (1996) Redistribution of high-pressure fluids during retrograde metamorphism of eclogite-facies (Voltri Massif, Italian Western Alps). *Lithos* **39**, 81-92.

Volkova N.I., Frenkel A.E., Budanov V.I. and Lepezin G.G. (2004) Geochemical signatures for eclogite protolith from the Maksyutov Complex, South Urals. *J. Asian Earth Sci.* **23**, 745-759.

Wan Y.S., Li R.W., Wilde S.A., Liu D.Y., Chen Z.Y., Yan L.L., Song T.R. and Yin X.Y. (2005) UHP metamorphism and exhumation of the Dabie Orogen, China: Evidence from SHRIMP dating of zircon and monazite from a UHP granitic gneiss cobble from the Hefei Basin. *Geochim. Cosmochim. Acta* **69**, 4333-4348.

Wang X.M., Liou J.G. and Mao H.K. (1989) Coesite-bearing from the Dabie Mountains in central China. *Geology* **17**, 1085-1088.

Wang X.M., Zhang R.Y. and Liou J.G. (1995) UHPM terrane in east central China. In: *Ultrahigh Pressure Metamorphism* (eds. Coleman R. and Wang X.M.). Cambridge University Press, Cambridge, p.356-390.

Wu X.L., Meng D.W. and Han Y.J. (2004) A TEM study on fluid inclusions in coesite-bearing jadeite quartzite in Shuanghe in the Dabie Mountains. *Acta Geol. Sin.* **78**, 121-124.

Wu Y.-B., Zheng Y.-F., Zhao Z.-F., Gong B., Liu X.M. and Wu F.-Y. (2006) U-Pb, Hf and O isotope evidence for two episodes of fluid-assisted zircon growth in marble-hosted eclogites from the Dabie orogen. *Geochim. Cosmochim. Acta* **70**, 3743-3761.

Wu Y.-B., Gao S., Zhang H.-F., Yang S. H., Liu X.-C., Jiao W.-F., Liu Y.-S., Yuan H.-L., Gong H.-J. and He M.C. (2009) U-Pb age, trace-element, and Hf-isotope compositions of zircon in a quartz vein from eclogite in the western Dabie Mountains: Constraints on fluid flow during early exhumation of ultra high-pressure rocks. *Am. Mineral.* **94**, 303-312.

Xia Q.-X., Zheng Y.-F. and Zhou L.-G. (2008) Dehydration and melting during continental collision: constraints from element and isotope geochemistry of low-T/UHP granitic gneiss in the Dabie orogen. *Chem. Geol.* **247**, 36-65.

Xia Q.-X., Zheng Y.-F., Yuan H.L. and Wu F.-Y. (2009) Contrasting Lu-Hf and U-Th-Pb isotope systematics between metamorphic growth and recrystallization of zircon from eclogite-facies metagranite in the Dabie orogen, China. *Lithos* **112**, 477-496.

Xia Q.-X., Zheng Y.-F. and Hu Z.-C. (2010) Trace elements in zircon and coexisting minerals from low-T/UHP metagranite in the Dabie orogen: implications for fluid regime during continental subduction-zone metamorphism. *Lithos* **114**, 385-413.

Xie Z., Zheng Y.-F., Jahn B.-m., Ballevre M., Chen J.F., Gautier P., Gao T.-S., Gong B. and Zhou J.-B. (2004) Sm-Nd and Rb-Sr dating for pyroxene-garnetite from North Dabie in east-central China: problem of isotope disequilibrium due to retrograde metamorphism. *Chem. Geol.* **206**, 137-158.

Xie L.-W., Zhang Y.-B., Zhang H.-H., Sun J.-F. and Wu F.-Y. (2008) In situ simultaneous determination of trace elements, U-Pb and Lu-Hf isotopes in zircon and baddeleyite. *Chinese Sci. Bull.* **53**, 1565-1573.

Xu S.T., Okay A.I., Ji S.Y., Sengor A.M.C., Su W., Liu Y.C. and Jiang L.L. (1992) Diamond from the Dabie Shan metamorphic rocks and its implication for tectonic setting. *Science* **256**, 80-82.

Xu Z.Q., Zeng L.S., Liu F.L., Yang J.S., Zhang Z.M., McWilliams M. and Liou J.G. (2006) Polyphase subduction and exhumation of the Sulu high-pressure-ultrahigh-pressure metamorphic terrane. *Geol. Soc. Am. Spec. Paper* **403**, 93-113.

Yang J.S., Xu Z.Q., Song S.G., Zhang X., Wu C., Shi R., Li H. and Brunel M. (2001) Discovery of coesite in the North Qaidam Early Paleozoic ultrahigh-pressure metamorphic belt, NW China. *C.R. Acad. Sci. Paris (Earth Planet. Sci.)* **333**, 719-724.

Yang J.S., Xu Z.Q., Dobrzhinetskaya L.F., Green II H.W., Pei X., Shi R., Wu C., Wooden J.L., Zhang J., Wan Y. and Li H. (2003) Discovery of metamorphic diamonds in Central China; an indication of a >4000 km-long-zone of deep subduction resulting from multiple continental collisions. *Terra Nova* **15**, 370-379.

Yardley B., Gleeson S., Bruce S. and Banks D. (2000) Origin of retrograde fluids in metamorphic rocks. *J. Geochem. Explor.* **69-70**, 281-285.

Ye K., Cong B.L. and Ye D.N. (2000) The possible subduction of continental material to depths greater than 200 km. *Nature* **407**, 734-736.

Yuan H.L., Gao S., Rudnick R.L., Jin Z.M., Liu Y.S., Puchtel I.S., Walker R.J. and Yu R.D. (2007) Re-Os evidence for the age and origin of peridotites from the Dabie-Sulu ultrahigh pressure metamorphic belt, China. *Chem. Geol.* **236**, 323-338.

Yuan H.L., Gao S., Dai M.N., Zong C.L., Günther D., Fontaine G.H., Liu X.M., Diwu C.R. (2008) Simultaneous determinations of U-Pb age, Hf isotopes and trace element compositions of zircon by excimer laser-ablation quadrupole and multiple-collector ICP-MS. *Chem. Geol.* **247**, 100-118.

Yui T.-F., Rumble D. and Lo C.-H. (1995) Unusually low $\delta^{18}O$ ultra-high-pressure metamorphic rocks from the Sulu Terrane, eastern China. *Geochim. Cosmochim. Acta* **59**, 2859-2864.

Zhang L.F., Ellis D.J. and Jiang W.B. (2002) Ultrahigh pressure metamorphism in western Tianshan, China, part I; evidences from the inclusion of coesite pseudomorphs in garnet and quartz exsolution lamellae in omphacite in eclogites. *Am. Mineral.* **87**, 853-860.

Zhang Z.M., Shen K., Sun W.D., Liu Y.S., Liou J.G, Shi C. and Wang J.L. (2008) Fluids in deeply subducted continental crust: petrology, mineral chemistry and fluid inclusion of UHP metamorphic veins from the Sulu orogen, eastern China. *Geochim. Cosmochim. Acta* **72**, 3200-3228.

Zhang R.Y., Liou J.G. and Ernst W.G. (2009a) The Dabie-Sulu continental collision zone: A comprehensive review. *Gondwana Res.* **16**, 1-26.

Zhang R.Y., Liou J.G., Zheng J.P., Griffin W.L., Yang Y.-H. and Jahn B.-m. (2009b) Petrogenesis of eclogites enclosed in mantle-derived peridotites from the Sulu UHP terrane: constraints from trace elements in minerals and Hf isotopes in zircon. *Lithos* **109**, 176-192.

Zhao Z.-F., Zheng Y.-F., Gao T.-S., Wu Y.-B., Chen B., Chen F.K. and Wu F.-Y. (2006) Isotopic constraints on age and duration of fluid-assisted high-pressure eclogite-facies recrystallization during exhumation of deeply subducted continental crust in the Sulu orogen. *J. Metamorph. Geol.* **24**, 687-702.

Zhao Z.-F., Zheng Y.-F., Chen R.-X., Xia Q.-X. and Wu Y.-B. (2007) Element mobility in mafic and felsic ultrahigh-pressure metamorphic rocks during continental collision. *Geochim. Cosmochim. Acta* **71**, 5244-5266.

Zheng Y.-F., Fu B., Gong B. and Li S.G. (1996) Extreme ^{18}O depletion in eclogite from the Su-Lu terrane in East China. *Eur. J. Mineral.* **8**, 317-323.

Zheng Y.-F., Fu B., Li Y.-L., Xiao Y.L. and Li S.G. (1998) Oxygen and hydrogen isotope geochemistry of ultrahigh-pressure eclogites from the Dabie Mountains and Sulu terrane. *Earth Planet. Sci. Lett.* **155**, 113-129.

Zheng Y.-F., Fu B., Xiao Y.L, Li Y.-L. and Gong B. (1999) Hydrogen and oxygen isotope evidence for fluid-rock interactions in the stages of pre- and post-UHP metamorphism in the Dabie Mountains. *Lithos* **46**, 677-693.

Zheng Y.-F., Wang Z.-R., Li S.G. and Zhao Z.-F. (2002) Oxygen isotope equilibrium between eclogite minerals and its constraint on mineral Sm-Nd chronometer. *Geochim. Cosmochim. Acta* **66**, 625-634.

Zheng Y.-F., Fu B., Gong B. and Li L. (2003a) Stable isotope geochemistry of ultrahigh pressure metamorphic rocks from the Dabie-Sulu orogen in China: implications for geodynamics and fluid regime. *Earth Sci. Rev.* **62**, 105-161.

Zheng Y.-F., Zhao Z.-F., Li S.G. and Gong B. (2003b) Oxygen isotope equilibrium ultrahigh-pressure metamorphic minerals and its constraints on Sm-Nd and Rb-Sr chronometers. *Geol. Soc. Spec. Publ.* **220**, 93-117.

Zheng Y.-F., Wu Y.-B., Chen F.K., Gong B., Li L. and Zhao Z.-F. (2004) Zircon U-Pb and oxygen isotope evidence for a large-scale ^{18}O depletion event in igneous rocks during the Neoproterozoic. *Geochim. Cosmochim. Acta* **68**, 4145-4165.

Zheng Y.-F., Wu Y.-B., Zhao Z.-F., Zhang S.-B., Xu P. and Wu F.-Y. (2005) Metamorphic effect on zircon Lu-Hf and U-Pb isotope systems in ultrahigh-pressure metagranite and metabasite. *Earth Planet Sci. Lett.* **240**, 378-400.

Zheng Y.-F., Wu Y.-B., Gong B., Chen R.-X, Tang J. and Zhao Z.-F. (2007a) Tectonic driving of Neoproterozoic glaciations: Evidence from extreme oxygen isotope signature of meteoric water in granite. *Earth Planet. Sci. Lett.* **256**, 196-210.

Zheng Y.-F., Gao T.-S., Wu Y.-B. and Gong B. (2007b) Fluid flow during exhumation of deeply subducted continental crust: Zircon U-Pb age and O isotope studies of quartz vein in eclogite. *J. Metamorph. Geol.* **25**, 267-283.

Zheng Y.-F. (2008) A perspective view on ultrahigh-pressure metamorphism and continental collision in the Dabie-Sulu orogenic belt. *Chinese Sci. Bull.* **53**, 3081-3104.

Zheng J.P., Sun M., Griffin W.L., Zhou M.F. and Zhao G.C. (2008) Age and geochemistry of contrasting peridotite types in the Dabie UHP belt, eastern China: petrogenetic and geodynamic implications. *Chem. Geol.* **247**, 282-304.

Zheng Y.-F. (2009a) 25 years of continental deep subduction. *Chinese Sci. Bull.* **54**, 4266-4270.

Zheng Y.-F. (2009b) Fluid regime in continental subduction zones: petrological insights from ultrahigh-pressure metamorphic rocks. *J. Geol. Soc.* **166**, 763-782.

Zheng Y.-F., Chen R.-X. and Zhao Z.-F. (2009a) Chemical geodynamics of continental subduction-zone metamorphism: Insights from studies of the Chinese Continental Scientific Drilling (CCSD) core samples. *Tectonophysics* **475**, 327-358.

Zheng L., Zhi X.C. and Reisberg L. (2009b) Re-Os systematics of the Raobazhai peridotite massifs from the Dabie orogenic zone, eastern China. *Chem. Geol.* **268**, 1-14.

Zheng Y.-F., Ye K. and Zhang L.F. (2009c) Developing the plate tectonics from oceanic subduction to continental collision. *Chinese Sci. Bull.* **54**, 2549-2555.

Zindler A. and Hart S.R. (1986) Chemical geodynamics. *Ann. Rev. Earth Planet. Sci.* **14**, 493-571.

Figure Captions

Figure 1. Frequency histogram of countries publishing the most cited 100 papers in ultrahigh pressure metamorphism and continental deep subduction (after Zheng, 2009a).

Figure 2. Histograms of SHRIMP U-Pb ages for zircon from UHP metamorphic rocks in the Dabie-Sulu orogenic belt (after Zheng et al., 2009a). (a) Dates for coesite-bearing domain of metamorphic zircons, and (b) dates for metamorphic zircons without corresponding identification of coesite inclusions in the dating domain.

Figure 3. Comparison of oxygen isotope compositions for the Dabie-Sulu UHP eclogites with the other eclogites in the world (revised after Zheng et al., 2003a).

Figure 4. Schematic diagram showing timescales of UHP/HP metamorphism in the Dabie-Sulu orogenic belt due to continental subduction to and exhumation from mantle depths (after Zheng, 2008).

Figure 5. The relationship between water concentration and hydrogen isotope composition of omphacite and garnet from UHP eclogite in the main hole of CCSD, the Sulu orogen (data after Chen et al., 2007a). The decrease in total water concentration is associated with the increase in δD values, pointing to the preferential loss of D-depleted molecular water during exhumation.

Figure 6. Zircon Lu-Hf isotopic relationship between metamorphic domains of different origins for UHP

Figure 8. Zircon Lu-Hf isotopic relationship between metamorphic domains of different origins for UHP eclogite and granitic gneiss from the Dabie orogen (revised after Zheng et al., 2005). While metamorphically grown zircon is characterized by decreased $^{176}Lu/^{177}Hf$ ratios but increased $^{176}Hf/^{177}Hf$ isotope ratios, metamorphically recrystallized zircon remains almost unchanged in both $^{176}Lu/^{177}Hf$ and $^{176}Hf/^{177}Hf$ isotope ratios.

Chemical composition of the continental crust: a perspective from China

Shan Gao[a,b,*]
[a] State Key Laboratory of Geological Processes and Mineral Resources, Faculty of Earth Sciences, China University of Geosciences, Wuhan, 430074, P.R. China
[b] State Key Laboratory of Continental Dynamics, Department of Geology, Northwest University, Xi'an, 710069, P.R. China
* corresponding author's email: sgao@263.net

Full Text (3.7 Mb PDF)

Abstract

The chemical composition of the continental crust is critically important for understanding its formation and evolution and, ultimately, understanding Earth differentiation. Here we provide a brief review of the chemical composition of the continental crust, with an emphasis on studies from China. The upper crustal composition reveals higher transition metal abundances compared to previous estimates that were based on results from the Canadian Shield. Inter-element correlations in clastic sedimentary rocks can be extended to many immobile as well as mobile elements. The significant correlations place constraints on the concentrations of the rarely analyzed elements (B, Be, Bi, Ge, In, Mo, Sb, Sn, Te, Tl, W) in the upper crust. Middle crustal compositional estimates based on sampling of amphibolite-facies rocks and seismic profiles yield a bulk composition with 62-69% SiO_2. The eastern China middle crust composition is more evolved and shows slightly slower compressional velocity than that of global middle crust. While there is a general consensus that the global lower continental crust is mafic in composition, eastern China is a remarkable exception to this generality with an intermediate bulk lower crust composition. The total crust composition of eastern China is also more evolved than the global model and characterized by a significant negative Eu anomaly. Delamination of the lower crust and its underlying lithospheric mantle are suggested to have played an important role in driving the continental crust to an evolved composition, loss of the Archean keel, and in producing the large volumes of intraplate magmatism in the North China Craton during the Mesozoic.

Keywords: Continental crust, chemical composition, seismic velocity, delamination, eastern China

1. Introduction

The composition of the continental crust is critically important for understanding its formation and evolution and ultimately, understanding Earth's differentiation, and for quantifying geodynamic processes within the Earth (e.g., Taylor and McLennan, 1995, 2009; Rudnick, 1995; Gao et al., 1998a; Rundick and Gao, 2003; Hawkesworth and Kemp, 2006a, b). It also provides baselines for assessing geochemical anomalies in exploration of ore deposits and environmental and agriculture investigations. For these reasons, determining the chemical composition of the continental crust has been an aim of geochemists since the first analyses of rocks were undertaken (Clarke, 1889).

The continental crust can be divided into upper, middle and lower layers and shows wide lithological and geochemical variations. The upper crust is readily accessible for direct sampling and its composition is reasonably well established for the major elements and many lithophile trace elements. In comparison, the composition of the deep (middle and lower) crust is less well established due to its general inaccessibility. Here we provide a brief review of the chemical composition of the continental crust, with an emphasis on studies from China. For detailed reviews of composition of the continental crust in the global context see Rudnick and Gao (2003) and Taylor and McLennan (2009).

2. The Upper Crust

Two approaches have generally been used to determine the composition of the upper continental crust (ref. Rudnick and Gao, 2003; Taylor and McLennan, 2009). One is to establish weighted averages of the compositions of rocks exposed at the surface by large-scale sampling campaigns. All major-element determinations of upper-crust composition rely upon this method. The other approach is to determine the average concentrations of insoluble elements in fine-grained clastic sediments and sedimentary rocks (e.g., shale, mudstone, graywacke, siltstone, loess, and tillite) and use these to infer the average composition of their source regions.

2.1 Weighted Averages of Exposed Crust

The Canadian Shield represents the first area in which large-scale sampling of the crust was undertaken for both major and trace element analyses (Shaw et al., 1967, 1976, 1986; Eade and Fahrig, 1971, 1973). More recently, two campaigns of systematic large-scale sampling and rock analyses were undertaken in eastern China in the 1980's and 1990's for the purpose of studying the chemical composition of the continental crust. The first was carried out in the Qinling orogen and the adjacent regions of the North China Craton and Yangtze Craton. The sampling covered an area of 153,200 km^2 and comprised over 4500 individual rock samples that represented all of the Late Archean to Neogene stratigraphic units, the 2/3 of the exposed granitoids, as well as all of the major mafic-ultramafic intrusions in the study area. These individual rocks were analyzed for thirteen major and thirty trace and rare earth elements. The results were used, in conjunction with seismic velocities of the deep crust and surface heat flow, to estimate the composition of the upper, deep and total crust of the Qingling region (Gao et al., 1992; Zhang et al., 1994).

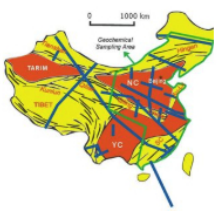

Figure 1

A second round of large-scale sampling was conducted over most of eastern China, covering a total area of ca 3,300,000 km^2 (Fig. 1) (Yan et al., 1997; Yan and Chi, 1997; Gao et al., 1998b; Zhang et al., 2002). A total of 28,253 individual rocks were sampled, from which 2,718 composite samples were prepared based on age, lithology and tectonic units. Between sixty-three to seventy-six major and trace elements were analyzed by a variety of methods, including elements that are rarely analyzed (e.g., Ag, As, Bi, Br, Cd, Cl, F, Ge, Hg, I, In, Mo, PGE, Te, Se, W) (Yan et al., 1997; Yan and Chi, 1997; Gao et al., 1998b; Zhang et al., 2002).

These studies revealed higher transition metal abundances of the upper crust compared to previous estimates that were based on results from the Canadian Shield studies (Shaw et al., 1967, 1976, 1986; Eade and

Shan Gao

About the Author

Shan Gao is a professor of geochemistry at China University of Geosciences (Wuhan) and an adjunct professor at Northwest University. He obtained a Ph.D. at China University of Geosciences (Wuhan) in 1989. His research interests are concerned with composition, formation and evolution of the continental crust and crust-mantle interactions as well as application of LA-ICP-MS to determine elemental and isotopic compositions of minerals. His current research focuses on tracing recycling of the lower continental crust in the mantle. He was elected Fellow of the Royal Society of Chemistry (UK) in 2009. He serves as a regional associate editor for *Journal of Analytical Atomic Spectrometry*, a member of editorial board for *Chemical Geology*, and a member of advisory board for *Earth and Planetary Science Letters*.

Fahrig, 1971, 1973; Taylor and McLennan, 1985; Wedepohl, 1995). A higher transition metal content of the upper crust has been supported by subsequent studies of fine-grained clastic sedimentary rocks (Condie, 1993; Plank and Langmuir, 1998; McLennan, 2001; Hu and Gao, 2008; Taylor and McLennan, 2009). The discrepancies between the Canadian Shield and eastern China studies were ascribed to differential erosion. The present-day surface of the Canadian Shield is dominated by amphibolite-facies granitoid gneisses, which are more typical of middle crust than upper crust. The uppermost crust of Archean regions typically contains more mafic volcanic rocks (Gao et al., 1998b). By contrast, unmetamorphosed to greenschist-facies rocks are well preserved in eastern China.

The influence of erosion on the upper crust composition was also demonstrated by Condie (1993), who added a 10 km thick layer of upper crust in Precambrian areas and a 5 km thick layer of upper crust in Phanerozoic areas to the present upper crust layer. This restoration model for the upper continental crust composition shows a remarkably good agreement with the eastern China upper crust composition in terms of Nb, Rb, Th, Zr, Co, Sc, and V, as well as K_2O concentrations. Although the Cr and Ni abundances of the restoration model are significantly greater than the eastern China estimates, the difference is small compared to estimates based on the Canadian Shield. We conclude that eastern China surface samples are a good representation of the average upper continental crust (Gao et al., 1992, 1998b).

Another important observation from eastern China is that various thicknesses of sedimentary cover, including carbonate, are an important component of the upper continental crust. Because carbonate and silicate rocks vary greatly in their chemical compositions and since the sedimentary cover in eastern China contains a significantly higher carbonate proportion with a carbonate/(pelite+sandstone) ratio of 0.31-2.23 compared to the global ratio of 0.18 (Taylor and McLennan, 1985), the upper crust compositions with and without carbonate are distinct in major elements (e.g., 58.5 vs 65.5% for SiO2 and 7.41 vs 3.31 for CaO) (Gao et al., 1998b). However, because carbonates have low abundances of trace elements, excepting Sr, the two estimates of the upper crust do not vary in relative trace element abundances (Yan et al., 1997; Gao et al., 1998b). The major element compositions without carbonate are also similar to previous estimates (Gao et al., 1998b).

In addition, trace elements associated with mineralization (e.g., B, Cl, Se, As, Bi, Pd, W, Th, Cs, Ta, Tl, Hg, Au, and Pb) show considerable inter-unit variability (by a factor of 2-5) in the upper crust (Gao et al., 1998b).

2.2 Fine-Grained Sedimentary Rocks

Estimates of the upper crustal composition from fine-grained clastic sedimentary rocks were applied by Taylor and McLennan (1985) to trace elements that are immobile during water-rock interaction and are not hosted in accessory minerals and, thus, are little fractioned during sedimentary processing and diagenesis. Such elements include REE, Y, Th, and Sc. The more mobile elements, such as K, U and Rb, can be estimated from assumed Th/U, K/U and K/Rb ratios (Taylor and McLennan, 1985). The fine-grained sediment approach has more recently been extended to elements such as Nb, Ta, Cs and transition metals (Cr, Ni, V, Co and Ti) (McDonough et al., 1992; Plank and Langmuir, 1998; Barth et al., 2000; McLennan, 2001).

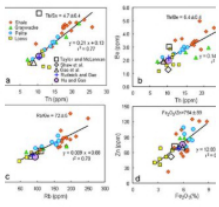

Figure 2

In a recent study, Hu and Gao (2008) analyzed 48 trace elements by ICP-MS (including the rarely analyzed elements As, B, Be, Bi, Cd, Ge, In, Mo, Sb, Sn, Te, Tl, W) in well-characterized upper crustal samples (shales, pelites, loess, graywackes, granitoids and their composites) from Australia, China, Europe, New Zealand and North American. The results reveal that inter-element correlations in clastic sedimentary rocks can be extended to many immobile as well as mobile elements (e.g., Ga-In, Th-Sn, Rb-Tl, Th-Tl, Rb-Be, Th-Be, Rb-Ge, Rb-W, Be-Bi, W-Bi, In-Li, B-Te, Fe-transition trace metals) (Fig. 2). The significant (r^2>0.6) correlations observed in clastic sediments and sedimentary rocks provide narrowly constrained upper continental crust elemental ratios, which can be used with abundances for certain key elements to place constraints on the concentrations of these rarely analyzed elements in the upper crust. Using the well-established upper crustal abundances of La (31 ppm), Th (10.5 ppm), Al_2O_3 (15.40%), K_2O (2.80%) and Fe_2O_3 (5.92%), these correlations lead to revised upper crustal abundances for B=47 ppm, Li=41 ppm, Cr=73 ppm, Ni=34 ppm, Sb=0.075, Te=0.027 ppm, W=1.4 ppm. Tl=0.53 ppm and Bi=0.23 ppm. No significant correlations exist between Mo and Cd and other elements in the clastic sediments and sedimentary rocks, probably due to their enrichment in organic carbon. If we assume that these two incompatible elements behave more or less like REE and Th, their abundances can be calculated by assuming the upper continental crust consists of 65% granitoid rocks plus 35% clastic sedimentary rocks. The validity of this bulk average approach for incompatible elements is supported by the similarity of SiO_2, Al_2O_3, La and Th abundances calculated in this way with their upper crustal abundances given in Rudnick and Gao (2003). The upper crustal abundances thus obtained are Mo=0.6 ppm and Cd=0.06 ppm. The data also suggest a ~20% increase of the Tm, Yb and Lu abundances reported in Rudnick and Gao (2003).

In summary, studies of surface samples from eastern China and clastic sediments establish significantly higher upper crustal abundances of transition metals compared to those based on surface samples from the Canadian Shield. The upper crustal compositions of the major elements and a majority of trace elements, as well as some key elemental ratios are well established. Such estimates can form basis of mass balance calculations for the Earth and provide geodynamic insights (e.g., Rudnick et al., 2000). However, the upper crustal abundances of some elements, notably platinum group elements, noble gases and the halogens are still highly uncertain.

3. The Deep Crust

Major uncertainties in the composition of the continental crust lie in the deep continental crust and particularly the lower crust, as it is far less accessible than the upper crust. Four approaches have been used to infer its composition (ref. Rudnick and Gao, 2003): (1) analyses of high-grade metamorphic (amphibolite or granulite facies) terrains and exposed crustal cross-sections in particular; (2) studies of granulite-facies xenoliths entrained in fast-rising magmas; (3) correlation of measured seismic velocities of deep crustal rocks with seismic profiles of the crust; and (4) surface heat flow measurements.

Studies of exposed crustal cross-sections and xenoliths indicate that, although exceptions exist, the middle crust is dominated by rocks metamorphosed at amphibolite-facies to lower granulite facies, while the lower crust consists mainly of granulite-facies rocks (Rudnick and Gao, 2003 and references therein). Exposed amphibolite- to granulite-facies terrains and middle crustal cross-sections show that, although they contain a wide variety of lithologies, including metasedimentary rocks, they are dominated by igneous and metamorphic rocks of the diorite-tonalite-trondhjemite-granodiorite (DTTG) and granite suites. This is true not only for Precambrian shields, but also for Phanerozoic crust and continental arcs. Such rock associations are consistent with the average middle crustal P-wave velocities of 6.4-6.5 km s^{-1} seen in all the tectonic settings except for active rifts and some intra-oceanic island arcs, which have higher average velocities suggesting a more mafic composition (Rudnick and Fountain, 1995).

Middle crust compositional estimates based on sampling of amphibolite-facies rocks and seismic profiles yield a bulk composition with 62-69% SiO_2. Trace element composition of the middle crust is poorly constrained, as systematic trace element studies of amphibolite-facies rocks are few. Nevertheless, the estimates of Rudnick and Fountain (1995) based on lithologies derived from seismic velocities and Gao et al. (1998b) based on eastern China surface sampling show a broadly similar composition in both major and trace elements, although the eastern China middle crust composition is more evolved, having higher SiO_2, K_2O, Ba, Li, Zr, and LREE and LaN/YbN and lower total FeO, Sc, V, Cr and Co with a

significant negative Eu anomaly. These differences are expected based on the slightly higher compressional velocity of Rudnick and Fountain's global middle crust compared to that of eastern China (6.6 vs. 6.4 km s^{-1}: Gao et al., 1998a, b). The consistency is surprising, considering that the two estimates are based on different sample sets and different approaches, one global and the other regional (Rudnick and Gao, 2003).

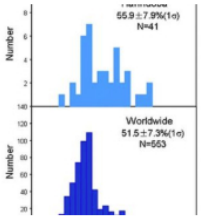

Figure 3

Like the middle crust, the lower crust also contains a wide variety of lithologies, as revealed by studies of granulite xenoliths, exposed high-pressure granulite terranes and crustal cross sections. Nevertheless, mafic rocks appear to dominate in the lower crust based on the relatively high seismic velocities, which are faster than 6.9 km s^{-1} (mostly ≥7.0 km s^{-1}) for various tectonic units (Rudnick and Fountain, 1995).

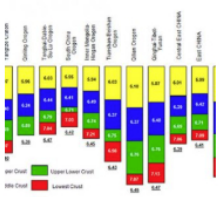
Figure 4

While there is a general consensus that the global lower continental crust is mafic in composition (ref. Rudnick and Fountain, 1995; Christensen and Mooney, 1995), Eastern China is a remarkable exception to this generality. Studies of exposed lower crustal cross-section and lower crustal granulite-facies xenoliths in eastern China indicate a bimodal lithological distribution in the lower crust, with felsic rocks being an important constituent, as exemplified by the Hannuoba granulite xenoliths, which have an average SiO_2 of 56% (Kern et al., 1995; Liu et al., 2001). This is unlike the worldwide compilations of lower crustal xenoliths, which are predominately mafic (Rudnick and Presper, 1990; Rudnick and Fountain, 1995) with an average SiO_2 of 51.5% (Fig. 3). This conclusion is supported by results of seismic profiling, which indicate a distinct two-layered structure to the lower crust for all of eastern China, except the Qingling orogen (Fig. 4). The upper lower crust has a mean velocity of 6.7 km s^{-1}, suggesting an evolved composition; only the lowermost crust has a mean velocity that is typical of mafic rocks (average velocity = 7.1 km s^{-1}) and is comparable to the global lower crust. The bulk lower crust of eastern China has a mean P-wave velocity of 6.82 km s^{-1} that is slower than the global average by 0.2-0.4 km s^{-1}, and is consistent with an intermediate bulk composition (Gao et al., 1998a, b). The slower velocity of the lower crust of eastern China is reinforced by recent compilations of seismic profiling in China (Li et al., 2006). We conclude that the evolved lower crust composition of eastern China is well established and is a remarkable feature exceptional to the global continental crust.

4. The total crust composition and its geodynamic implications

There is a general consensus that the bulk composition of the continental crust is andesitic. All estimates of the crust composition, including the pioneering work of Clarke (1889), have a total crustal SiO_2 that falls between 57.1-64.5% (Rudnick and Gao, 2003), regardless of the approaches and data sets that have been employed to derive these estimates. Moreover, all estimates show a continental crust that is characterized by enrichments in large-ion lithophile elements (e.g., Cs, Rb, Ba and, in particular, Pb) and depletions in high-field strength elements (Nb, Ta, Ti). These features are therefore considered robust and can be used to understand the formation and evolution of the continental crust.

The continental crust grows primarily by an igneous flux from the mantle, which in most cases should be basaltic. The demonstrably non-basaltic composition of the continental crust requires some form of crustal recycling through delamination, weathering and/or subduction (Rudnick, 1995).

Europium balance or imbalance in the continental crust may be useful for understanding the processes by which the crust evolved (e.g., Gao et al., 1998a; Hawkesworth and Kemp, 2006b). Mantle-derived additions to the crust would normally have no Eu anomaly. Intracrustal differentiation by granitic magmatism has led to a prominent negative Eu anomaly in the granitic upper crust (Eu/Eu^*=0.72; Rudnick and Gao, 2003), and should produce a restitic lower crust with a complementary positive Eu anomaly (Taylor and McLennan, 1985, 2009). However, if delamination of the dense mafic lower crust could occur, and if this crust contained cumulate or residual plagioclase, the total crust after delamination would evolve toward a felsic composition with a negative Eu anomaly. The total crust composition estimates of Rudnick and Gao (2003) has a weak negative Eu anomaly (Eu/Eu^*=0.93), which would accommodate some removal of plagioclase cumulates/restites, although given the uncertainties, there is no need to call upon plagioclase removal from the lower crust.

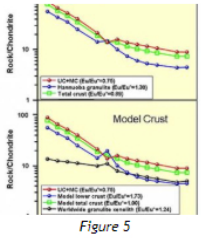

Figure 5

In contrast to the global average lower crust, the continental crust in eastern China has a pronounced negative Eu anomaly (Eu/Eu^*=0.80) (Gao et al., 1998a, b). The upper and middle crusts of eastern China have Eu/Eu^* of 0.73 and 0.78, respectively. Weighted by thickness, the upper plus middle crust as a whole has an average Eu/Eu^* of 0.75 (Fig. 5). The Hannuoba mafic and mafic to felsic granulite xenoliths have almost identical Eu/Eu^* of 1.28 and 1.30, respectively. If the eastern China lower crust is assumed to be represented by the average Hannuoba granulite xenoliths, the resultant total crust has Eu/Eu^* of 0.89 (Fig. 5). This magnitude of Eu anomaly is insufficient to compensate for the negative Eu anomaly of the upper and middle crust so as to produce no Eu anomaly in the total crust. The model lower crust is required to have Eu/Eu^* of 1.73 to make a balance, which is far greater than the average worldwide mafic (Eu/Eu^*=1.24) and mafic to felsic granulite xenoliths (Eu/Eu^*=1.14) (Fig. 5). Delamination of the lower crust plus underlying lithospheric mantle has been suggested to have occurred in eastern China based on studies of Mesozoic high-*Mg* adakitic magmas, picritic and basaltic lavas and entrained eclogitic xenoliths in the North China Craton (Gao et al., 2004, 2008; Xu et al., 2006). Although other models may also explain the andesitic composition of the continental crust (Rudnick and Gao, 2003; Arculus, 2006; Davidson and Arculus, 2006), we conclude that delamination of the deep lithosphere may have played an important role in driving the continental crust to an evolved composition, loss of the Archean keel, and in producing the large volumes of intraplate magmatism in the North China Craton during the Mesozoic (Gao et al., 2004, 2008; Xu et al., 2006).

Acknowledgments

I dedicate this paper to my graduate supervisor Prof. Benren Zhang. I thank the team of eastern China crust composition study for their samples and Mingcai Yan particularly for helping analysis of the composites. I also thank Roberta L. Rudnick, Zhaochu Hu, Yongsheng Liu, and Scott McLennan for their comments and discussion. I finally thank Yong-Fei Zheng and Stephen C. Komor for editorial handling. This research is supported by the National Nature Science Foundation of China (Grants 40821061, 90714010, 40973020), Chinese Ministry of Education and State Administration of Foreign Expert Affairs (B07039) as well as the MOST special funds from the State Key Laboratory of Continental Dynamics and the State Key Laboratory of Geological Processes and Mineral Resources.

References

Arculus R.J. (2006) The 'Andesite Model' of continental crust origins. *Geochim. Cosmochim. Acta* **70** (Issue, 18, Supplement 1), A20.

Barth M., McDonough W.F. and Rudnick R.L. (2000) Tracking the budget of Nb and Ta in the continental crust. *Chem. Geol.* **165**, 197-213.

Christensen N. I. and Mooney W. D. (1995) Seismic velocity structure and composition of the continental crust: A global view. *J. Geophys.Res.* **100**, 7961-9788.

Clarke F.W. (1889) The relative abundance of the chemical elements. *Phil. Soc. Washington Bull* **XI**, 131-142.

Condie K.C. (1993) Chemical composition and evolution of the upper continental crust: contrasting results from surface samples and shales. *Chem. Geol.* **104**, 1-37.

Eade K.E. and Fahrig W.F. (1971) Chemical evolutionary trends of continental plates-preliminary study of the canadian shield. *Geol. Sur. Can. Bull.* **179**, 1-51.

Eade K.E. and Fahrig W.F. (1973) Regional, lithological, and temporal variation in the abundances of some trace elements in the canadian shield. *Geol. Sur. Canada Paper* **72-46**, Ottawa, Ontario.

Davidson J.P. and Arculus R.J. (2006) The significance of Phanerozoic arc magmatism in generating continental crust. In *Evolution and Differentiation of the Continental Crust* (eds. M. Brown and T. Rushmer), pp. 135-172, Cambridge: Cambridge University Press.

Gao S., Zhang B.R., Luo T.C., Li Z.J., Xie Q.L., Gu X.M., Zhang H.F., Ouyang J.P., Wang D.P. and Gao C.L. (1992) Chemical composition of the continental-crust in the Qinling Orogenic Belt and its adjacent North China and Yangtze Cratons. *Geochim. Cosmochim. Acta* **56**, 3933-3950.

Gao S., Zhang B.-R., Jin Z.-M., Kern H., Luo T.-C., and Zhao Z.-D. (1998a) How mafic is the lower continental crust? *Earth Planet. Sci. Lett.* **106**, 101-117.

Gao S., Luo T.-C., Zhang B.-R., Zhang H.-F., Han Y.-W., Hu Y.-K. and Zhao Z.-D. (1998b) Chemical composition of the continental crust as revealed by studies in East China. *Geochim. Cosmochim. Acta* **62**, 1959-1975.

Gao S., Rudnick R.L., Yuan H.L., Liu X.M., Liu Y.S., Xu W.L., Ling W.L., Ayers J., Wang X.C. and Wang Q.H. (2004) Recycling lower continental crust in the North China craton. *Nature* **432**, 892-897.

Gao S., Rudnick R.L., Xu W.L.,Yuan H.L., Liu Y.S., Walker R.J., Puchtel I.S., Liu X.M., Huang H., Wang, X.R. and Yang, J. (2008) Recycling deep cratonic lithosphere and generation of intraplate magmatism in the North China craton. *Earth Planet. Sci. Lett.* **270**, 41-53.

Hawkesworth C.J. and Kemp A.I.S. (2006a) Evolution of the continental crust. *Nature* **443**, 811-817.

Hawkesworth C.J. and Kemp A.I.S. (2006b) The differentiation and rates of generation of the continental crust. *Chem. Geol.* **226**, 134-143.

Hu Z.C. and Gao S. (2008) Upper crustal abundances of trace elements: A revision and update. *Chem. Geol.* **253**, 205-221.

Kern H., Gao S. and Liu Q.-S. (1996) Seismic properties and densities of middle and lower crustal rocks exposed along the North China Geoscience Transect. *Earth Planet. Sci. Lett.* **139**, 439-455.

Li S.-L., Mooney W.D. and Fan J.C. (2006) Crustal structure of mainland China from deep seismic sounding data. *Tectonophysics* **420**, 239-252.

Liu Y.-S., Gao S., Jin S.-Y., Hu S.-H., Sun M., Zhao Z.-B. and Feng J.-L. (2001) Geochemistry of lower crustal xenoliths from Neogene Hannuoba Basalt, North China Craton: Implications for petrogenesis and lower crustal composition. *Geochim. Cosmochim. Acta* **65**, 2589-2604.

McDonough W.F., Sun S.S., Ringwood A.E., Jagoutz E. and Hofmann A.W. (1992) Potassium, rubidium, and cesium in the earth and moor and the evolution of the mantle of the earth. *Geochim. Cosmochim. Acta* **56**, 1001-1012.

McLennan S.M. (2001) Relationships between the trace element composition of sedimentary rocks and upper continental crust. *Geochem. Geophys. Geosys.* **2**, 2000GC000109.

Plank T. and Langmuir C.H. (1998) The chemical composition of subducting sediment and its consequences for the crust and mantle. *Chem. Geol.* **145**, 325-394.

Rudnick R.L. (1995) Making continental crust. *Nature* **378**, 571-578.

Rudnick R. L. and Presper T. (1990) Geochemistry of intermediate- to high-pressure granulites. In *Granulites and Crustal Evolution* (ed. D.Vielzeuf and P. Vidal), pp. 523-550. Kluwer.

Rudnick R.L. and Fountain D.M. (1995) Nature and composition of the continental crust: a lower crustal perspective. *Rev. Geophys.* **33**, 267-309.

Rudnick R. L. and Gao S. (2003) Composition of the continental crust. In *The Crust*, vol. 3 (ed. R. L. Rudnick). Elsevier, pp. 1-64.

Rudnick R.L., Barth M., Horn I. and McDonough W.F. (2000) Rutile-bearing refractory eclogites: missing link between continents and depleted mantle. *Science* **287**, 278-281.

Shaw D.M., Reilly G.A., Muysson J.R., Pattenden G.E. and Campbell F.E. (1967) An estimate of the chemical composition of the canadian precambrian shield. *Can. J. Earth Sci.* **4**, 829-853.

Shaw D.M., Dostal J. and Keays R.R. (1976) Additional estimates of continental surface precambrian shield composition in Canada. *Geochim. Cosmochim. Acta* **40**, 73-83.

Shaw D.M., Cramer J.J., Higgins M.D. and Truscott M.G. (1986) Composition of the Canadian Precambrian shield and the continental crust of the earth. In *The Nature of the Lower Continental Crust*, Geol. Soc. London, vol. 24 (eds. J.B. Dawson, D.A. Carswell, J. Hall and K.H. Wedepohl). pp. 257-282.

Taylor S. R. and McLennan S. M. (1985) *The Continental Crust: its Composition and Evolution*. Blackwell Blackwell Scientific, Oxford, 311p.

Taylor S. R. and McLennan S. M. (2009) *Planetary Crusts: Their Composition and Evolution*. Cambridge University Press, Cambridge. 378 pp.

Wedepohl K.H. (1995) The composition of the continental crust. *Geochim. Cosmochim. Acta* **59**, 1217-1232.

Xu W.L., Gao S., Wang Q.H., Wang D.Y. and Liu Y.S. (2006) Mesozoic crustal thickening of the eastern North China Craton: Evidence from eclogite xenoliths and petrologic implications. *Geology* **34**, 721-724.

Yan M.C. and Chi, Q.H. (1997) *The Chemical Composition of Crust and Rocks in the Eastern Part of China*. Science Press, Beijing, 292 pp.

Yan M.C., Chi Q.H., Gu T.X. and Wang C.S. (1997) Chemical composition of upper crust in eastern China. *Sci. China (D)* **40**, 530-539.

Zhang B.-R., Luo T.-C., Gao S., Ouyang J.-P., Chen D.X., Ma Z.-D., Han Y.-W., Gu X.-M. (1994)

Geochemical Study of the Lithosphere, Tectonism and Metalogenesis in the Qingling-Dabashan Region. Press of China University of Geosciences, Wuhan, 446 pp.

Zhang B.-R., Gao S., Zhang H.-F. and Han Y.W. (2002) *Geochemistry of Qingling Orogenic Belt*. Science Press, Beijing, 187 pp.

Zhang G. H., Zhou X. H., Chen S. H., and Sun M. (1998) Heterogeneity of the lower crust: Evidence from geochemistry of the Hannuoba granulite xenoliths, Hebei province (in Chinese). *Geochemica* **27**, 153-163.

Figure Captions

Figure 1. Generalized tectonic map of China showing distributions of seismic refraction profiles (blue lines) and the area of geochemical sampling (green line enclosed area) (Yan and Chi, 2007; Gao et al., 1998b). NC = North China Craton; YC = Yangtze Craton; SC = South China Orogen.

Figure 2. Examples of correlations between elements in various fine-grained clastic sedimentary rocks and loess (Hu and Gao, 2008): (a) Th-Sn, (b)Th-Be, (c) Rb-Ge, and (d) Fe_2O_3-Zn. Lines represent linear fit to data. r is correlation coefficient. Superimposed are upper crustal composition estimates of Taylor and McLennan (1985, 2009), Shaw et al. (1986), Gao et al. (1998b), Rudnick and Gao (2003), and Hu and Gao (2008).

Figure 3. Comparison of SiO_2 contents of granulite xenoliths from Hannuoba of the North China Craton (a) (Zhang et al., 1998; Liu et al., 2001) and worldwide compilations (b) (Rudnick, unpubl.). Numbers indicate the average SiO_2 content, one standard deviation and number of samples (N).

Figure 4. Average crustal structure for different tectonic units in China. All velocities are reported at 600 MPa and room temperature (Gao et al., 1998a). The underlined number below each column indicates average Vp for the total crust.

Figure 5. Eu anomalies of the continental crust in eastern China (upper panel) and model crust (lower panel). UC and MC indicate the upper and middle crusts, respectively.

Loess geochemistry and Cenozoic paleoenvironments

Zhengtang Guo[a,*]
[a]Institute of Geology and Geophysics, Chinese Academy of Sciences, Beijing, 100029, China
[*]corresponding author's email: ztguo@mail.iggcas.ac.cn

Full Text (2.4 Mb PDF)

Zhengtang Guo

About the Author

Zhengtang Guo is a professor of Cenozoic Geology. He obtained a PhD in 1990 from University of Pierre & Marie Curie, France. His main research interests center on the Cenozoic paleoclimates and biogeochemistry. He was a member of the Scientific Steering Committee of Past Global Change (PAGES), co-leader of PAGES's Australasian Pole-Equator-Pole (PEP-II) international project, Vice-President of the INQUA Commission on Paleoclimates. He and his colleagues extended the loess records in China from 8 Ma to 22 Ma, and use geochemical approaches to explore climate information from loess deposits.

Abstract

Loess-soil sequences are among the best terrestrial records of paleoenvironments. Those in northern China provide a 22 million-year (Ma) geological history of the Asian deserts (dust sources), winter monsoon (dust carrier) and summer monsoon (moisture carrier) winds, and the regional vegetation. Loess geochemistry represents one of the most dynamic research fields in loess-based Paleoclimatology. Some of the most frequent approaches are reviewed here with emphasis to the loess deposits in China.

Keywords: loess geochemistry, Cenozoic climate, paleosol, monsoon

1. Introduction

Loess is terrestrial eolian dust deposits covering ~10% of the land surface (Liu, 1985). The formation of loess fundamentally requires: (1) a sustained source of dust with poor vegetation, (2) adequate winds to transport the dust, and (3) a suitable accumulation site (positive, relatively flat and tectonically stable topography). Loess deposits usually contain numerous paleosols interbedded with loess layers within the band of Earth's orbital changes (Guo et al., 2002). The formation of these soils requires, in addition, a circulation as moisture-carrier (Guo et al., 2008).

All of these factors have left their imprints in the loess deposits. Consequently, loess-soil sequences are regarded as one of the best terrestrial records of paleoenvironments. World's longest loess records locate in the Loess Plateau in northern China. They include the well-known Quaternary (0-2.6 Ma) loess-soil sequences (Liu, 1985; Ding et al., 2001a), the eolian Red Clay (2.6-8.0 Ma) in the eastern Loess Plateau (Ding et al., 2001b), and the Mio-Pliocene loess-soil sequences in the western Loess Plateau (22-3.5 Ma) (Guo et al., 2002; Hao and Guo, 2004). Their combination provides a near continuous terrestrial record of climates for the past 22 Ma.

Geochemical approaches represent one of the most dynamic domains in loess-based Paleoclimatology. This short report aims at introducing some of the main achievements in the study of loess geochemistry with special emphasis to the loess records in China.

2. Chemical composition of loess

The chemical compositions of the Pleistocene loess from different continents have mostly been determined (e.g. Liu et al., 1993; Gallet et al., 1996; 1998; Jahn et al., 2001). Compilation of worldwide data shows a remarkable similarity of elemental geochemistry (Fig. 1), with the dominance of SiO_2, Al_2O_3, Fe_2O_3 and K_2O. Recent data from the Miocene (Guo et al., 2002; Liang et al., 2009) and Pliocene loess (Ding et al., 2001a; Guo et al., 2001) show similar features.

The major and trace elemental compositions of all the loess are encompassed between shales and sandstones, two principle clastic sedimentary end-members. They essentially resemble the average composition of upper continental crust (UCC) (Taylor et al., 1985).

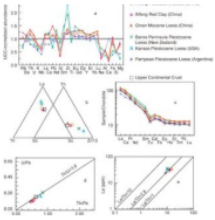

Figure 1

The REE (Rare-earth elements) patterns of different loess (Fig. 1) are hardly distinguishable, with enriched LREE and relatively flat HREE profiles, a restrict range of $(La/Yb)_N$ ratio (7-10) and a negative Eu anormaly. Eu/Eu* ratio varies between 0.53 to 0.67 for European loess, 0.74-0.83 for the loess in Argentina (Gallet et al., 1998), and 0.6-0.7 for the loess in China (Liang et al., 2009). They have nearly a constant La/Th ratio close to 2.8 despite the location and age differences.

The basic geochemical composition of loess, therefore, remarkably resembles the average composition of UCC, indicating that most of the loess materials were derived from well-mixed sedimentary protoliths, which had undergone numerous upper-crustal recycling processes. These reinforce an earlier conclusion (Taylor et al., 1983) that the average chemical composition of UCC might be obtained from eolian deposits, and suggest that the Neogene loess in China can provide equally good proxies for UCC.

3. Geochemical tracing of dust provenance and wind trajectory

Dust materials may be produced by eolian abrasion in the deserts and by glacial grinding of bedrocks (Liu, 1985). Eolian deflation of fine-grained materials may occur in large river-beds and on continental shelves during glacial periods, leading to the loess deposits on river terraces and in coastal regions. Despite of the general geochemical similarity to UCC (Fig. 1), loess of different origins are usually distinguishable through specific geochemical parameters.

The loess of different ages in northern China are characterized by slight TiO_2 positive and Na_2O, CaO negative anomalies and slightly lower Sr content compared to UCC (Fig. 1). These are attributable to their desert origin: the inland deserts in Asia were formed as early as 22 Ma ago (Guo et al., 2002), such that the materials would have experienced many cycles involving processes of sedimentary differentiation with moderate chemical weathering.

Another distinct feature of the loess in China is the higher Cs, lower Zr and Hf concentrations (Liang et al., 2009). They are explainable by the grain-size sorting during the transportation and can be regarded as another indication of the long trajectory of dust from the remote deserts in the Asian interior. These sorting processes are minimized for loess with closer sources.

Isotope tracers (e.g. Sr, Nd and Os) are particularly sensitive in the determination of dust provenance. Loess from different sources have

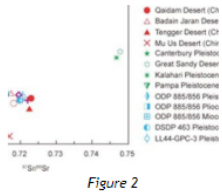

Figure 2

clearly distinct isotope signatures (Fig. 2). $\varepsilon_{Nd}(0)$ values for the Pleistocene, Pliocene and Miocene loess in China average -10.0, -10.1 and -9.5, respectively, indicating roughly similar sources and dust trajectories (Fig. 2). This is also supported by their narrower range of Eu/Eu* ratio between 0.6 and 0.7 (Liang et al., 2009). $^{87}Sr/^{86}Sr$ ratio averages 0.719874, 0.722026 and 0.719579 for the Pleistocene, Pliocene and Miocene samples, respectively. Their slight differences of $^{87}Sr/^{86}Sr$ are due to the coarser/finer textures of the Quaternary/Neogene loess. Isotope data from the main deserts in northern China (Fig. 2) suggest that the Taklimakan, Qaidam, Badain Jaran and Tengger deserts would have constantly been the main sources of the loess deposits in the Loess Plateau over the past 22 Ma.

These geochemical tracers confirm the onsets of the inland deserts (as dust sources) and monsoon-dominated climate (with the winter monsoon as dust carrier) in Asia by the early Miocene due to the uplift of the Himalayan-Tibetan complex and changes in the land-sea distribution pattern (Guo et al., 2008). Asian deserts have also been the main sources of the dust deposited in the North Pacific since the early Miocene (Ziegler et al., 2007), as is confirmed by the isotope data (Fig. 2). Some dust components, such as iron, may have significantly affected the concentration of atmospheric CO_2 and global climate through modulating marine bio-productivity (Jickells et al., 2005).

4. Loess geochemistry and paleoclimate proxies

Geochemical parameters are widely used as climate proxies in loess-based Paleoclimatology to document: (1) the conditions of dust sources; (2) the strength of dust-carrying winds; and (3) climates and vegetations in the depositional regions. In the case of the loess in China, these include the drying history of the Asian interior, the strengths of the Asian winter (dust carrier) and summer (moisture carrier) monsoons, and vegetation changes in the Loess Plateau.

Dust flux is positively correlative with the source aridity (Rea et al., 1998; Guo et al., 2004), but hardly measurable due to post-depositional modifications (e.g. pedogenesis and compaction). The flux of Al_2O_3 (An et al., 2001) and Be isotopes (Shen et al., 1992; Graham et al., 2001) were used to quantify the changes in dust flux. Some other elements, such as Fe_2O_3, have also the potential to document the long-term changes of dust flux because of their resistance to post-depositional weathering and the relatively small variability over time.

Grain-size of eolian sediments is indicative of the strength of dust carrying-winds, i.e. the westerly winds for the dust in North Pacific (Rea et al., 1998), and the Asian winter monsoon for the loess in China. However, grain-size of bulk samples were usually affected by post-depositional pedogenesis and weathering. SiO_2/Al_2O_3 molecular ratios were proven to be a sensitive proxy of the Asian winter monsoon for both Quaternary and Neogene loess in China (Guo et al., 2004), as SiO_2 and Al_2O_3 are stable under semi-arid conditions while quartz (SiO_2) is much more abundant in coarser dust fractions. Some other components, of which the concentrations are dependent of grain-size, were also used to reflect the strength of the winter monsoon (Liu et al., 1995).

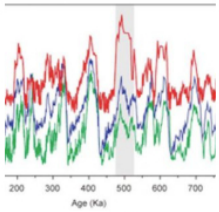

Figure 3

Chemical weathering in the monsoon zones mainly depends upon summer precipitation and temperature. Accordingly, chemical weathering indexes (e.g. Fed/FeT, CIW, Rb/Sr) are widely used to reflect the changes of the Asian summer monsoon (Guo et al., 1996; 2000; Chen et al., 1999; Ding et al., 2001b). These new proxies have documented a series of monsoon features that had not been reflected by magnetic susceptibility, an index that was widely used as a proxy of the summer monsoon. They brought some key insights for understanding the monsoon dynamics. For example, chemical weathering in the loess of China shows an overall declining trend (Liang et al., 2009) from the early Miocene to the Pleistocene, indicating a gradually weakened summer monsoon. This trend is broadly consistent with the late Cenozoic global cooling, suggesting that global temperature is an important forcing of the long-term monsoon changes. Also, correlation of the loess weathering history in China with the ice and marine records (Fig. 3) revealed a strong asymmetry of climates between the Northern and Southern Hemispheres ~500 ka ago that exercised a strong impact on the monsoon circulations and ocean conditions (Guo et al., 2009).

The loess deposits in China contain several hundred of paleosols (Guo et al., 2002). Carbon isotopes of soil carbonates and organic matter are reliable indicators of the proportions of C3 and C4 plant biomass as the C3 and C4 photosynthetic pathways fractionate carbon isotopes to different degrees. Data from the loess in China (e.g. An et al., 2005; Ding and Yang, 2000) yielded a faire history about the Neogene expansions of C4 grasslands in northern China, which significantly differs from that south to the Himalayan-Tibetan complex (Cerling et al., 1997).

In the regions with pure C3 vegetation, carbon isotopes are indicative of paleo-rainfall (Hatte et al., 2001). Oxygen isotopes of the authigenic carbonates in loess may reflect the changes in temperature, evaporation and rainwater sources (Ding and Yang, 2000; Li et al., 2007).

5. Summary and perspectives

This report summarizes some of the most frequent applications of Geochemistry in the study of loess. There are many other promising insights with regards to the loess geochemistry and Cenozoic environments. For example, geochemical methods may offer the means of resolving loess ages beyond the range of radiocarbon and luminescence dating (Oches and McCoy, 1995). Carbon isotopes of some molecular components in loess may bear more accurate information of paleo-vegetation (Xie et al., 2004). Elemental carbon in loess likely reflects the history of natural fires (Zhou et al., 2007). Hydrogen and nitrogen isotopes in loess may provide new environmental signals (Liu and Wang, 2008). Some of these results are still contentious, but it is rightly this kind of debates that add charms to the loess geochemistry field. In particular, there is a strong need to develop more accurate geochemical proxies and geochemical models for loess-based Paleoclimotology towards quantifying environmental parameters and climate dynamics.

Aknowledgments

This study was supported by the Natural Science Foundation of China (40730104).

References

An Z.S., Huang Y., Liu W.G., Guo Z.T., Clemens S., Li L., Prell W., Ning Y.F., Cai Y.J., Zhou W.J., Lin B.H., Zhang Q.L., Cao Y.N., Qiang X.K., Chang H. and Wu, Z.K. (2005) Multiple expansions of C4 plant biomass in East Asia since 7 Ma coupled with strengthened monsoon circulation. *Geology* **33**, 705-708.

An Z.S., Kutzbach J.E., Prell W.L. and Porter S. C. (2001) Evolution of Asian monsoons and phased uplift of the Himalaya-Tibetan plateau since Late Miocene times. *Nature* **411**, 62-66.

Basile I., Grousset F.E., Revel M., Petit J.R., Biscaye P.E. and Barkov N.I. (1998) Patagonian origin of glacial dust deposited in East Antarctica (Vostok and Dome C) during glacial stages 2, 4 and 6. *Earth and Planetary Science Letters* **146**, 573-589.

Cerling T.E., Harris J.M., macFadden B.J., Leakey M.G., Quade J., Eisenmann V. and Ehleringer J.R. (1997) Global vegetation change through the Miocene/Pliocene boundary. *Nature* **389**, 153-158.

Chen J., An Z.S. and Head J. (1999) Variation of Rb/Sr ratios in the loess-paleosol sequences of central China during the last 130,000 years and their implications for monsoon paleoclimatology. *Quaternary Research* **51**, 215-219.

Chen J., Li G., Yang J., Rao W., Lu H., Balsam W., Sun Y. and Ji J. (2007) Nd and Sr isotopic characteristics of Chinese deserts: Implications for the provenances of Asian dust. *Geochimica et Cosmochimica Acta* **71**, 3904-3914.

Ding Z.L., Yang S.L., Sun J.M. and Liu T.S. (2001a) Iron geochemistry of loess and red clay deposits in the Chinese Loess Plateau and implications for long-term Asian monsoon evolution in the last 7.0 Ma. *Earth and Planetary Science Letters* **185**, 99-109.

Ding Z.L., Sun J.M., Yang S.L. and Liu T.S. (2001b) Geochemistry of the Pliocene red clay formation in the Chinese Loess Plateau and implications for its origin, source provenance and aleoclimate change. *Geochimica et Cosmochimica Acta* **65**, 901-913.

Ding Z.L. and Yang S.L. (2000) C3/C4 vegetation evolution over the last 7.0 Myr in the Chinese Loess Plateau: evidence from pedogenic carbonate d13C. *Palaeogeography, Palaeoclimatology, Palaeoecology* **160**, 291-299.

Gallet S., Jahn B.-m. and Torii M. (1996) Geochemical characterization of the Luochuan loess-paleosol sequence, China, and paleoclimatic implications. *Chemical Geology* **133**, 67-88.

Gallet S., Jahn B.-m., Van Vliet Lanoe B., Dia A. and Rossello E. (1998) Loess geochemistry and its implications for particle origin and composition of the upper continental crust. *Earth and Planetary Science Letters* **156**, 157- 177.

Graham I., Ditchburn R. and Whitehead N. (2001) Be isotope analysis of a 0-500ka loess-paleosol sequence from Rangitatau East, New Zealand. *Quaternary International* **76/77**, 29-42.

Grousset F.E., Biscaye P.E., Revel M., Petit J.R., Pye K., Joussaume S. And Jouzel J. (1992) Antarctic (Dome C) ice-core dust at 18 k.y. B.P.: Isotopic constraints on origins. *Earth and Planetary Science Letters* **111**, 182-1750.

Guo Z.T., Liu T.S., Guiot J., Wu N.Q., Lu H.Y., Han J.M., Liu J.Q. and Gu Z.Y. (1996) High frequency pulses of East Asian monsoon climate in the last two glaciations: Link with the North Atlantic. *Climate Dynamics* **12**, 701-709.

Guo Z.T., Berger A., Yin Q.Z. and Qin L. (2009) Strong asymmetry of hemispheric climates during MIS-13 inferred from correlating China loess and Antarctica ice records. *Clim. Past.* **5**, 21-31.

Guo Z.T., Biscaye P., Wei L.Y., Chen X.H., Peng S.Z. and Liu T.S. (2000) Summer monsoon variations over the last 1.2 Ma from the weathering of loess-soil sequences in China. *Geophysical Research Letters* **27**, 1751-1754.

Guo Z.T., Ruddiman W.F., Hao Q.Z., Wu H.B., Qiao Y.S., Zhu R.X., Peng S.Z., Wei J.J., Yuan B.Y. and Liu T.S. (2002) Onset of Asian desertification by 22 Myr ago inferred from loess deposits in China. *Nature* **416**, 159-163.

Guo Z.T., Peng S.Z., Hao Q.Z., Biscaye P.E. and Liu T.S. (2001) Origin of the Miocene-Pliocene red-earth formation at Xifeng in Northern China and implications for paleoenvironments. *Palaeogeography, Palaeoclimatology, Palaeoecology* **170**, 11-26.

Guo Z.T., Peng S.Z., Hao Q.Z., Biscaye P.E., An Z.S. and Liu T.S. (2004) Late Miocene-Pliocene development of Asian aridification as recorded in the Red-Earth Formation in northern China. *Global and Planetary Change* **41**, 135-145.

Guo Z.T., Sun B., Zhang Z.S., Peng S.Z., Xiao G.Q., Ge J.Y., Hao Q.Z., Qiao Y.S., Liang M.Y., Liu J.F., Yin Q.Z. and Wei J.J. (2008) A major reorganization of Asian climate by the early Miocene. *Clim. Past.* **4**, 153-174.

Hao Q.Z. and Guo Z.T. (2004) Magnetostratigraphy of a late Miocene-Pliocene loess-soil sequence in the western Loess Plateau in China. *Geophysical Research Letters* **31**, L09209, doi: 10.1029/2003GL019392.

Hatte C., Antoine P., Fontugne M., Lang A., Rousseau D.D. and Zoller L. (2001) $\delta^{13}C$ of loess organic matter as a potential proxy for paleoprecipitation. *Quaternary Research* **55**, 33-38.

Jahn B.M., Gallet S. and Han J. (2001) Geochemistry of the Xining, Xifeng and Jixian sections, Loess Plateau of China: eolian dust provenance and paleosol evolution during the last 140 ka. *Chemical Geology* **178**, 71-94.

Jickells T.D., An Z.S., Andersen K.K., Baker A.R., Bergametti G., Brooks N., Cao J.J., Boyd P.W., Duce R.A., Hunter K.A., Kawahata H., Kubilay N., laRoche J., Liss P.S., Mahowald N., Prospero J.M., Ridgwell A.J., Tegen I. and Torres R. (2005) Global iron connections between desert dust, ocean biogeochemistry, and climate. *Science* **308**, 67-71.

Jouzel J., Masson-Delmotte V., Cattani O., Dreyfus G., Falourd S., Hoffmann G., Minster B., Nouet J., Barnola J.M., Chappellaz J., Fischer H., Gallet J.C., Johnsen S., Leuenberger M., Loulergue L., Luethi D., Oerter H., Parrenin F., Raisbeck G., Raynaud D., Schilt A., Schwander J., Selmo E., Souchez R., Spahni R., Stauffer B., Steffensen J.P., Stenni B., Stocker T.F., Tison J.L., Werner M. and Wolff E.W. (2007) Orbital and millennial Antarctic climate variability over the past 800,00 years. *Science* **317**, 793-796.

Li G., Sheng X., Chen J., Yang J. and Chen Y. (2007) Oxygen-isotope record of paleorainwater in authigenic carbonates of Chinese loess-paleosol sequences and its paleoclimatic significance. *Palaeogeography, Palaeoclimatology, Palaeoecology* **245**, 551-559.

Liang M.Y., Guo Z.T., Kahmann A.J. and Oldfield F. (2009) Geochemical characteristics of the Miocene eolian deposits in China: Their provenance and climate implications. *Geochemistry Geophysics Geosystems* **10**, Q04004, doi:10.1029/2008GC002331.

Lisiecki L.E. and Raymo M.E. (2005) A Plicene-Pleistocene stack of 57 globally distributed benthic $\delta^{18}O$ records. *Paleoceanography* **20**, PA1003, doi: 10.1029/2004PA001071.

Liu C.Q., Masuda A., Okada A., Yabuki S., Zhang J. and Fan Z.L. (1993) A geochemical study of loess and desert sand in northern China: Implications for continental crust weathering and composition. *Chemical Geology* **106**, 359-374.

Liu W.G. and Yang H. (2008) Multiple controls for the variability of hydrogen isotopic compositions in higher plant n-alkanes from modern ecosystems. *Global Change Biology* **14**, 2166-2177.

Liu T.S. (1985) Loess and the Environment (in Chinese with English abstract). China Ocean Press, Beijing.

Liu T.S., Guo Z.T., Liu J.Q., Han J.M., Ding Z.L., Gu Z.Y. and Wu N.Q. (1995) Variations of eastern Asian monsoon over the past 140,000 years. *Bulletin de la Societe Geologique de France* **166**, 221-229.

Nakai S., Halliday A.N. and Rea D.K. (1993) Provenance of dust in the Pacific Ocean. *Earth and Planetary Science Letters* **119**, 143-157.

Ochos E. and McCoy W. (1995) Amino acid geochronology applied to the correlation and dating of central

Oches E. and McCoy W. (1995) Amino acid geochronology applied to the correlation and dating of central European loess deposits. *Quaternary Science Reviews* **14**, 767-782.

Pettke T., Halliday A.N., Hall C.M. and Rea D.K. (2000) Dust production and deposition in Asia and the north Pacific Ocean over the past 12 Myr. *Earth and Planetary Science Letters* **178**, 397-413.

Rea D.K., Snoeckx H. and Joseph L.H. (1998) Late Cenozoic eolian deposition in the North Pacific: Asian drying, Tibetan uplift, and cooling of the northern hemisphere. *Paleoceanography* **13**, 215-224.

Shen C.D., Beer J., Liu T.S., Oeschger H., Bonani G., Suter M. and Wolfli W. (1992) 10Be in Chinese loess. *Earth and Planetary Science Letters* **109**, 169-177.

Taylor S.R. and McLennan S. (1985) *The Continental Crust: Its Composition and Evolution*. Blackwell, Oxford.

Taylor S.R., McLennan S.M. and McCulloch M.T. (1983) Geochemistry of loess, continental crustal composition and crustal model ages. *Geochimica et Cosmochimica Acta* **47**, 1897-1905.

Xie S., Guo J., Huang J., Chen F., Wang H. and Farrimond P. (2004) Restricted utility of $\delta^{13}C$ of bulk organic matter as a record of paleovegetation in some loess-paleosol sequences in the Chinese Loess Plateau. *Quaternary Research* **62**, 86-93.

Zhou B., Shen C.D., Sun W.D., Zheng H.B., Yang Y., Sun Y.B. and An Z.S. (2007) Elemental carbon record of paleofire history on the Chinese Loess Plateau during the last 420 ka and its response to environmental and climate changes. *Palaeogeography, Palaeoclimatology, Palaeoecology* **252**, 617-625

Ziegler C.L., Murray R.W., Hovan S.A. and Rea D.K. (2007) Resolving eolian, volcanogenic, and authigenic components in pelagic sediment from the Pacific Ocean. *Earth and Planeary Science Letters* **254**, 416-432.

Figure Captions

Figure 1. Elemental compositions of loess from different locations and ages. a. UCC-normalized abundances. b. La-Th-Sc and Th-Sc-Zr/10 discrimination diagrams. c. Chondrite-normalized REE distribution patterns. d. U/Pb versus Th/Pb ratios. e. La versus Th diagram. The Banks Peninsula (average of 5 samples) and Kansas (average of 3 samples) Pleistocene loess data are from Taylor et al. (1983). Data for the Pampean (average of 6 samples) Pleistocene loess are from Gallet et al. (1998). Data for the Xifeng Pleistocene loess (average of 6 samples), the Xifeng Pliocene Red Clay (average of 4 samples) and the Qinan Miocene (average of 7 samples) loess are from Liang et al. (2009). UCC data are from Taylor and McLennan (1985).

Figure 2. Isotopic signatures of loess/dust from different locations and ages. Data for the Xifeng Pleistocene loess (average of 5 samples), the Xifeng Pliocene Red Clay (average of 5 samples) and the Qinan Miocene loess (average of 5 samples) are from this study. Data for Taklimakan (average of 9 samples), Qaidam (average of 7 samples), Badain Jaran (average of 11 samples), Tengger (average of 5 samples) and Mu Us (average of 10 samples) deserts in China are from (Chen et al., 2007). Data for Canterbury (1 sample), Great Sandy Desert (average of 2 samples), Kalahari (average of 2 samples) and Pampa (average of 3 samples) Pleistocene loess are from Basile et al (1998). Date for the Pleistocene (average of 4 samples), Pliocene (average of 7 samples) and Miocene (average of 9 samples) at the ODP site 885/886 are from Pettke et al (2000). Data for DSDP 463 (1 sample) and LL44-GPC-3 (1 sample) sites are from Nakai et al (1993).

Figure 3. Correlation of loess weathering record at Xifeng in China (Guo et al., 2009) (red) with the Antarctic temperature (Jouzel et al., 2007) (green) and marine $\delta^{18}O$ records (Lisiecki and Raymo, 2005) (blue).

Geochronology of high-temperature rocks and hydrothermal ore deposits in China

Xian-hua LI[a,*]
[a] State Key Laboratory of Lithospheric Evolution, Institute of Geology and Geophysics, Chinese Academy of Sciences, Beijing 100029, China
[*] corresponding author's email: lixh@gig.ac.cn

Full Text (2.4 Mb PDF)

Xian-hua Li

Xian-hua Li is a professor and the director of the SIMS laboratory at the Institute of Geology and Geophysics, Chinese Academy of Sciences. He received his PhD in 1989 from the Institute of Geochemistry in Chinese Academy of Sciences. Between 1989 and 2005, he worked in the laboratory of isotope geochemistry at the Guangzhou Institute of Geochemistry and subsequently moved to the Institute of Geology and Geophysics in Beijing. His research interests are geochronology, isotope geochemistry, igneous petrogenesis and chemical geodynamics. He was elected as a Fellow of the Geological Society of America in 2006.

Abstract

Geochronological investigations in China were initiated nearly 50 years ago, mainly since the establishment of university programs teaching isotope geochemistry and the setup of geochronological laboratories. During the late 1970's and early 1990s, the geochronological framework of China's landmass has been established by numerous isotopic studies. Over the past decade, state-of-the-art geochronological laboratories have been established in China, contributing to the country's increasing role in many fields of Geosciences. This article highlights some of the major geochronological achievements of the past decades, with special focus on China's Precambrian geology, the improved understanding of age relationships in the Mesozoic Igneous Province of eastern China, and new developments in the dating of hydrothermal ore deposits.

Keywords: Geochronology, Precambrian continental evolution, Mesozoic Igneous Province, hydrothermal ore deposits, China.

1. History of geochronological research in China

Geochronological investigations in China have been evolved in three major stages: (1) early establishment of geochronological laboratories and initiation of education of isotope geochemistry during late 1950s and 1966; (2) increasing availability of commercial mass spectrometers and increased application of geochronology in geosciences during late 1970s and early 1990s; and (3) establishment of state-of-the-art geochronological laboratories, which represented an important stepping stone for much progress of China's geosciences during the past decade.

The initiation and development of geochronological research in China was a result of the recognition of its fundamental importance to the understanding of the geological evolution of China's landmass and its exploitation for mineral deposits. During the late 1950s and early 1960s, geochronological laboratories were firstly established in two institutions, namely the Chinese Academy of Sciences and the Chinese Academy of Geological Sciences in Beijing. The establishment of the K-Ar and U-Pb dating techniques at these institutions were initiated and led by Profs. Pu Li and Yuqi Chen, respectively. At the time, education of isotope geochronology and geochemistry was spearheaded by the Department of Geochemistry at the University of Science and Technology of China.

The first K-Ar age dates measured by China's isotopic laboratories were published by Li in 1963. A subsequent compilation of new K-Ar and U-Pb dates was given by Chen and Li (1964). These early geochronological investigations significantly promoted geological studies in China and the study of Precambrian geology. However, the early boom of geochronology was interrupted by the ten-year-long Cultural Revolution between 1966 and 1976. The isotopic laboratory at the Chinese Academy of Sciences was moved to Guiyang, the capital city of Guizhou Province in southwestern China. Here, the new Institute of Geochemistry was established. Despite these difficult times, geochronological research continued. The first National Conference on Isotope Geochronology and Geochemistry was held in 1975 at Guiyang and attended by over 200 scientists. The conference continued to be organized as quadrennial meeting. Its ninth meeting returned to Guiyang in 2009.

Isotope geochronology reemerged after the Cultural Revolution, and was booming again during the late 1970s and early 1990s. The increasing availability of commercial mass spectrometers enabled a number of isotopic laboratories to be established. The K-Ar and U-Pb methods were complemented by Rb-Sr, Sm-Nd and Ar/Ar as well as U-series and fission-track dating, ^{14}C and other cosmogenic isotopic systems. Methodology developments made zircon single grain U-Pb dating possible.

Over this period of time, the geochronological framework of China was established through the research efforts by numerous scientists, contributing to the development of the chronological time scale of China, the improved understanding of Precambrian geology, as well as the age dating of igneous rocks, regional tectonic processes, and the formation of ore deposits. A comprehensive review of work conducted during this period was presented by Yu and Li (1997). An English translation was made available by Tu et al. (1998). The majority of geochronological studies during this period was published in Chinese and is, therefore, not easily accessible to the international community.

In the early to middle 1990s, the number of geochronological studies in China decreased due to decreasing funding for basic sciences. This situation only gradually changed since late 1990s as the Chinese Academy of Sciences established new research programs. During the past decade, a number of state-of-the-art geochronological laboratories have been established in China. These are equipped with a series of high-performance mass spectrometers including high-resolution SIMS, AMS, TIMS, and noble gas mass spectrometers. In addition, a large number of MC-ICP-MS and ICP-MS equipped with laser ablation systems are now available for geochronology throughout the country. New geochronological methods established include in-situ zircon U-Pb and sulfide Re-Os. Amongst the different methods, in-situ U-Pb zircon geochronology clearly enjoyed the greatest success, enabling geological events and processes to be accurately placed within a firm time framework. U-Pb zircon geochronology contributed to many regional geological studies in China, in particular in the Eastern North China Craton, the Neoproterozoic Doushantuo Formation, the Early Paleozoic of NW China, the Northern Tibetan Plateau, and the South China Block.

2. Precambrian Geochronology of China's Landmass

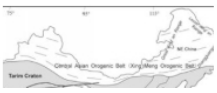

China's landmass contains three major Archean cratons, namely the North China Craton (NCC), the Tarim Craton (TC), and the Yangtze Craton (YC) (Fig. 1).

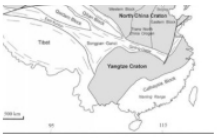

Figure 1

The oldest rocks identified in China are three small occurrences of trondhjemite gneiss dated at ca. 3.8 Ga in Anshan, northeastern NCC (Liu et al., 1992, 2008). Anshan is one of the four locations worldwide where ≥3.8 Ga rocks are exposed (Nutman et al., 2001). However, the crystallization ages of these trondhjemite gneisses are controversial because these rocks also contain 3.3-3.1 Ga zircons, suggesting that the ca. 3.8 Ga zircons may represent xenocrysts (Wu et al., 2008). More research is needed to resolve this inconsistency, especially as the undisputedly oldest rocks in the area are 3.3-3.0 Ga old granitoids.

One of the major advances in the understanding of the Precambrian history of the NCC was its division into three tectonic blocks, namely the Eastern and Western Blocks and the intervening belt of the Trans-North China Orogen (Zhao et al., 2007). Mesoarchean rocks are rare in the NCC, with only two localities being well documented. One is located in western Jiaodong, which occurs in the southeastern part of the Eastern Block. Here a biotite enclave and its hosting TTG gneiss are dated at 2.9 Ga (Jahn et al., 2008). The other is at Lushan in the far south of the Trans-North China Orogen where 2.8 Ga tonalite and amphibolite were found (Liu et al., 2009). Late Archean TTG gneisses surrounded by minor supracrustal rocks predominate in the Eastern and Western Blocks. Most of these rocks were formed within a short time interval at ca. 2.5 Ga (Zhao et al., 2005a), with a few ca. 2.7 Ga TTG occurring in Jiaodong (Jahn et al., 2008). Various interpretations for the genesis of these Archean TTG have been proposed including formation during arc-continent collision (Jahn et al., 2008) or underplating of mantle-derived magmas, presumably triggered by a mantle plume (Zhao et al., 1999). A salient feature is that these terminal Archean TTG were metamorphosed soon after their crystallization at 2.50-2.49 Ga, probably reflecting a mantle plume activity that resulted in significant growth of the continental crust (Yang et al., 2008a).

In the Trans-North China Orogen, a long-lived magmatic arc existed during 2.56-1.92 Ga. Collision of the Eastern and Western Blocks and final amalgamation of the NCC caused intense deformation and metamorphism at 1.88-1.82 Ga (Zhao et al., 2005a, 2007). The Trans-North China Orogen is coeval with 2.1-1.8 Ga collisional orogens in most continental blocks worldwide, marking the assembly of the supercontinent Columbia by ca. 1.8 Ga (Zhao et al., 2005b). Following its final assembly, the NCC experienced extensive anorogenic magmatism including 1.78 Ga giant mafic dike swarms and coeval volcanism that was related to rifting (Peng et al., 2008). Emplacement of the 1.75-1.68 Ga anorthosite-mangerite-alkali granitoid-Rapakivi granite suite (Zhang et al., 2007a) most likely manifests the initial phase of the breakup of Columbia (Zhai and Liu, 2003). Large-scale dolerite sills dated at ca. 1.35 Ga might indicate fragmentation of the NCC from other parts of Columbia (Zhang et al., 2009a). The Precambrian geochronological framework of NCC is summarized in Table 1.

Table 1: Precambrian geochronological framework of the North China, Yangtze and Tarim Cratons.

North China Craton	Yangtze Craton	Tarim Craton
	655-635 Ma Nantuo glaciation	0.74-0.54 Ga glaciation inferred from four layers of diamictites
	0.72-0.66 Ga Jiangkou glaciation	
	0.83-0.75 Ga magmatic flare-up and rift basins related to breakup of Rodinia	0.82-0.74 Ga anorogenic magmatism and rift basins related to breakup of Rodinia
	0.85 Ga dolerite dykes and alkaline intrusions	
	1.1-0.89 Ga orogenic magmatism and metamorphism related to assembly of Rodinia	1.05-0.9 Ga orogenic magmatism and metamorphism related to assembly of Rodinia
1.35 Ga dolerite sills and continental rifting related to fragmentation of Columbia?		
1.78-1.68 Ga intraplate igneous suites and continental rifting related to breakup of Columbia?		
1.88-1.82 Ga metamorphism in Trans-North China Orogen, collision of Eastern and Western Blocks related to assembly of Columbia	1.85 Ga granite	
		2.0-1.9 Ga metamorphism
2.5-1.9 Ga TTG of magmatic arc in Trans-North China Orogen		2.45-2.35 Ga intraplate bimodal magmatism
2.5 Ga TTG and metamorphism of plume-related (?) in Eastern Block		
		2.8-2.6 Ga TTG
2.9-2.7 Ga TTG in Lushan and Jiaodong	3.2-2.9 Ga TTG and amphibolite in Kongling	
3.3-3.0 Ga TTG in Anshan		
3.8 Ga TTG in Anshan?		

Due to a widespread sedimentary cover of middle Neoproterozoic to Cenozoic ages, outcrops of Early Precambrian crystalline basement rocks are scarce in the YC. The oldest rocks belong to the Mesoarchean Kongling Complex near the Yangtze Gorge Dam. These TTG and amphibolites have been dated at 3.2-2.9 Ga (Qiu et al., 2000; Zhang et al., 2006a; Jiao et al., 2009). The Kongling Complex was intruded by 1.85 Ga K-feldspar granites, probably indicating the final cratonization of the YC (Zhang et al., 2006b; Xiong et al., 2008). Metamorphic and calc-alkaline igneous rocks dated at 1.1-0.89 Ga are sporadically distributed around the YC (Ling et al., 2003; Li et al., 2009). They are interpreted to have formed in an active continental margin environment, broadly coeval with the global Grenville-aged orogenesis, marking the amalgamation of the YC with the Cathaysia Block (forming the coherent South China Block) to the south, and probably with the Australian continent to the northwest during the assembly of Rodinia. Neoproterozoic gantitoid and mafic-ultramafic intrusions and their extrusive counterparts dated at 0.83-0.75 Ga are widespread throughout the entire South China Block (Li et al., 2003). While petrogenesis and tectonic implications of these magmatic rocks are still controversial (Li et al., 1999, 2003; Zhou et al., 2002; Wang et al., 2006a; Zheng et al., 2007, 2008; Zhang et al., 2008a), identification of 0.83-0.81 Ga high-temperature komatiitic basalts, continental flood basalts, and 0.78-0.75 Ga mafic dykes (Wang et al., 2007, 2008; Lin et al., 2007), as well as development of continental

rift basins (Wang and Li, 2003) and bimodal volcanism (Li et al., 2002), suggest the possibility that these middle Neoproterozoic magmatic rocks were most likely formed by melting above a Neoproterozoic mantle superplume that triggered the breakup of Rodinia.

Neoproterozoic rift basins are well preserved in the YC. U-Pb zircon geochronological investigations provide a firm time scale of the basin evolution since ca. 820 Ma (Wang et al., 2003) and the timing of two intervening glaciations. The older Jiangkou glaciation is dated between 725 Ma and 663 Ma (Zhou et al., 2004; Zhang et al., 2008b), whereas the younger Nantuo glaciation occurred between 655 Ma and 635 Ma (Condon et al., 2005; Zhang et al., 2008c). The Precambrian geochronological framework of YC is presented in Table 1.

The TC in NW China is mostly covered by Cenozoic deserts, with the Precambrian rocks being sporadically exposed along the craton margins. The 2.8-2.6 Ga TTG gneisses are the oldest rocks identified in the TC (Lu et al., 2008), which are locally exposed on the eastern and northern margins of the craton. Early Paleoproterozoic granites and mafic dykes in the same areas are dated at 2.45-2.35 Ga. They are interpreted as bimodal igneous suites formed in a continental rift setting (Zhang et al. 2003; Lu et al., 2008). In the eastern TC, high-grade metamorphism took place at 2.0-1.9 Ga (Lu et al., 2008).

The late Mesoproterozoic and Neoproterzoic geology of the TC is characterized by 1.05-0.9 Ga orogenic magmatism and metamorphism and 0.82-0.74 Ga anorogenic magmatism and basin rifting (Xu et al., 2005; Zhang et al., 2007b; Lu et al., 2008), which is broadly contemporaneous to the YC. Together with the South China Block, the TC was, therefore, involved in the assembly and breakup of the supercontinent Rodinia. The Neoproterozoic basin at Quruqtagh in the northwestern TC preserves four layers of diamictites in the Bayisi, Altungol, Tereeken, and Hankalchough Formations that have ages between 740 Ma and the end of the Precambrian (Xu et al., 2009), providing an unique natural laboratory for studying the global complexity of Neoproterozoic glaciation. A Precambrian geochronological framework of TC is presented in Table 1. There is a striking similarity in geochronology between the YC and TC during the latest Meosoproterozoic and Neoproterozoic time.

3. Geochronology of the Mesozoic Igneous Province of eastern China

Eastern China comprises three major tectonic blocks, from north to south, the Xing-Mong Orogenic Belt in NE China, the Eastern Block of the NCC, and the eastern South China Block (SCB). These blocks amalgamated to form most of the Southeast-Asian landmass during the late Paleozoic to early Mesozoic (Li et al., 1993; Zhang et al., 2009b). Mesozoic igneous rocks are widespread throughout eastern China, consisting predominantly of granitoid intrusions and their extrusive counterparts along with subordinate mafic and alkaline rocks. Over the past decade, numerous investigations helped establishing a firm geochronological framework for the igneous activity in this part of China.

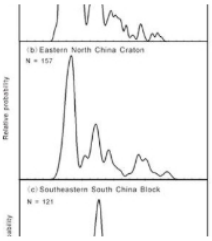

Figure 2

Mesozoic igneous rocks in the XMOB of NE China occurred mainly in the Lesser Xing'an-Zhangguangcai Ranges to the east and northeast, and the Great Xing'an Range to the west, which are separated by the Cenozoic Songliao Basin in the middle (Fig. 1). The total exposed area of the Mesozoic igneous rocks is almost 400,000 km^2. Igneous activity occurred largely during the Cretaceous (140-110 Ma) and to a lesser degree during the Jurassic (190-150 Ma) and Triassic (Fig. 2a) (Wu et al., 2002, 2003; Zhang et al., 2008d). There is a younging trend landwards from the continental margin for Jurassic rocks, whereas Cretaceous rocks show the opposite trend (Wang et al., 2006b). In combination with petrological and geochemical data, the Jurassic igneous rocks are thought to have formed in an active continental margin environment that was related to the westward subduction of an oceanic slab. Cretaceous igneous rocks formed in response to asthenosphere upwelling and crustal melting in an extensional setting due to large-scale lithospheric delamination (Wu et al., 2005a).

Mesozoic igneous rocks in the eastern NCC crop out in four discrete areas that are separated by extensive areas of Cenozoic sedimentary cover (i.e., the Jiaodong, Yan-Liao, Taihang and Jiaodong-Luxi areas). Age patterns (Fig. 2b) of these rocks are broadly similar to those in NE China, with most of the igneous activity being of Cretaceous age (130-120 Ma). Rocks of Jurassic (180-150 Ma) and Triassic (250-200 Ma) age occur in subordinate amounts (Wu et al., 2005a, b; Yang et al., 2005, 2008b). The minor Triassic rocks formed by post-orogenic magmatism along the northern and eastern margin of the NCC, which collided with the XMOB of NE China and YC in late Permian and in early Triassic, respectively. The intensive Jurassic-Cretaceous magmatism is likely associated with the progressive reactivation, replacement, and final 'decratonization' of the Precambrian lithosphere beneath the eastern NCC (Yang et al., 2008b).

The southeastern SCB is characterized by widespread of igneous rocks in age between 270 and 80 Ma (Fig. 2c) (Li and Li, 2007), with a total exposed area of ca. 280,000 km^2. The 270-210 Ma magmatism is associated with the northeasterly trending, ~1300-km-wide South China Fold Belt (SCFB). There is a northwesterly younging trend from the continental margin for these syn-orogenic magmatic rocks as well as coeval deformation and metamorphism in the broad SCFB, which is best explained by a flat-slab subduction model (Li and Li, 2007). Jurassic igneous rocks are distributed in the inland, consisting of an early phase of minor amount of bimodal magmatic rocks (basalts and A-type felsic volcanic rocks and their intrusive counterparts) dated at ca. 190-170 Ma and a later phase of flare-up of fractionated I- and A-type granites dated at 165-155 Ma (Li et al., 2007). These Jurassic rocks are thought to be anorogenic products formed in response to the upwelling of asthenosphere mantle caused by the break-up and foundering of an early Mesozoic subducted flat-slab beneath southeastern China. Cretaceous igneous rocks occur mostly along the coastal region, consisting of ca. 95% felsic volcanic and intrusive rocks and ca. 5% mafic rocks dated at 140-80 Ma. A coastward migration of both extensional and arc-related magmatism is likely formed in a retreating arc system (Li and Li, 2007).

4. Dating of hydrothermal ore deposits

Precise and accurate isotopic geochronology is crucial for constraining the timing and genesis of mineral deposits. However, direct age determination of hydrothermal ore deposits is often difficult due to the lack of minerals suitable for conventional radiometric age dating. Over the past decades, several new methods have been developed and are now widely applied in ore deposit research in China.

Pyrite, one of the most common sulfides in many hydrothermal deposits, contains variable concentrations of Rb and Sr with diverging Rb/Sr ratios, thus permitting direct dating of deposits. Yang and Zhou (2001) presented a method of direct Rb-Sr age determination of pyrite from a lode gold deposit in the Jiaodong area, demonstrating that this method is a promising geochronological technique. Li et al. (2008) further improved this method, which can now be used to date single grains of pyrite.

The Re-Os isotopic system proved to be an ideal geochronometer for molybdenite-bearing ores. In China, Du et al. (1993) developed the first molybdenite Re-Os dating method. This isotopic system has subsequently been applied to the dating of other sulfide minerals such as pyrite (Liu et al., 2004) and arsenopyrite (Yu et al., 2005). In China, the sulfide Re-Os isotopic system has become one of the most widely used geochronometers for the dating of hydrothermal ore deposits.

Direct dating of fluid inclusions can also provide robust constrains on the timing of hydrothermal ore deposits. Early attempts of Rb-Sr isochron age determination were conducted on quartz (Li et al., 1992, 2000), but were not always successful due to the complexity of inclusion assemblages and the presence of K-bearing phases as impurities in the dated quartz. The ^{40}Ar/^{39}Ar age dating of quartz following the

of K-bearing phases as impurities in the dated quartz. The Ar/Ar age dating of quartz following the crushing of quartz under vacuum, combined with a step heating process (Qiu 1996; Qiu et al., 2002), proved to be advantageous for the dating of fluid inclusions. Gases released by the crushing are mainly derived from the fluid inclusions whereas those emitted from the sample during heating are largely sourced by inclusions of K-bearing minerals. The combined use of progressive crushing and heating has also been successfully applied in the Ar/Ar dating of sphalerite from the world-class Fankou Pb-Zn deposit in South China (Qiu and Jiang, 2007). One of the major advantages of this technique is that primary and secondary fluid inclusions within sphalerite can be clearly distinguished.

The Sm-Nd isotopic system represents another useful geochronometer permitting direct dating of hydrothermal ore deposits. Jiang et al. (2000) demonstrated that the Sm-Nd method can be used for the age determination of hydrothermal tourmaline- and sulfide-bearing ores. At the Shizhuyuan polymetallic skarn and greisen deposit in southeast China, hydrothermal minerals include garnet, fluorite, and wolframite proved to be suitable for Sm-Nd isochron dating as these cogenetic phases display a wide range of Sm and Nd concentrations at variable Sm/Nd ratios (Li et al., 2004).

5. Conclusions

Geochronological research has achieved great success in many areas of geosciences research in China. Examples of past and current trends for the dating of high-temperature rocks and hydrothermal minerals are highlighted in the present contribution. However, much work is still needed in both geochronological method developments and their application in the real world. For instance, despite great success of in-situ U-Pb zircon dating by SIMS and LA-ICP-MS, the high-precision TIMS U-Pb techniques is still not available in China due to the lack of appropriate isotopic spikes. These shortcomings will likely be overcome in the next couple years through international collaboration and the involvement of Chinese scientists in the EARTHTIME project.

References

Chen Y.Q. and Li P. (1964) Discussions on the geochronological research achievements in China. *Chinese Sci. Bull.* (in Chinese) **9**, 659-666.

Chen C.H., Lee C.Y., Lu H.Y. and Hsieh P.S. (2008) Generation of Late Cretaceous silicic rocks in SE China: age, major element and numerical simulation constraints. *J. Asian Earth Sci.* **31**, 479-498.

Condon D., Zhu M., Bowring S.A., Wang W., Yang A. and Jin Y. (2005) U-Pb ages from the Neoproterozoic Doushantuo Formation, *China. Science* **308**, 95-98.

Du A.D., He H.L., Yin N.W., Zou X.Q., Sun Y.L., Sun D.Z., Chen S.Z. and Qu W.J. (1993) direct dating of molybdenites using the Re-Os geochronometer. *Chinese Sci. Bull.* **38**, 1319-1320.

Jahn B.-m., Liu D.Y., Wan Y.S., Song B. and Wu J.S. (2008) Archean crustal evolution of the Jiaodong Peninsula, China, as revealed by zircon SHRIMP geochronology, elemental and Nd-isotope geochemistry. *Am. J. Sci.* **308**, 232-269.

Jiang S.Y., Slack J.F. and Palmer M.R. (2000) Sm-Nd dating of the giant Sullivan Pb-Zn-Ag deposit, British Columbia. *Geology* **28**, 751-754.

Jiao W.F., Wu Y.B., Yang S.H., Peng M. and Wang J. (2009) The oldest basement rock in the Yangtze Craton revealed by zircon U-Pb age and Hf isotope composition. *Sci. China (D)* **52**, 1393-1399.

Li P. (1963) Potassium-argon absolute ages of micas from the pegmatites and granites of Inner Mongolia and Nanling Region of China. *Sci. Sin.* **12**, 1041-1048.

Li Z.X. and Li X.H. (2007) Formation of the 1300 km-wide intra-continental orogen and post-orogenic magmatic province in Mesozoic South China: a flat-slab subduction model. *Geology* **35**, 179-182.

Li H., Chen F. and Cai H. (2000) Study on Rb-Sr isotopic ages of gold deposits in West Junggar Area, Xinjiang. *Acta Geol. Sin.* (in Chinese with English abstract) **74**, 181-192.

Li X.H., Gui X.T., Cheng J.P. and Yin G.Q. (1992) Rb-Sr and ^{40}Ar-^{39}Ar dating of Gaofeng gold deposit, Guangdong Province. *Min. Dep.* (in Chinese with English abstract) **11**, 367-373.

Li S.G., Xiao Y.L., Liu D.L., Chen Y.Z., Ge N.J., Zhang Z.Q., Sun S.S., Cong B.L., Zhang R.Y., Hart S.R. and Wang S.S. (1993) Collision of the North China and Yangtse Blocks and formation of coesite-bearing eclogites: timing and processes. *Chem. Geol.* **109**, 89-111.

Li Z.X., Li X.H., Kinny P.D. and Wang J. (1999) The breakup of Rodinia: did it start with a mantle plume beneath South China? *Earth Planet. Sci. Lett.* **173**, 171-181.

Li X.H., Li Z.X., Zhou H., Liu Y. and Kinny P.D. (2002) U-Pb zircon geochronology, geochemistry and Nd isotopic study of Neoproterozoic bimodal volcanic rocks in the Kangdian Rift of South China: implications for the initial rifting of Rodinia. *Precambrian Res.* **113**, 135-155.

Li Z.X., Li X.H., Kinny P.D., Wang J., Zhang S. and Zhou H. (2003) Geochronology of Neoproterozoic syn-rift magmatism in the Yangtze Craton, South China and correlations with other continents: evidence for a mantle superplume that broke up Rodinia. *Precambrian Res.* **122**, 85-109.

Li X.H., Liu D.Y., Sun M., Li W.X., Liang X.R. and Liu Y. (2004) Precise Sm-Nd and U-Pb isotopic dating of the super-giant Shizhuyuan polymetallic deposit and its host granite, Southeast China. *Geol. Mag.* **141**, 225-231.

Li X.H., Li Z.X., Li W.X., Liu Y., Yuan C., Wei G.J. and Qi C.S. (2007) U-Pb zircon, geochemical and Sr-Nd-Hf isotopic constraints on age and origin of Jurassic I- and A-type granites from central Guangdong, SE China: a major igneous event in response to foundering of a subducted flat-slab? *Lithos* **96**, 186-204.

Li Q.L., Chen F., Yang J.H., Fan H.R. (2008) Single grain pyrite Rb-Sr dating of the Linglong gold deposit, eastern China. *Ore Geol. Rev.* **34**, 263-270.

Li X.H., Li W.X., Li Z.X., Lo C.H., Wang J., Ye M.F. and Yang Y.H. (2009) Amalgamation between the Yangtze and Cathaysia Blocks in South China: constraints from SHRIMP U-Pb zircon ages, geochemistry and Nd-Hf isotopes of the Shuangxiwu volcanic rocks. *Precambrian Res.* **174**, 117-128.

Lin G.C., Li X.H. and Li W.X. (2007) SHRIMP U-Pb zircon age, geochemistry and Nd-Hf isotopes of the Neoproterozoic mafic dykes from western Sichuan: petrogenesis and tectonic implications. *Sci. China (D)* **50**, 1-16.

Ling W., Gao S., Zhang B., Li H., Liu Y. and Cheng J. (2003) Neoproterozoic tectonic evolution of the northwestern Yangtze Craton, South China: implications for amalgamation and break-up of the Rodinia Supercontinent. *Precambrian Res.* **122**, 111-140.

Liu D.Y., Nutman A.P., Compston W., Wu J.S. and Shen Q.H. (1992) Remnants of ≥3800Ma crust in the Chinese part of the Sino-Korean Craton. *Geology* **20**, 339-342.

Liu Y.L., Yang G., Chen J.F., Du A.D. and Xie Z. (2004) Re-Os dating of pyrite from giant Bayan Obo REE-Nb-Fe deposit. *Chinese Sci. Bull.* **24**, 2627-2631.

Liu D.Y., Wilde S.A., Wan Y.S., Wu J.S., Zhou H.Y., Dong C.Y. and Yin X.Y. (2008) New U-Pb and Hf isotopic data confirm Anshan as the oldest preserved segment of the North China Craton. *Am. J. Sci.* **308**, 200-231.

Liu D.Y., Wilde S.A., Wan Y.S., Wang S., Valley J.W., Kita N., Dong C., Xie H., Yang C., Zhang Y. and Gao L. (2009) Combined U-Pb, hafnium and oxygen isotope analysis of zircons from meta-igneous rocks in the southern North China Craton reveal multiple events in the Late Mesoarchean-Early Neoarchean. *Chem. Geol.* **261**, 140-154.

Lu S.N., Li H.K., Zhang C.L. and Niu G.H. (2008) Geological and geochronological evidence for the Precambrian evolution of the Tarim Craton and surrounding continental fragments. *Precambrian Res.* **160**, 94-107.

Nutman A.P., Friend C.R.L. and Bennett V.C. (2001) Review of the oldest (4400-3600 Ma) geological and mineralogical record: glimpses of the beginning. *Episodes* **24**, 93-101.

Peng P., Zhai M.G., Ernst R.E., Guo J.H., Liu F. and Hu B. (2008) A 1.78 Ga large igneous province in the North China Craton: the Xiong'er Volcanic Province and the North China dyke swarm. *Lithos* **101**, 260-280.

Qiu H.N. (1996) ^{40}Ar-^{39}Ar dating of the quartz samples from two mineral deposits in western Yunnan (SW China) by crushing in vacuum. *Chem. Geol.* **127**, 211-222.

Qiu H.N. and Jiang Y.D. (2007) Sphalerite $^{40}Ar/^{39}Ar$ progressive crushing and stepwise heating techniques. *Earth Planet. Sci. Lett.* **256**, 224-232.

Qiu Y.M., Gao S., McNaughton N.J., Groves D.L. and Ling W.L. (2000) First evidence of >3.2 Ga continental crust in the Yangtze Craton of South China and its implications for Archean crustal evolution and Phanerozoic tectonics. *Geology* **28**, 11-14.

Qiu H.N., Zhu B.Q. and Sun D.Z. (2002) Age significance interpreted from ^{40}Ar-^{39}Ar dating of quartz samples from the Dongchuan Copper Deposits, Yunnan, SW China, by crushing and heating. *Geochem. J.* **36**, 475-491.

Tu G.Z., Chow T.J., Yu J.S., Chen Y.W. and Li Y.S. (1998) *Isotope Geochemistry Researches in China*. Science Press, Beijing, 590 pp.

Wang J. and Li Z.X. (2003) History of Neoproterozoic rift basins in South China: implications for Rodinia breakup. *Precambrian Res.* **122**, 141-158.

Wang J., Li X.H., Duan T.Z., Liu D.Y., Song B., Li Z.X. and Gao, Y.H. (2003) Zircon SHRIMP U-Pb dating for the Cangshuipu volcanic rocks and its implications for the lower boundary age of the Nanhua strata in South China. *Chinese Sci. Bull.* **48**, 1663-1669.

Wang X.L., Zhou J.C., Qiu J.S., Zhang W.L., Liu X.M. and Zhang G.L. (2006a) LA-ICP-MS U-Pb zircon geochronology of the Neoproterozoic igneous rocks from northern Guangxi, South China: implications for tectonic evolution. *Precambrian Res.* **145**, 111-130.

Wang F., Zhou X.H., Zhang L.C., Ying J.F., Zhang Y.T., Wu F.Y. and Zhu R.X. (2006b). Late Mesozoic volcanism in the Great Xing'an Range (NE China): Timing and implications for the dynamic setting of NE Asia. *Earth Planet. Sci. Lett.* **251**, 179-198.

Wang X.C., Li X.H., Li W.X. and Li Z.X. (2007) Ca. 825 Ma komatiitic basalts in South China: first evidence for >1500 °C mantle melts by a Rodinian mantle plume. *Geology* **35**, 1103-1106.

Wang X.C., Li X.H., Li W.X., Li Z.X., Liu Y., Yang Y.H., Liang X.R. and Tu X.L. (2008) The Bikou basalts in northwestern Yangtze Block, South China: remnants of 820-810 Ma continental flood basalts? *Geol. Soc. Am. Bull.* **120**, 1478-1492.

Wu F.Y., Sun D.Y., Li H.M., Jahn B.M. and Wilde S.A. (2002) A-type granites in northeastern China: age and geochemical constraints on their petrogenesis. *Chem. Geol.* **187**, 143-173.

Wu F.Y., Jahn B.M., Wilde S.A., Lo C.H., Yui T.F., Lin Q., Ge W.C. and Sun D.Y. (2003) Highly fractionated I-type granites in NE China (I): geochronology and petrogenesis. *Lithos* **66**, 241-273.

Wu F.Y., Lin J.Q., Wilde S.A., Zhang X.O. and Yang J.H. (2005a) Nature and significance of the Early Cretaceous giant igneous event in eastern China. *Earth Planet. Sci. Lett.* **233**, 103-119.

Wu F.Y., Yang J.H., Wilde S.A. and Zhang X.O. (2005b) Geochronology, petrogenesis and tectonic implications of Jurassic granites in the Liaodong Peninsula, NE China. *Chem. Geol.* **221**, 127-156.

Wu F.Y., Zhang Y.B., Yang J.H., Xie L.W. and Yang Y.H. (2008) Zircon U-Pb and Hf isotopic constraints on the Early Archean crustal evolution in Anshan of the North China Craton. *Precambrian Res.* **167**, 339-362.

Xiong Q., Zheng J.P, Yu C.M., Su Y.P., Tang H.Y. and Zhang Z.H. (2009) Zircon U-Pb age and Hf isotope of Quanyishang A-type granite in Yichang: signification for the Yangtze continental cratonization in Paleoproterozoic. *Chinese Sci. Bull.* **54**, 436-446.

Xu B., Jian P., Zheng H., Zou H., Zhang L. and Liu D.Y. (2005) U-Pb zircon geochronology and geochemistry of Neoproterozoic volcanic rocks in the Tarim Block of northwest China: implications for the breakup of Rodinia supercontinent and Neoproterozoic glaciations. *Precambrian Res.* **136**, 107-123.

Xu B., Xiao S.H., Zou H.B., Chen Y., Li Z.X., Song B., Liu D.Y., Zhou C.M. and Yuan X.L. (2009) SHRIMP zircon U-Pb age constraints on Neoproterozoic Quruqtagh diamictites in NW China. *Precambrian Res.* **168**, 247-258.

Yang J.H. and Zhou X.H. (2001) Rb-Sr, Sm-Nd and Pb isotope systematics of pyrite: implications for the age and genesis of lode gold deposits. *Geology* **29**, 711-714.

Yang J.H., Wu F.Y., Chung S.L., Wilde S.A., Chu M.F., Lo C.H. and Song B. (2005) Petrogenesis of Early Cretaceous intrusions in the Sulu ultrahigh-pressure orogenic belt, east China and their relationship to lithospheric thinning. *Chem. Geol.* **222**, 200-231.

Yang J.H., Wu F.Y., Wilde S.A. and Zhao G.C. (2008a) Petrogenesis and geodynamics of Late Archean magmatism in eastern Hebei, eastern North China Craton: Geochronological, geochemical and Nd-Hf isotopic evidence. *Precambrian Res.* **167**, 125-149.

Yang J.H., Wu F.Y., Wilde S.A., Belousova E. and Griffin W.L. (2008b) Mesozoic decratonization of the North China block. *Geology* **36**, 467-470.

Yu J.S. and Li Y.S. (1997) *Isotope Geochemistry Researches in China*. Science Press, Beijing, 621 pp (in Chinese).

Yu G., Yang G., Chen J.F., Qu W.J., Du A.D. and He W. (2005) Re-Os dating of gold-bearing arsenopyrite of the Maoling gold deposit, Liaoning Province, northeast China and its geological significance. *Chinese Sci. Bull.* **50**, 1509-1514.

Zhai M.G. and Liu W.J. (2003) Palaeoproterozoic tectonic history of the North China Craton: a review. *Precambrian Res.* **122**, 183-199.

Zhang C.L., Wang Z., Shen J.L., Bi H., Guo K.Y. and Wang A.G. (2003) Zircon SHRIMP dating and geochemistry characteristics of Akazi rock mass of western Kunlun. *Acta Petrol. Sin.* (in Chinese with English abstract) **19**, 523-529.

Zhang S.B., Zheng Y.F., Wu Y.B., Zhao Z.F., Gao S. and Wu F.Y. (2006a) Zircon isotope evidence for ≥3.5 Ga continental crust in the Yangtze Craton of China. *Precambrian Res.* **146**, 16-34.

Zhang S.B., Zheng Y.F., Wu Y.B., Zhao Z.F., Gao S. and Wu F.Y. (2006b) Zircon U-Pb age and Hf-O isotope evidence for Paleoproterozoic metamorphic event in South China. *Precambrian Res.* **151**, 265-288.

Zhang S.H., Liu S.W., Zhao Y., Yang J.H., Song B. and Liu X.M. (2007a) The 1.75-1.68 Ga anorthosite-mangerite-alkali granitoid-Rapakivi granite suite from the northern North China Craton: magmatism related to a Paleoproterozoic orogen. *Precambrian Res.* **155**, 287-312.

Zhang C.L., Li X.H., Li Z.X., Lu S.N., Ye H.F. and Li H.M. (2007b) Neoproterozoic ultramafic-mafic-carbonatite complex and granitoids in Quruqtagh of northeastern Tarim Block, western China: geochronology, geochemistry and tectonic implications. *Precambrian Res.* **152**, 149-168.

Zhang S.B., Zheng Y.F., Zhao Z.F., Wu Y.B., Liu X.M. and Wu F.Y. (2008a) Neoproterozoic anatexis of Archean lithosphere:geochemical evidence from felsic to mafic intrusives at Xiaofeng in the Yangtze George, South China. *Precambrian Res.* **163**, 210-238.

Zhang Q.R., Li X.H., Feng L.J., Huang J. and Biao S. (2008b) A new age constraint on the onset of the Neoproterozoic glaciations in the Yangtze Platform, South China. *J. Geol.* **116**, 423-429.

Zhang S.H., Jiang G. and Han Y. (2008c) The age of the Nantuo Formation and Nantuo glaciation in South China. *Terra Nova* **20**, 289-294.

Zhang J.H., Ge W.C., Wu F.Y., Wilde S.A., Yang J.H. and Liu X.M. (2008d). Large-scale Early Cretaceous volcanic events in the northern Great Xing'an Range, Northeastern China. *Lithos* **102**, 138-157.

Zhang S.H., Zhao Y., Yang Z.Y., He Z.F. and Wu H. (2009a) The 1.35 Ga diabase sills from the northern North China Craton: implications for breakup of the Columbia (Nuna) supercontinent. *Earth Planet. Sci. Lett.* **288**, 588-600.

Zhang S.H., Zhao Y., Song B., Hu J.M., Liu S.W., Yang Y.H., Chen F.K., Liu X.M., and Liu J. (2009b) Contrasting Late Carboniferous and Late Permian-Middle Triassic intrusive suites from the northern margin of the North China Craton: geochronology, petrogenesis, and tectonic implications. *Geol. Soc. Am. Bull.* **121**, 181-200

Zhao G.C., Wilde S.A., Cawood P.A. and Lu L.Z. (1999) Tectonothermal history of the basement rocks in the western zone of the North China Craton and its tectonic implications. *Tectonophysics* **310**, 37-53.

Zhao G.C., Sun M., Wilde S.A. and Li S. (2005a) Late Archean to Paleoproterozoic evolution of the North China Craton: key issues revisited. *Precambrian Res.* **136**, 177-202.

Zhao G.C., Sun M., Wilde S.A. and Li S. (2005b) A Paleo-Mesoproterozoic supercontinent: assembly, growth and breakup. *Earth Sci. Rev.* **67**, 91-123.

Zhao G.C., Kröner A., Wilde S.A., Sun M., Li S., Li X., Zhang J., Xia X. and He Y. (2007) Lithotectonic elements and geological events in the Hengshan-Wutai-Fuping belt: a synthesis and implications for the evolution of the Trans-North China Orogen. *Geol. Mag.* **144**, 753-775.

Zheng Y.F., Zhang S.B., Zhao Z.F., Wu Y.B., Li X., Li Z. and Wu F.Y. (2007) Contrasting zircon Hf and O isotopes in the two episodes of Neoproterozoic granitoids in South China: implications for growth and reworking of continental crust. *Lithos* **96**, 127-150.

Zheng Y.F., Wu R.X., Wu Y.B., Zhang S.B., Yuan H.L. and Wu F.Y. (2008) Rift melting of juvenile arc-derived crust: geochemical evidence from Neoproterozoic volcanic and granitic rocks in the Jiangnan Orogen, South China. *Precambrian Res.* **163**, 351-383.

Zhou M.F., Yan D.P., Kennedy A.K., Li Y. and Ding J. (2002) SHRIMP U-Pb zircon geochronological and geochemical evidence for Neoproterozoic arc-magmatism along the western margin of the Yangtze Block, South China. *Earth Planet. Sci. Lett.* **196**, 51-67.

Zhou C.M., Tucker R. and Xiao S.H. (2004) New constraints on the age of Neoproterozoic glaciation in South China. *Geology* **32**, 437-440.

Figure Captions

Figure 1. Sketched tectonic map of China showing the major Precambrian cratons and younger orogens.

Figure 2. Histogram of isotopic ages for Mesozoic igneous rocks form eastern China: (a) the XMOB in NE China, (b) the eastern NCC, and (c) the southeastern SCB.

Geochemical applications of in situ isotopic analyses by laser ablation

Fu-Yuan WU [a,*]

[a] State Key Laboratory of Lithospheric Evolution, Institute of Geology and Geophysics, Chinese Academy of Sciences, Beijing 100029, China

[*] corresponding author's email: wufuyuan@mail.igcas.ac.cn

Full Text (3.5 Mb PDF)

Fu-Yuan WU

About the Author

Fu-Yuan Wu is a professor and the deputy director of the Institute of Geology and Geophysics, Chinese Academy of Sciences. He obtained his PhD in 1990 from Changchun College of Geology (now the College of Earth Sciences in Jilin University). He worked on granite petrology in Changchun until 2003, when he moved to the Institute of Geology and Geophysics in Beijing. His research is focused on granite petrogenesis, mantle geochemistry, geochronology, and isotopic geochemistry. He is a member of editorial board for *Chemical Geology*.

Abstract

Isotopic compositions of geological material are a kind of 'DNA' that has been widely used in geochemistry to identify various sources of rocks and processes that have shaped our Earth. Traditionally, radiogenic Sr, Nd and Hf isotopic ratios were determined on whole-rock samples through dissolution, chemical separation using time-consuming liquid chromatographic exchange and measurement by thermal ionization mass spectrometry (TIMS). This kind of bulk analysis cannot provide spatial information with high resolution, although it is commonly thought that most geological materials are heterogeneous in both occurrence and composition. The advent of inductively coupled plasma mass spectrometry (ICP-MS), however, makes it possible to measure isotopic ratios on the scale of sub-grains if laser ablation sampling is used. China, like other countries in the world, has installed numerous quadruple and multi-collector (MC) ICP-MS instruments with laser ablation systems, which are currently being used for *in situ* zircon U-Pb dating, and Sr-Nd and Hf isotopic measurements. After reviewing technical developments, this paper briefly describes the geochemical applications of *in situ* laser ablation techniques for *in situ* isotopic analysis of minerals, deciphering the petrogenesis of magmatic rocks, and identifying sediment provenances.

Keywords: Geochemical applications; Isotopic analysis; *In situ* analysis; Laser ablation

1. Introduction

Traditionally, isotopic data were obtained by chemical separation using ion-exchange columns after complete sample digestion, followed by purification of Sr, Nd and Hf fractions, and then measurement by Thermal Ionization Mass Spectrometry (TIMS). However, this solution method is a bulk analysis and the obtained isotope data are therefore an average of the sample. Since natural geological materials are generally heterogeneous, isotopic analyses should be conducted using high resolution micro-analytical techniques, such as *in situ* analyses by Secondary Ionization Mass Spectrometry (SIMS) and Laser Ablation (LA) Inductively Coupled Plasma Mass Spectrometry (ICP-MS), or Multi-collector (MC) ICP-MS. During the past few decades, *in situ* LA-(MC) -ICP-MS techniques have developed rapidly, and have been widely applied in geochemistry, including measurements of trace elements, radiogenic Pb, Sr, Nd, Hf and Os isotopes, and non-traditional Li, B and Mg isotopes (Sylvester, 2001, 2008).

Chinese Earth sciences have greatly benefited from the above technical developments since the first installation of ICP-MS in early 1990s. Subsequently, laser ablation attached analytical systems have been established in numerous universities and institutes, with *in situ* laser ablation data first reported for Pb isotopes by Liu et al. (1998) and Yan et al. (1998), for Sr isotopes by Wei et al. (2002), for Nd isotopes by Yang et al. (2008) and for Hf isotopes by Li et al. (2003).

2. In situ laser ablation techniques

LA-ICP-MS analytical systems consist of three essential parts, LA (laser ablation), ICP (Inductively coupled plasma) and MS (mass spectrometry, quadruple (Q) or multi-collector (MC)). Whatever isotopes are being analysed, instrumental mass bias or discrimination, elemental fractionation and potential matrix effects must be overcome.

2.1 *In situ* zircon U-Pb age determination

The first *in situ* zircon U-Pb age data conducted by laser ablation were published in early 1990s (Feng et al., 1993; Fryer et a., 1993). Due to the low efficiency of older generation laser systems, only $^{207}Pb/^{206}Pb$ ages from Precambrian zircons were obtained by these pioneer works. To overcome elemental fractionation, Li et al. (2000) proposed a raster scanning mode to get reliable age data for the Phanerozoic zircons. Subsequently, Li et al. (2001) developed a method to simultaneously obtain U-Pb age and trace element compositions, which was used by Yuan et al. (2003, 2004) and many others (Liu et al., 2007; Xie et al., 2008). Since then, laser ablation has become a common method for zircon U-Pb age measurements in China although, two SIMS instrument facilities, SHRIMP II and CAMECA 1280, have also been established (Liu et al., 2006; Li et al., 2009). Laser ablation has now become a routine technique to date zircon and other accessory minerals, such as baddeleyite, monazite, titanite, rutile, allanite, perovskite, xenotime, eudialyte, zirconolite, calzirtite, uraninite, and davidite (KoÅ¡ler et al., 2001; Jackson et al., 2004; Chang et al., 2006; Simonetti et al., 2006; Cocherie and Robert, 2008; Frei and Gerdes, 2009). In China, for example, perovskite, titanite and eudialyte have been dated by U-Pb using *in situ* laser ablation techniques (Yang et al., 2009; Wu et al., 2010a; Li et al., 2010). The U-Pb ages obtained by laser ablation in China were mostly with quadruple ICP-MS. There is no report that ion counters in MC-ICP-MS instruments have been used, which would permit more accurate detection of common lead.

2.2 *In situ* Sr isotopic analysis

The first reported *in situ* Sr isotopic analysis was by Christensen et al. (1995) on gastropods and plagioclase crystals. With 150-300 μm spot sizes and raster mode, they obtained $^{87}Sr/^{86}Sr$ ratios identical within errors to those obtained by TIMS analyses. Since then, in situ Sr isotopic data have been reported for apatite, carbonate, allanite, titanite, clinopyroxene, perovskite, eudialyte, basalt groundmass and melt inclusions (c.f. Vroon et al., 2008). Lately, Sr isotopic analysis of fluid inclusions has been reported from China (Yuan et al., 2009). The main obstacle in Sr isotopic analysis is interference of ^{87}Rb on ^{87}Sr, which requires that the analysed material must have extremely low Rb/Sr ratios ofin situ Sr isotopic data have great potential to decipher the petrogenesis of magmatic rocks, melt-rock interactions, and seawater isotopic variations (Davidson et al., 2007), although high precision Sr isotopic data comparable to Nd isotopic data are difficult to obtain (Figure 1a).

2.3 *In situ* Nd isotopic analysis

Nd isotopic compositions are important tracers for petrogenesis and

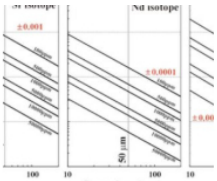

Figure 1

Nd isotopic compositions are important tracers for petrogenesis and crust-mantle evolution of the Earth. However, there is a paucity of studies of mineral *in situ* Nd isotopic analyses except for apatite, titanite, ferromanganese nodules, perovskite, monazite, allanite, eudialyte, zirconolite, and calzirtite (Foster and Vance, 2006; McFarlane and McCulloch, 2007; Yang et al., 2009; Wu et al., 2010b, 2010c). Theoretically, any material with high Nd concentrations can be analyzed *in situ* for Nd isotopes. For example, a precision of 100 ppm can be obtained for 60-80μm spot sizes (Figure 1b) on NIST610, which has a Nd concentration of 440 ppm (Yang et al., 2008). The main difficulty is isobaric interferences of Ce and Sm on Nd, which can be reasonably corrected (Yang et al., 2009).

Although high precision *in situ* Nd isotopic compositions are easier to obtain than those of Sr, appropriate external standards for *in situ* Nd isotopic analysis are lacking because almost all natural materials show some variations in Sm/Nd ratios. Synthetic standards have been recently developed (McFarlane and McCulloch, 2007), but natural mineral standards are required to overcome potential matrix effects.

2.4 In situ Hf isotopic analysis

Hf is another important isotopic tracer used to study geological processes. However, Hf isotopes cannot be determined easily by traditional TIMS techniques, and MC-ICP-MS techniques are best suited for Hf isotopic analysis. In terms of *in situ* analysis by laser ablation, the minerals commonly used are zircon and baddeleyite since both of them have high Hf concentrations and low Lu/Hf ratios (Thirlwall and Walder 1995; Griffin et al., 2000; Kinny and Mass, 2003; Wu et al., 2007). More recently, Hf isotopic compositions have been reported for eudialyte, zirconolite and calzirtite (Wu et al., 2010b). The main interference is ^{176}Yb on ^{176}Hf. This correction was traditionally done assuming Yb has the same fractionation as Hf during the analysis (Li et al., 2003; Xu et al., 2004), but later experiments indicated that this is not the case (Woodhead et al., 2004; Iizuka and Hirata, 2005; Wu et al., 2006). Therefore, the most commonly used protocol is measuring the mass bias of Yb directly during analyses. Evidently, it is impossible to get reliable Hf isotopic data if the Yb/Hf ratio is as high as 0.02 (Wu et al., 2006). In our experience, the minerals that can be analyzed *in situ* for Hf isotopes include zircon, baddeleyite, rutile, eudialyte, zirconolite and calzirtite. With a spot size of 60 μm or less, Hf concentrations in excess of 1000 ppm are required to get reasonable Hf isotopic ratios (Figure 1c).

In situ analytical techniques developed in China include the simultaneous determination of zircon U-Pb ages, Hf isotopic compositions and trace element contents (Yuan et al., 2008; Xie et al., 2008). The ablated aerosol is carried by helium and split into two transport tubes using a three-way pipe and introduced simultaneously into the Q-ICPMS and MC-ICPMS. The proportion of ablated material carried into the two instruments was controlled by three mass flow controllers. There is no significant mass fractionation when different proportions of ablated material were carried into the Q-ICPMS and MC-ICPMS (Xie et al., 2008). This simultaneous technique can also be applied to other accessory minerals for U-Pb ages, Sr or Nd isotopic compositions and trace element analyses (Yang et al., 2009; Wu et al., 2010a, 2010b), such as used in metamorphic zirconology (Xia et al., 2009; Chen et al., 2010). Table 1 presents a summary of object minerals that can be analyzed by the simultaneous *in situ* technique.

Table 1 Simultaneous determination of isotopic compositions using Q-ICP-MS and MC-ICP-MS

Q-ICP-MS	MC-ICP-MS	Mineral
U-Pb age and/or trace elements	Sr isotopes	Apatite, calcite, allanite, epidote, titanite, perovskite, eudialyte
	Nd isotopes	Apatite, calcite, titanite, perovskite, mozanite, allanite, epidote, eudialyte, zirconolite, calzirtite
	Hf isotopes	Zircon, baddeleyite, eudialyte, zirconolite, calzirtite

Another achievement is the combined analyses of Hf isotope by MC-ICP-MS and O isotope by CAMECA 1280 for zircons (Li et al., 2009b, 2010), a technique that has been used by other researchers to decipher the petrogenesis of granite and continental crustal growth (Hawkesworth and Kemp, 2006; Kemp et al., 2006, 2007). Similarly, numerous studies in China have used a combination of *in situ* U-Pb dating, Hf isotopic compositions and O isotope analysis (Zhang et al., 2006, 2008; Zheng et al., 2006, 2007; Zhao et al., 2008).

3. Geochemical applications

3.1 Isotopic investigation of eudialyte

Eudialytes are a group of complex Na-Ca zirconosilicate minerals that generally occur in peralkaline agpaitic syenites. Given that eudialytes are easily altered and commonly contain inclusions of earlier-crystallized minerals, *in situ* laser ablation is the most suitable method to determine their U-Pb ages, and Sr, Nd and Hf isotopic compositions. Electron microprobe and LA-ICP-MS analysis of eudialytes from nepheline syenites in numerous localities indicate that this mineral typically has high contents of U, Pb, Nb, Ta, Zr, Hf and REEs. Analysis of an in-house standard eudialyte by both solution and laser ablation methods demonstrates that precise and accurate U-Pb ages can be obtained after correction for the common Pb content. The high Sr, Nd and Hf contents in most eudialyte, coupled with the generally low Rb/Sr and Lu/Hf ratios, also permit the precise determination of *in situ* Sr, Nd and Hf isotopic ratios by LA-MC-ICP-MS methods. In our experience, eudialyte is the only mineral investigated to date for which it is possible to determine simultaneously U-Pb ages and Sr, Nd and Hf isotopic compositions (Wu et al., 2010b).

3.2 Hf isotopic constraint on magma mixing

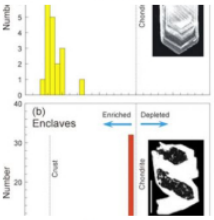

Figure 2

Magma mixing has been widely recognized from field observations, whole rock geochemistry and Nd and Sr isotopic data in both plutonic and volcanic environments. The basis of such interpretations is the recognition of the primitive sources of mafic and felsic magmas. However, identifying the specific sources that contributed to the origin of granitoids has long been a problem, since both magma mixing and wall-rock assimilation can significantly modify the rock chemistry. This can result in homogeneous Nd and Sr isotopic compositions in what were initially discrete components within a single pluton or batholith. Considering that zircon, a ubiquitous accessory mineral in both granites and enclosed microgranular enclaves, is extremely resistant to later geological processes and can survive post-crystallization thermal disturbances, Yang et al. (2007) conducted a comprehensive *in situ* zircon U-Pb and Hf isotopic study of mafic microgranular enclaves and host granitoids from the Early Cretaceous Gudaoling batholith in NE China. The zircon U-Pb age of the enclaves (120 ± 1 Ma) is identical to that of the host monzogranite (120 ± 1 Ma), establishing that the mafic and felsic magmas were coeval. The enclaves have $\varepsilon_{Hf}(t)$ values of +4.5 to -6.2, which is distinct from $\varepsilon_{Hf}(t)$ of -15.1 to -25.4 obtained for the host monzogranite (Figure 2). This indicates that both depleted mantle and ancient crustal sources contributed to their origin. The depleted mantle component was not previously revealed by whole-rock geochemical and Sr-Nd isotopic studies, demonstrating that the zircon Hf isotopic data can be a powerful geochemical tracer with the potential to provide unique petrogenetic information. Some ancient crustal contamination is indicated by inherited zircons with considerably older U-Pb ages and low $\varepsilon_{Hf}(t)$ values. Hafnium isotopic variations in

the Early Cretaceous zircons rule out simple crystal-liquid fractionation or restite unmixing as the major genetic link between enclaves and host rocks. Instead, mixing of mantle-derived mafic and ancient crustal-derived felsic magmas can reasonably explain these data (Yang et al., 2007).

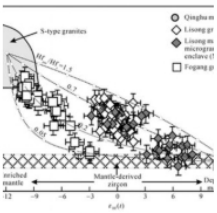

Figure 3

An interesting discovery during previous studies is that zircons from granites always show Hf isotopic variations, which are definitively beyond the analytical precision, and should shed light on the composition of magma from which the zircon crystallized. A typical example comes from Hf-O isotopic analyses of granites in southeastern China by Li et al. (2009b), who demonstrated that granitic rocks (Figure 3), whether granite (Lisong granite), dioritic enclave (Lisong diorite) or individual pluton (Fogang granite), show a systematic Hf-O variation, such as previously shown by Kemp et al. (2007) for the granites in the Lachlan Fold Belt of southeastern Australia. Evidently, the studied Lisong dioritic enclave crystallized from depleted mantle-derived magma which is constrained by data from the Qinghu monzonite, whereas the Lisong and Fogang granites were formed by magma mixing to varying degrees between mantle- and crustal-derived melts. Therefore, *in situ* analysis of zircon Hf-O isotopes is a powerful tool to identify mixing during magma evolution.

3.3 Juvenile Hf isotopic compositions of the Ladakh-Gangdese batholith in Tibet

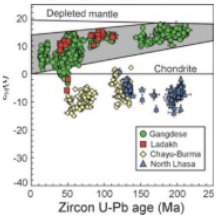

Figure 4

In Tibet, during oceanic closure, terrane amalgamation and collision and subsequent post-orogenic processes between India and Asia, resulted in the production of various kinds of granites. The best studied granites in the region are the Transhimalayan batholith, exposed along the southern margin of the Lhasa terrane and extending from the Kohistan-Ladakh batholith in the west through the Gangdese batholith in the middle to the Chayu-western Yunnan (Dianxi)-Burma batholith in the east, with a length of >3000km. Although this gigantic batholith has attracted much academic attention over the past decades, its geochronological framework, petrogenesis and relationship with Tethysan ocean closure and India-Asia collision remain unclear. Our U-Pb age data suggest four discrete stages of magmatic activities, specifically ~205-152, ~109-80, ~65-41 and ~33-13 Ma, with the stage of 65-41 Ma being the most prominent. The Hf isotopic data indicate that the Gangdese batholith has positive $\varepsilon_{Hf}(t)$ values (Figure 4, Chiu et al., 2009; Ji et al., 2009), which are comparable to those of the Kohistan-Ladakh batholiths in the west (Ravikant et al., 2009), but markedly different from those of the Chayu-Burma batholiths in the east (Liang et al., 2008). This newly established zircon U-Pb age and Hf isotope database for the Gangdese batholith can be used as a tracer for the source-to-sink relation of the sediments eroded from the southern Tibetan Plateau (Liang et al., 2008; Cina et al., 2009; Hoang et al., 2009; Wu et al., 2010c).

3.4 *In situ* Sr-Nd isotopic compositions of Mengyin kimberlitic perovskites

Kimberlite is a kind of igneous rock from which the initial isotopic compositions of magmas are hard to be obtained because it is commonly contaminated by both crustal and mantle materials and also shows extensive alteration and weathering following emplacement. Fortunately, perovskite ($CaTiO_3$) can be used to circumvent this problem since it occurs mainly in the kimberlite groundmass and crystallizes early in the magmatic history, along with ilmenite, rutile and magnesian chromite. Therefore, perovskite has the potential to record the primary geochemical and isotopic signature of the magma prior to any contamination. Furthermore, perovskite is normally resistant to weathering and tends to remain fresh when other constituents have been intensely altered.

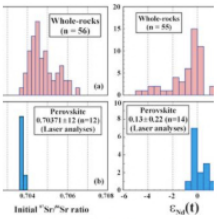

Figure 5

Numerous kimberlitic samples from Mengyin in eastern China were selected for U-Pb dating and Sr-Nd-Hf isotopic analysis of perovskite. *In situ* U-Pb analyses of fresh perovskite yield an age of 470 ± 4 Ma, which is considered the emplacement age of the Mengyin kimberlite. However, altered perovskite shows Pb loss and yields Paleozoic-Mesozoic ages, indicating that perovskite is not as resistant to isotopic modification as suggested previously. *In situ* Sr-Nd isotopic analyses by laser ablation of perovskite grains collected from the main Mengyin kimberlite record uniform Sr and Nd isotopic compositions with an average initial 87Sr/86Sr ratio of 0.70371 ± 12 and $\varepsilon_{Nd}(t)$ value of 0.13 ± 0.22, which are identical, within uncertainties, to the values obtained by solution analyses of the perovskite. However, they are significantly different from the whole rock data (Figure 5), indicating that initial Sr-Nd isotopic ratios calculated from whole rock measurements on kimberlites are likely to record mixed isotopic signatures due to crustal contamination and subsequent alteration. This conclusion is also supported by the Hf isotopic data for perovskite. Therefore, our studies (Yang et al., 2009; Wu et al., 2010a), combined with those by others (Paton et al., 2007a, 2007b; Woodhead et al., 2009), indicate that meaningful isotopic ratios for kimberlite can only be obtained from single minerals such as perovskite.

4. Concluding remarks

Most natural materials show compositional zoning, hence isotopic variations within individual mineral grains are vital to deciphering precise and detailed geodynamic processes. For this reason, *in situ* laser ablation analysis has become an important frontier in geochronology and isotopic geochemistry. LA-(MC)-ICP-MS techniques have distinct advantages over traditional bulk analysis. Firstly, *in situ* laser ablation can decipher subtle isotopic variations at high spatial resolution on a sub-grain scale. For example, we can obtain reliable isotopic data from thin section with clear petrogenetic implications. Secondly, LA-(MC)-ICP-MS works under atmospheric pressure, which makes it convenient to change the sampling mode during analyses. Thirdly, laser ablation does not need time-consuming sample preparation, with isotopic analyses within minutes. However, laser ablation is destructive to the sample, although the consumed volume is much smaller than by the traditional TIMS method, but larger than SIMS, which has an ablation depth of only 2-3 μm. Therefore, for precious samples, such as minerals from meteorites, our suggestion is that the laser ablation should be conducted after SIMS analyses. Other factors that should be considered during laser ablation analyses are the potential matrix effects, necessitating the use of various standards. In addition, *in situ* laser ablation is a relative analysis, with TIMS being the only analysis that produces absolute isotopic data.

Acknowledgments

This study has been financially supported by the Natural Science Foundation of China and the Chinese Academy of Sciences. Thanks are given to Yue-Heng Yang, Lie-Wen Xie, Jin-Hui Yang and Yan-Bin Zhang for their help during analytical development of the above-mentioned isotope analyses. Yue-Heng Yang also helped to complete the Figure 1. Yong-Fei Zheng read the early draft and provided invaluable suggestions.

References

Chang Z. S., Vervoort, J. D., McClelland W. C. and Knaack, C. (2006) U-Pb dating of zircon by LA-ICP-MS. *Geochemistry, Geophysics, Geosystems* **7**, 2005GC001100.

Chen R.-X., Zheng Y.-F. and Xie L.-W. (2010) Metamorphic growth and recrystallization of zircon:

Chen R. X., Zheng Y. F. and Xie L. W. (2010) Metamorphic growth and recrystallization of zircon: distinction by simultaneous in-situ analyses of trace elements, U-Th-Pb and Lu-Hf isotopes in zircons from eclogite-facies rocks in the Sulu orogen. *Lithos* **114**, 132-154.

Chiu H. Y., Chung S. L., Wu F. Y., Liu D. Y., Liang Y. H., Lin I. J., Iizuka Y., Xie L. W., Wang Y. B. and Chu M. F. (2009) Zircon U-Pb and Hf isotopic constraints from eastern Transhimalayan batholiths on the pre-collisional magmatic and tectonic evolution in southern Tibet. *Tectonophysics* **477**, 3-19.

Christensen J. N., Halliday A. N., Lee D. C. and Hall C. M. (1995) *In situ* isotopic analysis by laser ablation. *Earth and Planetary Science Letters* **136**, 79-85.

Cina S. E., Yin A., Grove M., Dubey C. S., Shukla D. P., Lovera, O. M., Kelty T. K., Gehrels G. E. and Foster D. A. (2009) Gangdese arc detritus within the eastern Himalayan Neogene foreland basin: Implications for the Neogene evolution of the Yalu-Brahmaputra River system. *Earth and Planetary Science Letters* **285**, 150-162.

Cocherie A. and Robert M. (2008) Laser ablation coupled with ICP-MS applied to U-Pb zircon geochronology: A review of recent advances. *Gondwana Research* **14**, 597-608.

Davidson J. P., Morgan D. J., Charlier B. L. A., Harlou R. and Hora J. M. (2007) Microsampling and isotopic analysis of igneous rocks: implications for the study of magmatic systems. *Annual Review of Earth and Planetary Sciences* **35**, 273-311.

Feng R., Machado N. and Ludden J. (1993) Lead geochronology of zircon by laser-inductively coupled plasma mass spectrometry (ICP-MS). *Geochimica et Cosmochimica Acta* **57**, 3479-3486.

Foster G. L. and Vance D. (2006) *In situ* Nd isotopic analysis of geological materials by laser ablation MC-ICP-MS. *Journal of Analytical Atomic Spectrometry* **21**, 288-296.

Frei D. and Gerdes A. (2009) Precise and accurate *in situ* U-Pb dating of zircon with high sample throughput by automated LA-SF-ICP-MS. *Chemical Geology* **261**, 261-270.

Fryer B. J., Jackson S. E. and Longerich H. (1993) The application of laser ablation microprobe-inductively coupled plasma-mass spectrometry (LAM-ICP-MS) to *in situ* (U)-Pb geochronology. *Chemical Geology* **109**, 1-8.

Griffin W. L., Pearson N. J., Belousova E., Jackson S. E., van Achterbergh E., O'Reilly S. Y. and Shee, S. R. (2000) The Hf isotope composition of cratonic mantle: LAM-MC-ICPMS analysis of zircon megacrysts in kimberlites. *Geochimica et Cosmochimica Acta* **64**, 133-147.

Hawkesworth C. J. and Kemp A. I. S. (2006) Using hafnium and oxygen isotopes in zircons to unravel the record of crustal evolution. *Chemical Geology* **226**, 144-162.

Hoang V. L., Wu F. Y., Clift P. D., Wysocka A. and Swierczewska A. (2009) Evaluating the evolution of the Red River system based on in-situ U-Pb dating and Hf isotope analysis of zircons. *Geochemistry, Geophysics, Geosystems* **10**, 2009GC002819.

Iizuka T. and Hirata, T. (2005) Improvements of precision and accuracy in *in situ* Hf isotope microanalysis of zircon using the laser ablation-MC-ICPMS technique. *Chemical Geology* **220**, 121-137.

Jackson S. E., Pearson N. J., Griffin W. L. and Belousova E. A. (2004) The application of laser ablation-inductively coupled plasma-mass spectrometry (LA-ICP-MS) to *in situ* U-Pb zircon geochronology. *Chemical Geology* **211**, 47-69.

Ji W. Q., Wu F. Y., Chung S. L., Li J. X. and Liu C. Z. (2009) Zircon U-Pb geochronological and Hf isotopic constraints on petrogenesis of the Gangdese batholith in Tibet. *Chemical Geology* **262**, 229-245.

Kemp A. I. S., Hawkesworth C. J., Paterson B. A. and Kinny P. D. (2006) Episodic growth of the Gondwana supercontinent from hafnium and oxygen isotopes in zircon. *Nature* **439**, 580-583.

Kemp A. I. S., Hawkesworth C. J., Foster G. L., Paterson B. A., Woodhead J. D., Hergt J. M., Gray, C. M. and Whitehouse M. J. (2007) Magmatic and crustal differentiation history of granitic rocks from Hf-O isotopes in zircon. *Science* **315**, 980-983.

Kinny P. D. and Maas R. (2003) Lu-Hf and Sm-Nd isotope systems in zircon. In: Hanchar J. M. and Hoskin P. W. O (eds.), Zircon. *Reviews in Mineralogy and Geochemistry* **53**, 327-341.

KoÅ¡ler J., Tubrett M. and Sylvester P. (2001) Application of laser ablation ICPMS to U-Th-Pb dating of monazite. *Geostandards Newsletter* **25**, 375-386.

Li J. W., Deng X. D., Zhou M. F., Liu Y. S., Zhao X. F. and Guo J. L., 2010. Laser ablation ICP-MS titanite U-Th-Pb dating of hydrothermal ore deposits: A case study of the Tonglushan Cu-Fe-Au skarn deposit, SE Hubei Province, China. *Chemical Geology* **270**, 56-67.

Li X. H., Liang X., Sun M., Liu Y. and Tu X. L. (2000) Geochronology and geochemistry of single-grain zircons: Simultaneous *in-situ* analysis of U-Pb age and trace elements by LAM-ICP-MS. *European Journal of Mineralogy* **12**, 1015-1024.

Li X. H., Liang X. R., Sun M., Guan H. and Malpas G. (2001) Precise $^{206}Pb/^{238}U$ age determination on zircons by laser ablation microprobe-inductively coupled plasma-mass spectrometry using continuous linear ablation. *Chemical Geology* **175**, 209-219.

Li X. H., Liang X. R., Wei G. J. and Liu Y. (2003) Precise analysis of zircon Hf isotopes by LAM-MC-ICPMS (in Chinese with English abstract). *Geochimica* **32**, 86-90.

Li, X. H., Liu Y., Li Q. L., Guo C. H. and Chamberlain K. R. (2009a) Precise determination of Phanerozoic zircon Pb/Pb age by multi-collector SIMS without external standardization. *Geochemistry, Geophysics, Geosystems* **10**, 2009GC002400.

Li X. H., Li W. X., Wang X. C., Li Q. L., Liu Y. and Tang G. Q. (2009b) Role of mantle-derived magma in genesis of early Yanshanian granites in the Nanling Range, South China: *in situ* zircon Hf-O isotopic constraints. *Science in China (D)* **52**, 1262-1278.

Li X. H., Li W. X., Li Q. L., Wang X. C., Liu Y. and Yang Y. H. (2010) Petrogenesis and tectonic significance of the ~ 850 Ma Gangbian alkaline complex in South China: Evidence from *in situ* zircon U-Pb dating, Hf-O isotopes and whole-rock geochemistry. *Lithos* **114**, 1-15.

Liang Y. H., Chung S. L., Liu D. Y., Xu Y. G., Wu F. Y., Yang J. H., Wang Y. B. and Lo C. H. (2008) Detrital zircon evidence from Burma for reorganization of the eastern Himalayan river system. *American Journal of Science* **308**, 618-638.

Liu D. Y., Jian P., Kroner A. and Xu S. T. (2006) Dating of prograde metamorphic events deciphered from episodic zircon growth in rocks of the Dabie-Sulu UHP complex, China. *Earth and Planetary Science Letters* **250**, 650-666.

Liu H. C., Zhu B. Q. and Zhang Z. X. (1998) Single zircon dating by LAM-ICPMS (in Chinese). *Chinese Science Bulletin* **43**, 1103-1106.

Liu X. M., Gao S., Diwu C. R., Yuan H. L. and Hu C. C. (2007) Simultaneous *in-situ* determination of U-Pb age and trace elements in zircon by LA-ICP-MS in 20 μm spot size. *Chinese Science Bulletin* **52**, 1257-1264.

McFarlane C. R. M. and McCulloch M. T. (2007) Coupling of *in-situ* Sm-Nd systematics and U-Pb dating of monazite and allanite with applications to crustal evolution studies, *Chemical Geology* **245**, 45-60.

Paton C., Woodhead J., Hergt J., Phillips D. and Shee S. (2007a) Sr-isotope analysis of kimberlitic groundmass perovskite via LA-MCICPMS. *Geostandards and Geoanalytical Research* **31**, 321-330.

Paton C., Hergt J. M., Phillips D., Woodhead J. D. and Shee S. R. (2007b) New insights into the genesis of Indian kimberlites from the Dharwar Craton via *in situ* Sr isotope analysis of groundmass perovskite. *Geology* **35**, 1011-1014.

Ravikant V., Wu F. Y. and Ji W. Q. (2009) Zircon U-Pb and Hf isotopic constraints on petrogenesis of the Cretaceous-Tertiary granites in eastern Karakoram and Ladakh, India. *Lithos* **110**, 153-166.

Simonetti A., Heaman L. M., Hartlaub R. P., Creaser R. A., MacHattie T. G. and Bohm C. (2005) U-Pb zircon dating by laser ablation-MC-ICP-MS using a new multiple ion counting Faraday collector array. *Journal of Analytical Atomic Spectrometry* **20**, 677-686.

Sylvester P (ed). (2001) Principles and Applications. *Mineralogical Association of Canada, Short Course* **29**, 1-243.

Sylvester P (ed). (2008) Laser ablation ICP-MS in the Earth Sciences: current practices and outstanding issues. *Mineralogical Association of Canada, Short Course* **40**, 1-348.

Thirlwall M. F. and Walder A. J. (1995) *In situ* hafnium isotope ratio analysis of zircon by inductively coupled plasma multiple collector mass spectrometry. *Chemical Geology* **122**, 241-247.

Vroon P. Z., van der Wagt B., Koornneef J. M. and Davies G. R. (2008) Problems in obtaining precise and accurate Sr isotope analysis from geological materials using laser ablation MC-ICPMS. *Analytical and Bioanalytical Chemistry* **390**, 465-476.

Wei G. J., Liang X. R., Li X. H. and Liu Y. (2002) Precise measurement of Sr isotopic composition of liquid and solid base using (LA) MC-ICPMS (in Chinese with English abstract). *Geochimica* **31**, 295-299.

Woodhead J., Hergt J., Shelley M., Eggins S. and Kemp R. (2004) Zircon Hf-isotope analysis with an excimer laser, depth profiling, ablation of complex geometries, and concomitant age estimation. *Chemical Geology* **209**, 121-135.

Woodhead J., Hergt J., Phillips D. and Paton C. (2009) African kimberlites revisited: *in situ* Sr-isotope analysis of groundmass perovskite. *Lithos* **112s**, 311-317.

Wu F. Y., Yang Y. H., Xie L. W., Yang J. H. and Xu P. (2006) Hf isotopic compositions of the standard zircons and baddeleyites used in U-Pb geochronology. *Chemical Geology* **234**, 105-126.

Wu F. Y., Li X. H., Zheng Y. F. and Gao S. (2007) Lu-Hf isotopic systematics and their applications in petrology (in Chinese with English abstract). *Acta Petrologica Sinica* **23**, 185-220

Wu F. Y., Yang Y. H., Mitchell R. H. and Zhang Y. B. (2010a) *In situ* U-Pb age determination and Nd isotopic analyses of perovskites from kimberlites in southern Africa and Somerset Island, Canada. *Lithos* doi:10.1016/j.lithos.2009.12.010.

Wu F. Y., Yang Y. H., Marks M., Liu Z. C., Zhou Q., Ge W. C., Yang J. S., Zhao Z. F., Mitchell R. H. and Markl G. (2010b) *In situ* U-Pb, Sr, Nd, and Hf isotopic analysis of eudialyte by LA-(MC)-ICP-MS. *Chemical Geology* in press.

Wu F. Y., Ji W. Q., Liu C. Z. and Chung S. L. (2010c) Detrital zircon U-Pb and Hf isotopic constraints from the Xigaze fore-arc basin, southern Tibet on the source provenance and Transhimalaya magmatic evolution. *Chemical Geology* **271**, 13-25.

Xia Q.-X., Zheng Y.-F., Yuan H. L. and Wu F.-Y. (2009) Contrasting Lu-Hf and U-Th-Pb isotope systematics between metamorphic growth and recrystallization of zircon from eclogite-facies metagranite in the Dabie orogen, China. *Lithos* **112**, 477-496.

Xie L. W., Zhang Y. B., Zhang H. H., Sun J. F. and Wu F. Y. (2008) *In situ* simultaneous determination of trace elements, U-Pb and Lu-Hf isotopes in zircon and baddeleyite. *Chinese Science Bulletin* **53**, 1565-1573.

Xu P., Wu F. Y., Xie L. W. and Yang Y. H. (2004) Hf isotopic compositions of the standard zircons for U-Pb dating. *Chinese Science Bulletin* **49**, 1642-1648.

Yan X., Chu Z. Y., Sun M., Xu P. and Zhou X. H. (1998) $^{207}Pb/^{206}Pb$ determination of zircons by laser probe inductively coupled plasma mass spectrometry (in Chinese). *Chinese Science Bulletin* **43**, 2101-2105.

Yang J. H., Wu F. Y., Wilde S. A., Xie L. W., Yang Y. H. and Liu X. M. (2007) Tracing magma mixing in granite genesis: *in situ* U-Pb dating and Hf-isotope analysis of zircons. *Contributions to Mineralogy and Petrology* **153**, 177-190.

Yang Y. H., Sun J. F., Xie L. W., Fan H. R. and Wu F. Y. (2008) *In situ* Nd isotopic measurement of geological samples by laser ablation. *Chinese Science Bulletin* **53**, 1062-1070.

Yang Y. H., Wu F. Y., Wilde S. A., Liu X. M., Zhang Y. B., Xie L. W. and Yang J. H. (2009) *In-situ* perovskite Sr-Nd isotopic constraints on the petrogenesis of the Ordovician Mengyin kimberlites in the North China Craton. *Chemical Geology* **264**, 24-42.

Yuan H. L., Wu F. Y., Gao S., Liu X. M., Xu P. and Sun D. Y. (2003) Determination of U-Pb age and rare earth element concentrations of zircons from Cenozoic intrusions in northeastern China by laser ablation ICP-MS. *Chinese Science Bulletin* **48**, 2411-2421.

Yuan H. L., Gao S., Liu X. M., Li H. M., Günther D. and Wu F. Y. (2004) Precise U-Pb age and trace element determinations of zircon by laser ablation-inductively coupled plasma mass spectrometry. *Geostandards and Geoanalytical Research* **28**, 353-370.

Yuan H. L., Gao S., Dai M. N., Zong C. L., Günther D., Fontaine G. H., Liu X. M. and Diwu C. R. (2008) Simultaneous determinations of U-Pb age, Hf isotopes and trace element compositions of zircon by excimer laser ablation quadrupole and multiple collector ICP-MS. *Chemical Geology* **247**, 100-118.

Yuan H. L., Gao S., Dai M. N., Zong C. L. and Li R. X. (2009) *In situ* strontium isotope analysis of fluid inclusion using LA-MC-ICPMS (in Chinese with English abstract). Bulletin of Mineralogy, Petrology and Geochemistry 28, 313-317.

Zhang S.-B., Zheng Y.-F., Wu Y.-B., Zhao Z.-F., Gao S. and Wu F.-Y. (2006) Zircon U-Pb age and Hf-O isotope evidence for Paleoproterozoic metamorphic event in South China. *Precambrian Research* **151**, 265-288.

Zhang S.-B., Zheng Y.-F., Zhao Z.-F., Wu Y.-B., Liu X. M. and Wu F.-Y. (2008) Neoproterozoic anatexis of Archean Lithosphere: Geochemical evidence from felsic to mafic intrusives at Xiaofeng in the Yangtze George, South China. *Precambrian Research* **163**, 210-238.

Zhao Z.-F., Zheng Y.-F., Wei C. S., Chen F. K., Liu X. M. and Wu F.-Y. (2008) Zircon U-Pb ages, Hf and O isotopes constrain the crustal architecture of the ultrahigh-pressure Dabie orogen in China. *Chemical*

Geology **253**, 222-242.

Zheng Y.-F., Zhao Z.-F., Wu Y.-B., Zhang S.-B., Liu X. M. and Wu F.-Y. (2006) Zircon U-Pb age, Hf and O isotope constraints on protolith origin of ultrahigh-pressure eclogite and gneiss in the Dabie orogen. *Chemical Geology* **231**, 135-158.

Zheng Y.-F., Zhang S.-B., Zhao Z.-F., Wu Y.-B., Li X. H., Li Z. X. and Wu F.-Y. (2007) Contrasting zircon Hf and O isotopes in the two episodes of Neoproterozoic granitoids in South China: implications for growth and reworking of continental crust. *Lithos* **96**, 127-150.

Figure Captions

Figure 1. Relationship between element concentrations and precision of isotopic measurement for LA-ICP-MS (Neptune MC-ICP-MS in Beijing, 193nm GeoLas+ laser). The repetition rate is fixed at 8-10 Hz (after Wu et al., 2010b).

Figure 2. Histograms of $\varepsilon_{Hf}(t)$ values of zircons from (a) host granite and (b) mafic enclaves from the Gudaoling batholith in NE China. The $\varepsilon_{Hf}(t)$ values of all zircons were calculated at 120 Ma, the crystallization age of mafic enclaves and host granite. Scale bar is 50 μm (after Yang et al., 2007).

Figure 3. Hf-O isotopic variations of zircons from Qinghu, Lisong and Fogang plutons (after Li et al., 2009b). The dotted lines denote two-component mixing trends between mantle- and crustal-derived magmas.

Figure 4. Comparisons of zircon Hf isotopic compositions from different batholiths in the Transhimalayan belt and the northern Lhasa terrane. Zircons from the Gangdese and Ladakh batholiths have positive $\varepsilon_{Hf}(t)$ values; whereas those from the Chayu-Burma batholith and the North Lhasa terrane have negative $\varepsilon_{Hf}(t)$ values, suggesting their derivation from the juvenile and ancient crusts, respectively (after Ji et al., 2009).

Figure 5. Histograms comparing the initial Sr-Nd isotopic compositions of perovskite with whole-rock values for the Mengyin kimberlites (after Yang et al., 2009). (a) Whole-rock Sr isotopes; (b) Perovskite Sr isotopes (laser analyses); (c) Whole-rock Nd isotopes, and (d) Perovskite Nd isotopes (laser analyses).

Geochemical Processes of Organic Pollutants in a Typical Subtropical Watershed: A Case Study with Decabromodiphenyl Ether

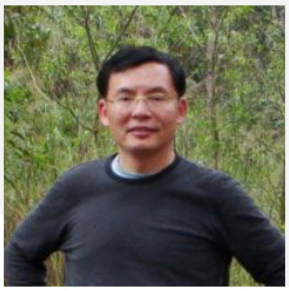

Eddy Y. ZENG [a,*]
[a] State Key Laboratory of Organic Geochemistry, Guangzhou Institute of Geochemistry, Chinese Academy of Sciences, Guangzhou 510640, China
* corresponding author's email: eddyzeng@gig.ac.cn

Full Text (3.3 Mb PDF)

Abstract

The Pearl River Delta (PRD) is a subtropical watershed located in South China and noted for its fast-growing economic development. As a result of the high industrial and agricultural productivities, as well as primitive handling of electronic waste (e-waste), organic contamination has become a serious threat to the sustainability of socioeconomic growth in the region. To provide a better understanding of the fate of organic pollutants within the environment of the PRD, this study examined various inter-compartmental fluxes and constructed a mass transport budget using decabromodiphenyl ether (BDE-209), a major constituent in brominated fire retardants abundantly embedded in e-waste, as the target analyte. The results show that atmospheric deposition (9,200 kg/yr annually for dry and wet depositions combined) was the most important vector in cycling of BDE-209; particularly, wet deposition (2,500 kg/yr) was in the same order of magnitude as dry deposition (6,700 kg/yr), which is obviously attributed to the large amounts of precipitations encountered in the PRD subject to the East Asian monsoon system. Riverine runoff, on the other hand, carried an unexpectedly small amount (1,960 kg/yr) of BDE-209 from the PRD; however, most (1,550 kg/yr) of this amount continues to be discharged into deeper oceans. The soil inventory (44,000 kg/yr) of BDE-209 was only several times the amount of annual atmospheric deposition, probably because BDE-209 is still being released from current sources. Nevertheless, imported e-waste (particularly from industrialized countries, mostly from the United States) appears to be a potentially gigantic source of BDE-209 with an annual accumulation rate estimated at 9,400,000 kg/yr. Finally, useful inferences can be drawn for the fate of other organic pollutants from the present study.

Keywords: Organic pollutants; Inter-compartmental flux; Geochemical process; e-Waste; Decabromodiphenyl ether; Pearl River Delta

1. Introduction

The Pearl River Delta (PRD), located in a subtropical region of South China to the north of the South China Sea and with an area of 53,580 km^2 within Guangdong Province (Figure 1), is one of the most economically prosperous areas in China. Rapid economic development and accelerated urbanization in the region over the last three decades have resulted in elevated levels of pollution in various environmental compartments of the PRD. Aside from traditional contaminant inputs such as waste discharges from industrial, agricultural and domestic activities, primitive handling of electronic waste (e-waste), largely derived from importation to the PRD, containing heavy metals and organic pollutions has drastically added to the magnitude of the problem (Ni and Zeng, 2009). The fact that China has been importing the largest portion of e-waste generated worldwide, with the PRD being the main destiny, has raised great concerns worldwide (Ogunseitan et al., 2009; Stone, 2009).

Polybrominated diphenyl ethers (PBDEs) are major constituents of brominated fire retardants (BFRs) abundantly used in a variety of electronic and electric devices, which become obsolete at the end of their life cycles. Because huge amounts of BFRs have been used in the manufacture of electronics and appliances in the PRD and have been imported to the region in the form of e-waste (a fair amount of BFRs is used locally in manufacturing electronics and appliances, but much larger amounts of BFRs are imported to the region via e-waste), high levels of PBDEs have been detected in various PRD sample matrices including riverine runoff (Guan et al., 2007), soil (Zou et al., 2007), sediment (Mai et al., 2005), air (Chen et al., 2006; Zhang et al., 2009), precipitation (Zhang et al., 2009), aquatic products (Guo et al., 2007; Meng et al., 2007), human breast milk (Bi et al., 2006) and blood plasma (Bi et al., 2006; Qu et al., 2007). In addition, because of their persistency in the environment, ability to accumulate in biota, toxic potency to both the ecological system and human health, and potential for long-range atmospheric transport, tetrabromodiphenyl ethers and pentabromodiphenyl ethers were included in the Stockholm Convention on Organic Persistent Pollutants in May 2009 (http://chm.pops.int/).

Despite the tremendous efforts to characterize the occurrence of organic pollutants in the environment of the PRD, it remains relatively unclear how organic pollutants such as PBDEs are transported among various environmental compartments of the PRD. Such information is critical for understanding the dynamics of inter-compartmental fluxes of organic pollutants, and would allow a better assessment of the environmental behavior and effects of organic pollutants. To this end, we will use decabromodiphenyl ether (BDE-209), the most abundant component among the BDE congeners found in the environment of the PRD, as the target compound to construct a mass transport budget using data available from the literature.

To accomplish the above-mentioned goal, individual inter-compartmental processes for BDE-209 have to be examined. The main inter-compartmental processes, specifically applicable to the geographical setting of the PRD, include riverine runoff, dry and wet atmospheric depositions, air-soil and air-water gaseous exchange, long-range atmospheric transport in and out of the region, and e-waste emissions. Minor routes include city emission and bioprocess (e.g., uptake and release by terrestrial and aquatic biota). In addition, soil (and sediment) is perhaps the largest reservoir of BDE-209 and may become a buffer mediating the geochemical cycling of BDE-209. Because the Pearl River Estuary (PRE, Figure 1) connects the main portion of the PRD with the northern South China Sea, the geochemical processes (Figure 2) occurring in the PRE play an important role in controlling the outflows of BDE-209 to deep seas and is also considered in the present study.

In the rest of this paper, I will summarize the procedures used to obtain the fluxes of BDE-209 for riverine runoff, dry and wet atmospheric depositions and e-waste emission, as well as soil inventory of BDE-209, from available literature or current knowledge. Finally, the implications of the mass transport

About the Author

Eddy Y. Zeng is a professor and director of the State Key Laboratory of Organic Geochemistry. He obtained a Ph.D. in 1992 from the Department of Chemistry at the University of Southern California, USA. He worked as a principal scientist at the Southern California Coastal Water Research Project for more than 12 years, where he led a research group focusing on studies concerning the occurrence and fate of organic pollutants in the marine coastal environment off southern California. He has been conducting research in the field of environmental geochemistry, focusing mainly in the environmental geochemical processes of persistent organic pollutants. He also serves as an editor of *Environmental Toxicology and Chemistry*, an associate editor of *Journal of Hydrology*, an editorial board member of *Chemosphere*.

budget will be briefly discussed.

2. Riverine Runoff Transport

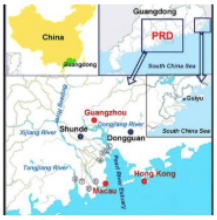

In the upper right hand quadrant - One box has PRD in it and is blown up on the left below. Guiyu's location is shown in the smaller box on the right.
Figure 1

Because of the rich river network in the PRD (Figure 1), riverine runoff is an important mode to carry BDE-209, derived from all sources such as industrial, agricultural and residential discharge, surface washoff and precipitation, into the coastal ocean and further to the global oceans. Four main rivers (Xijiang, Beijiang, Dongjiang and Tangjiang Rivers) flow into the PRD and merge into the northern South China Sea through eight outlets, i.e., Humen, Jiaomen, Hongqili, Hengmen, Modaomen, Jitimen, Hutiaomen and Yamen (Figure 1). Monthly flux of BDE-209 through the eight outlets into the coastal ocean was calculated with $F_{i,j} = kC_{i,j} \times D_{i,j}$, where k is a unit conversion factor, $C_{i,j}$ is the concentration of BDE-209 in riverine runoff collected from a specific outlet for a given month, and $D_{i,j}$ stands for the corresponding total water discharge for the same month. The total annual flux (F_i) from the ith outlet was then estimated by

$$F_i = \sum_{j=1}^{12} F_{i,j} \qquad (1)$$

Based on Eq. (1), our previous study obtained an annual riverine input of BDE-209 at 1.96 tons/yr (Guan et al., 2007). For comparison, the annual riverine mass emissions of polycyclic aromatic hydrocarbons (PAHs; sum of 28 components), dichlorodiphenyltrichloroethanes (DDTs; sum of *o,p'*- and *p,p'*-DDT, DDD and DDE), hexachlorocyclohexanes (sum of α-HCH, ß-HCH, γ-HCH, and δ-HCH) and PBDEs (sum of 10 congeners including BDE-209) were 33.9 (Wang et al., 2007), 1.3 (Guan et al., 2009b), 1.23 (Guan et al., 2009b) and 2.14 tons/yr (Guan et al., 2007), respectively. Further analyses of the data unveiled considerably linear correlations between the riverine inputs of organic pollutants and water discharge (Guan et al., 2007; Guan et al., 2009b; Wang et al., 2007; Wang et al., 2008), suggesting that water discharge is likely to be the crucial factor in controlling the pollutant riverine inputs in the PRD.

3. Atmospheric Depositional Rates

Atmospheric depositional rates can be contributed from dry and wet depositions, and they are defined as Fdry and Fwet, respectively and estimated with the following equations (Cetin and Odabasi, 2007; Venier and Hites, 2008):

$$F_{dry} = C_p v_d A = (C_{p,u} A_u + C_{p,r} A_r)\, v_d \qquad (2)$$

$$F_{wet} = (VWM)pA = (VWM_u A_u + VWM_r A_r)p \qquad (3)$$

where C_p is the BDE-209 concentration in the atmospheric particulate phase (kg/m^3), v_d is the particle dry depositional velocity (m/yr), A is the study area (m^2), *VWM* is the volume weighted mean BDE-209 concentration in precipitation (kg/m^3), p is the precipitation rate (m/yr), and u and r denote the urban and rural areas, respectively.

Concentrations of BDE-209 in air (Chen et al., 2006) and rain (Zhang et al., 2009) of Guangzhou, the capital of Guangdong Province (Figure 1), have been measured, and were used as the urban data for Eqs. (2) and (3). In addition, Zhang et al. (2009) measured the concentrations of BDE-209 in air and precipitation from Dongguan and Shunde (Figure 1), which were regarded as the rural concentrations. As a result, the annual dry and wet depositional rates of BDE-209 were estimated at 6,700 and 2,500 kg/yr, respectively, for the entire PRD (Zhang et al., 2009). Apparently, dry deposition is the predominant mode to remove BDE-209 from the atmosphere in the PRD, but wet deposition also contributes substantially to the overall atmospheric fallout of BDE-209. The sizeable contribution from wet deposition can be attributable to the generally large amount of precipitations in the region, e.g., average 1300 to 2284 mm in various parts of Guangzhou Province embracing the PRD in 2008 (Statistical Bureau of Guangdong Province, 2009).

4. Potential Loading from E-Waste

The amount of BDE-209 potentially emitted from e-waste to the PRD (I; tons/yr) was estimated with the following equation:

$$I = kVC \qquad (4)$$

where k is a unit conversion constant, V stands for the volume (V does not necessarily represent volume. In the current example, weight is used to designate the amount of e-waste generally annually worldwide. In eq. (4), k is used to transform different units) of e-waste annually generated in and/or imported to the PRD area, and C represents the average concentration of BDE-209 in e-waste. A literature survey indicated that the gross amount of e-waste generated annually worldwide is 20-50 million tons/yr, approximately 70% of which is shipped to China (Ni et al., 2010). In addition, plastics account for ~12-20% of the e-waste weight and the concentration of BDE-209 in plastics is 21,000,000 ng/g (Choi et al., 2009). If 16% is taken as the relative abundance of plastics in e-waste, substituting the above values into Eq. (4) yields the annual potential loading of BDE-209 from e-waste imported to China at 47,000-118,000 tons/yr. If it is assume that 20% of the total amount of e-waste imported to China is shipped to the PRD, the low end of the annual loading of BDE-209 from e-waste to the PRD is ~9,400 tons/yr. This assumption is extremely conservative as Guiyu, located in Guangdong Province (Figure 1), is home to some of the world's largest e-waste dismantling and recycling facilities; as a result, large amounts of e-waste are expected to be processed in the region.

5. Mass Inventory in Soil

A hypothetical 20-cm deep layer of soil was used to estimate the mass inventory (I; kg) of BDE-209 in the surface soil of the PRD using

$$I = kCAd\rho \qquad (5)$$

where k is a unit conversion factor, C is the area weighted concentration of BDE-209 (ng/g), A is the study area (m^2), d stands for the soil depth (20 cm), and ρ is the ideal soil density (1.5 g/cm^3). With Eq. (5) Zou et al. (2007) obtained the soil inventory of BDE-209 in the PRD at 44,000 kg. Inevitably, this value should be quite dynamic as the atmospheric deposition estimated above contributes

approximately 9,200 kg/yr or ~20% at the current level to the soil inventory annually.

6. Geochemical Dynamics in the Pearl River Estuary

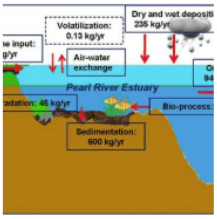

Figure 2

As mentioned above, the geochemical dynamics occurring in the PRE (Figure 2) dictates the outflows of BDE-209 into the coastal ocean. The main processes considered include air-water gaseous exchange, dry and wet depositions, sedimentation and degradation and are discussed below.

6.1. Atmospheric Deposition

Dry and wet depositional fluxes can be estimated with Eqs. (2) and (3). For air-water gaseous exchange, the flux (F_g) can be estimated with the following equation:

$$F_g = k_g(C_g - C_w H')A \quad (6)$$

where k_g is the overall gas-phase mass transfer coefficient (m/s), C_w and C_g are the BDE-209 concentrations in the dissolved phase of water and in the gas phase of air (kg/m^3), and H' is the unitless Henry's Law constant (Venier and Hites, 2008). Because no measured data are available, the gas-phase concentration of BDE-209 in the atmosphere of the PRE is assumed to be the same as the average concentration (which was below the detection limit and taken as zero in the present study) of BDE-209 obtained in samples collected from the atmosphere of Guangzhou (Chen et al., 2006). Guan et al. (2009a) determined a value of -0.13 kg/yr for air-water exchange flux of BDE-209 in the PRE with the negative sign indicating vaporization was the dominant transport mode. In addition, the annual combined dry and wet depositional input amounted to 235 kg/yr (Guan et al., 2009a).

6.2. Sedimentation and Degradation

The sedimentation rate of BDE-209 in the PRE (with an area of 2016 km^2) was estimated from a previous study investigating the time trend of BDE-209 in the sediment column of the PRE (Chen et al., 2007). The result indicated that nearly 600 kg/yr of BDE-209 settled into the sediment of the PRE annually in recent years (Chen et al., 2007). Furthermore, a mass attenuation model was used to estimate the degradation rate of BDE-209 in the PRE:

$$M_d = M_o[1 - (1/2)^{t/T}] \quad (7)$$

where M_d is the amount of the degraded BDE-209, M_o is the initial mass, t is the time duration for degradation and T is the degradation half-time of BDE-209. With the hydraulic turnover time (~6 days) regarded as the degradation time (Wong and Cheung, 2008) and the riverine input (1350 kg/yr) of BDE-209 from the four eastern riverine runoff outlets (Figure 1) as the initial mass (Guan et al., 2007), the annual degradation rate of BDE-209 was estimated at 45 kg/yr (Guan et al., 2009a).

With the above considerations, a mass balance diagram can be constructed for BDE-209 in the PRE (Figure 2). It is clear that the majority (70%) of BDE-209 discharged from the PRD into the PRE eventually flows to the adjacent ocean, which indicates that riverine runoff from the PRD significantly contributes to the mass loadings of BDE-209 (and other organic pollutants) to the global oceans.

7. Mass Transport Budget: Implications and Perspectives

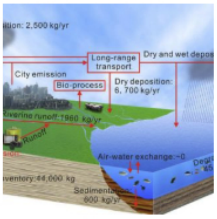

Figure 3

After all the above processes are taken into account, a mass transport budget can be constructed (Figure 3). It should be noted that the riverine runoff input in the budget is 610 kg/yr higher than that entering the PRE (Figure 2); this additional amount was discharged from the four western outlets (Modaomen, Jitimen, Hutiaomen and Yamen) and directly to the coastal ocean (Figure 1). Figure 3 shows that dry deposition is an important mode to recycle BDE-209 from the atmosphere to the ground, and soil remains the largest sink. On the other hand, fluxes associated with air-soil and air-water gaseous exchange within the PRD should be noticeably less significant compared to dry and wet depositional fluxes as indicted by the small amount of air-water exchange relative to that of dry/wet deposition in the PRE (Figure 2). Terrestrial sediment inventories (e.g., those in rivers, lakes, reservoir and ponds etc.) may be important because of the possibility of receiving point-source inputs from manufacturing plants or e-waste recycling centers, but their impacts on the overall geochemical cycling are largely accounted for by riverine runoff or air-water exchange. The amounts of BDE-209 flowing in and out of the PRD via long-range transport are also unknown; however, the net effect may be small and largely reflected in dry and wet atmospheric depositions. Biological processes that impact BDE-209 cycling are also unknown but are expected to be negligible because the amount of biota (or equivalently biomass) available for accumulation of BDE-209 is expected to be substantially smaller than those of soil/sediment and water. Finally, it should be emphasized that the amount of BDE-209 for a specific inter-compartmental flux or within an environmental compartment in the PRD is no more than a drop in the bucket compared to the potential emission of BDE-209 from e-waste (Figure 3). Apparently, vast amounts of BDE-209 remain in e-waste and commercial products embedded with BFRs, that can explode in the future if no appropriate mitigation measures are immediately installed.

Although this study has examined the geochemical process of BDE-209 only, useful inferences can be derived for other organic pollutants. For example, PAHs are similar to BDE-209 in that both are still being released from current sources and considerably persistent in the environment. It can be deduced that the amount of annual atmospheric PAH depositions would be substantial compared to the current soil inventory as in the case of BDE-209 (9.2 tons/yr for dry and wet depositions versus 44 tons for soil inventory; Figure 3). Based on a field measurement of atmospheric depositions of PAHs (12 components) in an urban lake in Guangzhou (Li et al., 2009), we obtained the annual dry and wet depositional rate of PAHs at 106 tons/yr for the entire PRD. In addition, the soil inventory of the same PAHs in the PRD was estimated at 4,600 tons by extrapolating the results from the study of Ma et al. (2009). On the other hand, the amount of annual atmospheric deposition of DDTs is expected to be fairly small relative to its soil inventory because DDTs in the environment are mostly residues from history uses. In fact, our preliminary assessment indicates that the soil DDT inventory in the PRD is three orders of magnitude higher than the annual dry and wet atmospheric deposition of DDTs (unpublished data). Nevertheless, more refined studies are needed to verify this hypothesis, and more importantly to gain better understanding of the governing mechanisms for the geochemical processes of organic pollutants in general.

Acknowledgements

The funding of the present study was gracefully provided by the National Natural Science Foundation of China (No. 40821003), Chinese Academy of Sciences (KZCX2-YW-Q02-06) and Earmarked Fund of the State Key Laboratory of Organic Geochemistry (SKLOG2009A04). Thanks also go to Kai Zhang and Baozhong Zhang for their precious time and efforts in compiling the literature data as well as drawing

the figures, which was critical for completing this manuscript.

References

Bi, X., Qu, W., Sheng, G., Zhang, W., Mai, B., Chen, D., Yu, L., and Fu, J. (2006) Polybrominated diphenyl ethers in South China maternal and fetal blood and breast milk. *Environ. Pollut.* **144**, 1024-1030.

Cetin, B. and Odabasi, M. (2007) Air-water exchange and dry deposition of polybrominated diphenyl ethers at a coastal site in Izmir, Turkey. *Environ. Sci. Technol.* **41**, 785-791.

Chen, L. G., Mai, B. X., Bi, X. H., Ran, Y., Luo, X. J., Chen, S. J., Sheng, G. Y., Fu, J. M., and Zeng, E. Y. (2006) Concentration levels, compositional profiles, and gas-particle partitioning of polybrominated diphenyl ethers in the atmosphere of an urban city in South China. *Environ. Sci. Technol.* **40**, 1190-1196.

Chen, S. J., Luo, X. J., Lin, Z., Luo, Y., Li, K. C., Peng, X. Z., Mai, B. X., Ran, Y., and Zeng, E. Y. (2007) Time trends of polybrominated diphenyl ethers in sediment cores from the Pearl River Estuary, South China. *Environ. Sci. Technol.* **41**, 5595-5600.

Choi, K. I., Lee, S. H., and M., O. (2009) Leaching of brominated flame retardants from TV housing plastics in the presence of dissolved humic matter. . *Chemosphere* **74**, 460-466.

Guan, Y. F., Sojinu, O. S. S., Li, S. M., and Zeng, E. Y. (2009a) Fate of polybrominated diphenyl ethers in the environment of the Pearl River Estuary, South China. *Environ. Pollut.* **157**, 2166-2172.

Guan, Y. F., Wang, J. Z., Ni, H. G., Luo, X. J., Mai, B. X., and Zeng, E. Y. (2007) Riverine inputs of polybrominated diphenyl ethers from the Pearl River Delta (China) to the coastal ocean. *Environ. Sci. Technol.* **41**, 6007-6013.

Guan, Y. F., Wang, J. Z., Ni, H. G., and Zeng, E. Y. (2009b) Organochlorine pesticides and polychlorinated biphenyls in riverine runoff of the Pearl River Delta, China: A assessment of mass loading, input source and environmental fate. *Environ. Pollut.* **157**, 618-624.

Guo, J.-Y., Wu, F.-C., Mai, B.-X., Luo, X.-J., and Zeng, E. Y. (2007) Polybrominated diphenyl ethers in seafood products of South China. *J. Agric. Food Chem.* **55**, 9152-9158.

Li, J., Cheng, H. R., Zhang, G., Qi, S. H., and Li, X. D. (2009) Polycyclic aromatic hydrocarbon (PAH) deposition to and exchange at the air-water interface of Luhu, an urban lake in Guangzhou, China. *Environ. Pollut.* **157**, 273-279.

Ma, X. X., Ran, Y., Gong, J., and Zou, M. Y. (2009) Concentrations and inventories of polycyclic aromatic hydrocarbons and organochlorine pesticides in the watershed soils of the Pearl River Delta, China. *Environ. Monitor. Assess.* **145**, 453-464.

Mai, B. X., Chen, S. J., Luo, X. J., Chen, L. G., Yang, Q. S., Sheng, G. Y., Peng, P. A., Fu, J. M., and Zeng, E. Y. (2005) Distribution of polybrominated diphenyl ethers in sediments of the Pearl River Delta and adjacent South China Sea. *Environ. Sci. Technol.* **39**, 3521-3527.

Meng, X.-Z., Zeng, E. Y., Yu, L.-P., Mai, B.-X., Luo, X.-J., and Ran, Y. (2007) Persistent halogenated hydrocarbons in consumer fish of China: regional and global implications for human exposure. *Environ. Sci. Technol.* **41**, 1821-1827.

Ni, H. G. and Zeng, E. Y. (2009) Law enforcement and global collaboration are the keys to containing e-waste tsunami in China. *Environ. Sci. Technol.* **43**, 3991-3994.

Ni, H. G., Zeng, H., Tao, S., and Zeng, E. Y. (2010) Environmental and human exposure to persistent halogenated compounds derived from e-waste in China. Environ. Toxicol. Chem. (in press).Ogunseitan, O. A., Schoenung, J. M., Saphores, J.-D. M., and Shapiro, A. A. (2009) The electronics revolution: from e-wonderland to e-wasteland. *Science* **326**, 670-671.

Qu, W. Y., Bi, X. H., Sheng, G. Y., Lu, S. Y., Fu, H., Yuan, J., and Li, L. P. (2007) Exposure to polybrominated diphenyl ethers among workers at an electronic waste dismantling region in Guangdong, China. *Environ. Int.* **33**, 1029-1034.

Statistical Bureau of Guangdong Province (2009) Guangdong Statistical Yearbook. http://www.gdstats.gov.cn/tjnj/ml_c.htm (accessed January 2010).

Stone, R. (2009) Confronting a toxic blowback from the electronics trade. *Science* **325**, 1055-1055.

Venier, M. and Hites, R. A. (2008) Atmospheric deposition of PBDEs to the Great Lakes featuring a Monte Carlo analysis of errors. *Environ. Sci. Technol.* **42**, 9058-9064.

Wang, J.-Z., Guan, Y.-F., Ni, H.-G., Luo, X.-L., and Zeng, E. Y. (2007) Polycyclic aromatic hydrocarbons in riverine runoff of the Pearl River Delta (China): concentrations, fluxes and fate. *Environ. Sci. Technol.* **41**, 5614-5619.

Wang, J. Z., Ni, H. G., Guan, Y. F. G., and Zeng, E. Y. (2008) Occurrence and mass loadings of *n*-alkanes in riverine runoff of the Pearl River Delta, South China: Global implications for levels and inputs. *Environ. Toxicol. Chem.* **27**, 2036-2041.

Wong, M. H. and Cheung, K. C. (2008) Pearl River Estuary and Mirs Bay, South China. http://nest.su.se/MNODE/asia/China/pearlmirs/PMbudsrev2.htm (accessed January 2010).

Zhang, B. Z., Guan, Y. F., Li, S. M., and Zeng, E. Y. (2009) Occurrence of polybrominated diphenyl ethers in air and precipitation of the Pearl River Delta, South China: annual washout ratios and depositional rates. *Environ. Sci. Technol.* **43**, 9142-9147.

Zou, M. Y., Ran, Y., Gong, J., Mai, B. X., and Zeng, E. Y. (2007) Polybrominated diphenyl ethers in watershed soils of the Pearl River Delta: Occurrence, inventory, and fate. *Environ. Sci. Technol.* **41**, 8262-8267.

Figure Captions

Figure 1. General locality of the study region in the Pearl River Delta (PRD) and Pearl River Estuary (PRE) within Guangdong Province of South China. Upper left-hand quadrant: Locality of Guangdong province. Upper right-hand quadrant: Locality of the PRD within Guangdong Province; the smaller box on the right indicates the location of Guiyu, one of the largest e-waste recycling centers in the world (also enlarged directly below). Lower quadrant: Detailed map showing the various sampling sites within the PRD with the numbers designating the eight major riverine runoff outlets: (1) - Humen; (2) - Jiaomen; (3) - Hongqili; (4) - Hengmen; (5) - Modaomen; (6) - Jitimen; (7) - Hutiaomen; and (8) - Yamen.
In the upper right hand quadrant - One box has PRD in it and is blown up on the left below. Guiyu's location is shown in the smaller box on the right.

Figure 2. Schematic showing the geochemical process of BDE-209 in the Pearl River Estuary (Figure 1).

Figure 3. Mass transport budget of BDE-209 within the Pearl River Delta, South China (Figure 1).

The Geochemical Society · 5241 Broad Branch Rd, NW · Washington, DC 20015-1305